Copy 199
RM L54B08

NACA RM L54B08

TECH LIBRARY KAFB, NM
0144323

RESEARCH MEMORANDUM

7521

HINGE-MOMENT, LIFT, AND PITCHING-MOMENT CHARACTERISTICS OF A FLAP-TYPE CONTROL SURFACE HAVING VARIOUS HINGE-LINE LOCATIONS ON A 4-PERCENT-THICK 60° DELTA WING

TRANSONIC-BUMP METHOD

By Robert F. Thompson

Langley Aeronautical Laboratory
Langley Field, Va.

CLASSIFIED DOCUMENT

[redacted]

NATIONAL ADVISORY COMMITTEE FOR AERONAUTICS

WASHINGTON
March 24, 1954

[redacted]

[redacted]

Classification cancelled (or changed to) Unclassified

By Authority Navtel RL Announcement #97
(OFFICER MAKING CHANGE)

By 24 Feb 56

NK
(GRADE OF OFFICER MAKING CHANGE)

7 April 61
DATE

TECH LIBRARY KAFB, NM
0144323

[redacted]

NATIONAL ADVISORY COMMITTEE FOR AERONAUTICS

RESEARCH MEMORANDUM

HINGE-MOMENT, LIFT, AND PITCHING-MOMENT CHARACTERISTICS OF A FLAP-TYPE CONTROL SURFACE HAVING VARIOUS HINGE-LINE LOCATIONS ON A 4-PERCENT-THICK 60° DELTA WING

TRANSONIC-BUMP METHOD

By Robert F. Thompson

SUMMARY

An investigation was made in the Langley high-speed 7- by 10-foot tunnel to determine the hinge-moment, lift, and pitching-moment characteristics of a 4-percent-thick 60° delta wing equipped with a trailing-edge flap-type control. The control spanned the inboard 66 percent of the semispan and had various overhang nose balances. Balance chord was varied by shifting the flap hinge line with the total control chord held constant at 11.3 percent of the wing mean aerodynamic chord. Ratios of balance chord to flap chord were 0.07, 0.32, 0.50, 0.79, and 1.03. The model was tested through an angle-of-attack range of -6° to 15°, a Mach number range from 0.60 to 1.18, and a flap-deflection range of approximately ±30°.

Shifting the control hinge line rearward had a balancing effect on the control hinge moments for all test conditions but caused the variation of hinge-moment coefficient with control deflection to become very nonlinear. For ratios of balance chord to flap chord equal to or greater than 0.50, the control was overbalanced over part of the test range and there were abrupt breaks and changes in slope of the curves of hinge-moment coefficient against control deflection. Rearward movement of the hinge line also resulted in large losses in control lift and pitch effectiveness for all but relatively low control deflections. Increasing the wing angle of attack from -6° to 15° had little effect on the general variation of hinge-moment, lift, and pitching-moment coefficients with control deflection.

[redacted]

[redacted]

INTRODUCTION

The large hinge moments associated with trailing-edge flaps when used on high-speed aircraft have necessitated the use of powered-control systems. To reduce the requirements of the powered-control system and enable the pilot to fly the airplane in the event of power failure, it is desirable to aerodynamically balance a large part of the control force. As part of a continuing program to evaluate various aerodynamic balances, the present investigation on plain overhang balances was made in the Langley high-speed 7- by 10-foot tunnel using the transonic-bump test technique. A bibliography of previous work on aerodynamic balances is given in reference 1.

This investigation presents experimental hinge-moment, lift, and pitching-moment data for a 4-percent-thick 60° delta wing equipped with a 66-percent-span inboard flap-type control. The hinge line of the control was shifted to give various ratios of balance chord to flap chord. Data were obtained over an angle-of-attack range of -6° to 15°, a flap-deflection range of approximately ±30°, and a Mach number range from 0.60 to 1.18.

COEFFICIENTS AND SYMBOLS

The lift and pitching-moment data represent the aerodynamic effects that would be obtained on a complete wing with both control surfaces deflected in the same direction.

C_h flap hinge-moment coefficient, $H/q2M_1$

C_L lift coefficient, $\frac{\text{Twice lift of semispan model}}{qS}$

C_m pitching-moment coefficient referred to $0.25\bar{c}$,

$$\frac{\text{Twice pitching moment of semispan model}}{qS\bar{c}}$$

ΔC_L increment of lift coefficient due to flap deflection

ΔC_m increment of pitching-moment coefficient due to flap deflection

H flap hinge moment measured about hinge line, ft-lb

[redacted]

M_1 area moment about hinge line of flap area rearward of hinge line, ft^3 (see fig. 1(b))

M_2 area moment about pitching-moment axis of flap area rearward of hinge line, ft^3

q effective dynamic pressure over span of model, $\rho V^2/2$, lb/sq ft

S twice wing area of semispan model, 0.278 sq ft

S_f twice flap area of semispan model rearward of hinge line, sq ft

$\bar{c}$ mean aerodynamic chord of wing, 0.462 ft, based on relationship $\frac{2}{S}\int_0^{b/2} c^2 dy$

b twice span of semispan model, 0.802 ft

c local wing chord, ft

c_b balance chord, (distance from hinge line forward to leading edge of control, see fig. 1(b)), ft

c_f flap chord, (distance from hinge line rearward to trailing edge of control, see fig. 1(b)), ft

y spanwise distance from plane of symmetry, ft

ρ mass density of air, slugs/cu ft

V free-stream air velocity, ft/sec

M effective Mach number over span of model, $\frac{2}{S}\int_0^{b/2} cM_a \, dy$

M_a average chordwise local Mach number

M_l local Mach number

R Reynolds number of wing based on $\bar{c}$

α angle of attack, deg

δ control-surface deflection, measured in a plane perpendicular to control-surface hinge line, positive when control-surface trailing edge is below wing-chord plane, deg

[redacted]

$C_{h_\delta} = \left(\frac{\partial C_h}{\partial \delta}\right)_\alpha$ averaged over a δ range of $\pm 5^\circ$

$C_{h_\alpha} = \left(\frac{\partial C_h}{\partial \alpha}\right)_\delta$ averaged over an α range of $\pm 6^\circ$

$C_{l_\delta} = \left(\frac{\partial C_l}{\partial \delta}\right)_\alpha$ averaged over a δ range of $\pm 5^\circ$

$C_{m_\delta} = \left(\frac{\partial C_m}{\partial \delta}\right)_\alpha$ averaged over a δ range of $\pm 5^\circ$

The subscript outside the parentheses indicates the factor held constant during the measurement of the parameter.

MODEL AND APPARATUS

The steel semispan wing was triangular in plan form having 60° sweepback of the leading edge, an aspect ratio of 2.31, and a taper ratio of 0. The airfoil section thickness was constant at 4 percent of the local wing chord at all chordwise stations from 30 to 70 percent of the local wing chord. Rearward of the 70-percent-chord station, the airfoil section tapered to a sharp trailing edge. Forward of the 30-percent-chord station the airfoil section tapered to a 0.0018c leading-edge radius. A drawing of the wing giving pertinent dimensions and data is shown in figure 1(a).

The wing was equipped with a constant-chord trailing-edge flap-type control spanning the inboard 66 percent of the semispan. Variation in overhang balance was accomplished by having five different interchangeable controls of equal total chord ($c_b + c_f = 0.113\bar{c}$). The ratio of balance chord c_b to flap chord c_f was varied by shifting the hinge line, and the flap section contour was unchanged. Ratios of balance chord to flap chord tested were as follows: 0.07 (radius nose, unbalanced flap), 0.32, 0.50, 0.79, and 1.03. (See fig. 1(b).) The flap was hinged to the wing with a hinge pin at the outboard end of the flap and a hinge rod below the bump surface. Flap hinge moments were measured by a calibrated beam-type electric strain gage fastened rigidly to the hinge rod below the bump surface. (See fig. 1(a).)

The model was mounted on an electrical strain-gage balance and the aerodynamic forces and moments were recorded by means of calibrated

potentiometers. The balance was mounted in a chamber within the bump and the model butt passed through a hole in the bump surface angle-of-attack turntable. Leakage through this hole was kept to a minimum by the use of a sponge-wiper seal fastened to the undersurface of the turntable cover plate. (See fig. 1(a).) A photograph of the model as mounted in the tunnel is given in figure 2.

TESTS

The tests were made in the Langley high-speed 7- by 10-foot tunnel by utilizing the transonic-bump technique. This technique involved the mounting of the model in the high-velocity flow field generated over the curved surface of a bump located on the tunnel floor.

Typical contours of local Mach number in the vicinity of the model location on the bump, obtained with no model in position, are shown in figure 3. The long dashed line shown near the model root chord indicates a local Mach number that is 5 percent below the maximum value and represents the estimated extent of the bump boundary layer. The effective test Mach numbers were obtained from contour charts similar to those of figure 3 by using the relationship

$$M = \frac{2}{S}\int_0^{b/2} cM_a \, dy$$

The variation of Reynolds number with Mach number for typical test conditions is presented in figure 4. The Reynolds numbers were based on a mean aerodynamic chord of 0.462 foot. Hinge moment, lift, and pitching moment were obtained through a Mach number, angle-of-attack, and flap-deflection range. Data for the flaps having c_b/c_f equal to 0.07, 0.50, and 1.03 were obtained through a Mach number range from 0.60 to 1.18, angle-of-attack range from -6° to 15°, and a flap-deflection range of approximately $\pm 30^\circ$. For the flaps having c_b/c_f equal to 0.32 and 0.79, data were obtained over a Mach number range from 0.60 to 1.10, an angle-of-attack range of $\pm 6^\circ$, and flap deflection from approximately -5° to 30°.

CORRECTIONS

No corrections have been applied to the data for the chordwise and spanwise velocity gradients or for distortion of the wing due to air loads, but these corrections are believed to be small. Flap deflections

have been corrected for twisting of the hinge rod between the hinge-moment strain gage and the flap. Flap-deflection corrections were determined from a static hinge-moment calibration and applied according to the measured test hinge moment. This correction was approximately 10 percent of the original flap setting for the extreme loading condition.

RESULTS AND DISCUSSION

Presentation of Data

The variation of C_h, C_L, and C_m with flap deflection for the five values of c_b/c_f tested, is presented for all test conditions in figures 5 to 9. The effect of hinge location on the variation of C_h, C_L, and C_m with flap deflection at $\alpha = 0^\circ$ is presented for three representative test Mach numbers in figure 10. A crossplot of the data of figures 5 to 9 to obtain the variation of C_h with α at $\delta = 0^\circ$ is given in figure 11. The effect of Mach number on the hinge-moment parameters C_{h_δ} and C_{h_α} is given in figure 12. Figure 13 shows the variation of C_{L_δ} and C_{m_δ} with Mach number. Figure 14, taken from the data of figure 10, is a correlation of the incremental lift and pitching-moment coefficient with the area and area moment, respectively, of the flap rearward of the hinge line for a given flap deflection.

Hinge-Moment Characteristics

Angle of attack had little effect on the general variation of C_h with δ for all flaps tested (figs. 5 to 9). Therefore, the data of figure 10(a) which is a comparison of some typical curves from figures 5 to 9 are a good representation of the effects of hinge location on the variation of C_h with δ. The slope of C_h with δ for the unbalanced flap ($c_b/c_f = 0.07$) was negative (underbalanced) for all test conditions and was fairly constant over a deflection range of about $\pm 20^\circ$. Shifting the hinge line rearward (increasing c_b/c_f) had a balancing effect on the flap hinge-moment coefficient for all test conditions but caused the variation of C_h with δ to become very nonlinear. At subsonic speeds, most of the balancing effect of the overhang was obtained over a δ range of about $\pm 10^\circ$. For ratios of c_b to c_f of 0.50, 0.79, and 1.03, abrupt breaks and reversals in slope of C_h with δ occurred throughout the test range except for the flap having $c_b/c_f = 0.50$ at supersonic speeds. Increasing Mach number had a tendency to decrease the nonlinearities in the basic data.

The variations of C_h with α shown in figure 11 were obtained by crossplotting the data of figures 5 to 9 at $\delta = 0^\circ$. The curves (C_h plotted against α) are linear over an α range of at least $\pm 6^\circ$ and are summarized within this α range by the hinge-moment parameter C_{h_α} of figure 12. Above $\alpha = 6^\circ$, there is an increase in tendency to float with the relative wind for $c_b/c_f = 0.07$ and 0.50 and an increase in tendency to float against the relative wind for $c_b/c_f = 1.03$.

Since nonlinearities exist in the basic data, the hinge-moment parameter C_{h_δ} (fig. 12) has limited meaning and is applicable only over a δ range of $\pm 5^\circ$ for most of the data except for the unbalanced flap ($c_b/c_f = 0.07$). The hinge-moment parameter C_{h_δ} for the unbalanced flap was negative and had a small negative increase with Mach number up to $M = 0.90$. There was a large negative increase in C_{h_δ} in the speed range from $M = 0.90$ to $M = 1.05$, indicating a large rearward shift in flap center of pressure above $M = 0.90$. The negative values of C_{h_δ} above $M = 1.05$ were more than twice the negative values at $M = 0.60$. In the δ range of $\pm 5^\circ$, increasing c_b/c_f shifted C_{h_δ} in a positive direction and there was always a large rearward shift in flap center of pressure above $M \approx 0.85$. For $c_b/c_f \geqq 0.50$, C_{h_δ} was positive and increased with Mach number up to $M \approx 0.90$. For Mach numbers greater than 1.00, C_{h_δ} for all controls was negative or underbalanced.

Increasing c_b/c_f shifted C_{h_α} (fig. 12) in a positive direction. The value of C_{h_α} was negative through the speed range for the unbalanced flap and was positive for the flaps having $c_b/c_f = 0.79$ and 1.03. In general, the variation of C_{h_α} with Mach number was of the same nature for all values of c_b/c_f. The value of C_{h_α} was essentially constant with Mach number up to $M = 0.85$ and above $M = 1.05$. From $M = 0.85$ to $M = 1.05$, there were large changes in C_{h_α}. The variation in C_{h_α} with M was least for the control having $c_b/c_f = 0.79$.

Lift and Pitching-Moment Characteristics

All flaps produced increments of lift and pitching-moment coefficient in the proper direction although for each value of c_b/c_f there were certain combinations of α and δ where a further increase in δ did not give a further increase in C_L or C_m (figs. 5 to 9). Angle of attack had only small effect on the general variation of C_L and C_m with δ. To provide a direct comparison of the effects of increasing

c_b/c_f at $\alpha = 0^\circ$, incremental values of C_L and C_m are plotted against δ in figure 10(b) for three representative test Mach numbers. At subsonic speeds, C_L and C_m for the unbalanced flap ($c_b/c_f = 0.07$; fig. 5) had essentially a linear variation over a δ range of at least $\pm 10^\circ$ with the effectiveness decreasing at higher deflections. At supersonic speeds there was a tendency for the effectiveness to increase at the high flap deflections. Shifting the hinge line rearward caused a large decrease in the effectiveness for all but relatively low flap deflections. For $c_b/c_f \geq 0.50$, deflecting the flap more than $\pm 10^\circ$ at the lower test speeds had little or no effect on C_L and C_m and in some cases caused an increment in the wrong direction (fig. 10(b)). At the higher test speeds, C_L and C_m had a more linear variation throughout the δ range.

Increasing c_b/c_f had a relatively small effect on the absolute magnitudes of C_{l_δ} and C_{m_δ} as averaged over a δ range of at least $\pm 5^\circ$ (fig. 13). The parameters C_{l_δ} and C_{m_δ} generally increased in magnitude with an increase in α. There was a gradual decrease in values of C_{l_δ} and C_{m_δ} with increasing Mach number for the unbalanced flap ($c_b/c_f = 0.07$). In most cases, increasing c_b/c_f caused values of C_{l_δ} and C_{m_δ} to remain constant or increase with Mach number up to $M \approx 0.90$ and then have a more abrupt decrease in the transition from subsonic to supersonic speeds.

Since shifting the hinge line rearward had little effect on C_{l_δ} and C_{m_δ} as measured for small control deflections, it would appear that as a first-order approximation these parameters are dependent on total-control area and area moment, respectively. This, however, would not account for the large losses in ΔC_L and ΔC_m at the higher control deflections due to shifting the hinge line rearward. Therefore, an attempt was made to correlate these lift and pitching-moment losses with the rearward movement in control hinge line. The correlation of figure 14 is presented as a particular result of the present investigation and is not intended for general usage. Data of figure 10(b) were used and the symbols are not test data points but are a means of identification.

In figure 14, ΔC_L for a given flap deflection is plotted against a nondimensional area ratio factor based on the control area rearward of the hinge line. The line drawn from the origin to the values of ΔC_L for the unbalanced flap $\left(c_b/c_f = 0.07,\ \frac{S_f}{S} = 0.092\right)$ indicates values of ΔC_L that are proportional to the flap area rearward of the hinge line. At the higher flap deflections, the reduction in control lift

effectiveness due to shifting the hinge line rearward is approximately proportional to the reduction in area rearward of the hinge line. In the low-deflection range ($\pm 10^\circ$ at $M = 0.6$ and $\pm 5^\circ$ at $M = 0.95$ and 1.10) flap lift effectiveness tends to be independent of hinge location and ΔC_L shows little variation with S_f/S. These results, at low flap deflections, are in qualitative agreement with results obtained at $M = 1.61$ in reference 1 and with two-dimensional results obtained at low speed on a 9-percent-thick wing in reference 2, where, for a given chord flap c_f the flap effectiveness parameter increased with an increase in c_b/c_f.

Figure 14 also presents ΔC_m for a given flap deflection plotted against a nondimensional area-moment ratio factor based on the area moment of the control area rearward of the hinge line. Essentially the same correlation is obtained for the pitching-moment data with the reduction in ΔC_m at the higher flap deflections being proportional to the reduction in area moment of the control area rearward of the hinge line. In the low-deflection range, flap pitch effectiveness tends to be independent of hinge location.

CONCLUSIONS

The results of the investigation of a 4-percent-thick 60° delta wing equipped with a trailing-edge flap-type control surface having various hinge-line locations indicated the following conclusions:

1. Shifting the flap hinge line rearward (increasing the ratio of balance chord to flap chord c_b/c_f) had a balancing effect on the flap hinge-moment coefficient C_h for all test conditions but caused the variation of C_h with flap deflection to become very nonlinear. Increasing Mach number tended to decrease the nonlinearities.

2. For $c_b/c_f \geq 0.50$, the control was overbalanced over part of the test range and abrupt breaks and reversals in slope of hinge-moment coefficient with flap deflection occurred.

3. Increasing angle of attack from -6° to 15° had little effect on the general variation of hinge-moment, lift, and pitching-moment coefficients with control deflection.

4. Increasing c_b/c_f resulted in a large decrease in lift and pitch effectiveness for all but relatively low control deflections.

5. At the higher control deflections the lift and pitch effectiveness tends to be proportional to the area and area moment of the flap area rearward of the hinge line. This conclusion is made only as a first-order approximation for the particular controls of the present investigation.

Langley Aeronautical Laboratory,
National Advisory Committee for Aeronautics,
Langley Field, Va., January 21, 1954.

REFERENCES

1. Lord, Douglas R., and Czarnecki, K. R.: Recent Information on Flap and Tip Controls. NACA RM L53I17a, 1953.

2. Sears, Richard I.: Wind-Tunnel Data on the Aerodynamic Characteristics of Airplane Control Surfaces. NACA ACR 3L08, 1943.

[redacted]

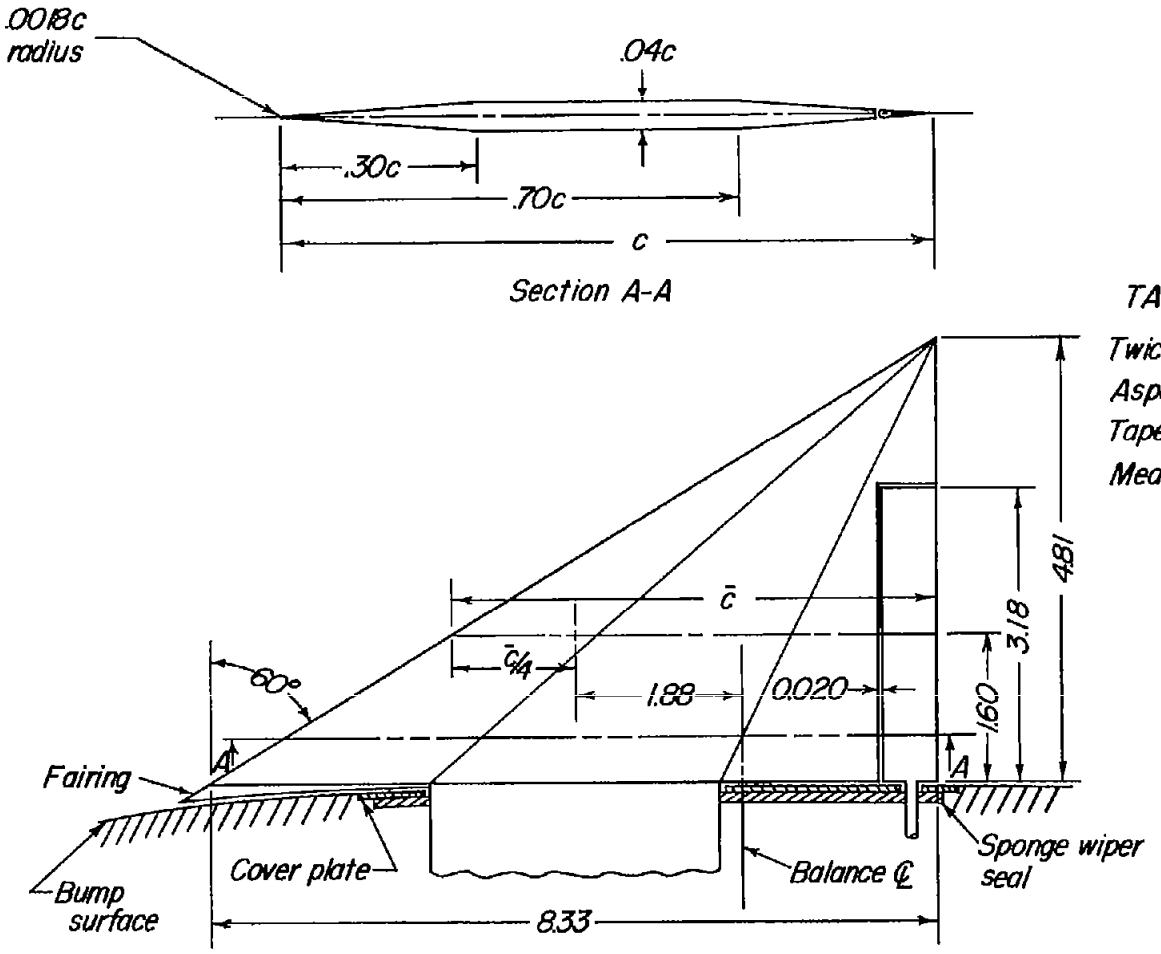

(a) Model details.

Figure 1.- Drawing of model and flaps. All dimensions are in inches.

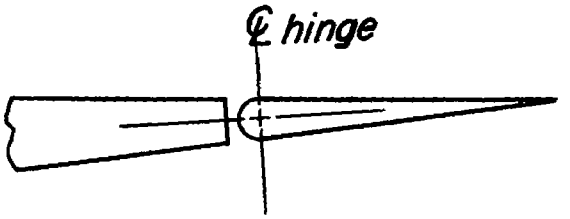

C_b/C_f = 0.07 ; $2M_1$ = .000611 ft^3

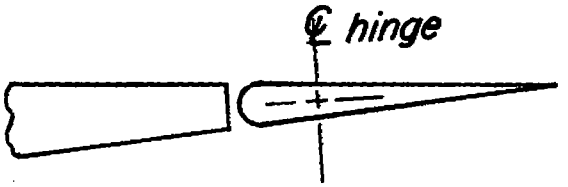

C_b/C_f = 0.32 ; $2M_1$ = .000413 ft^3

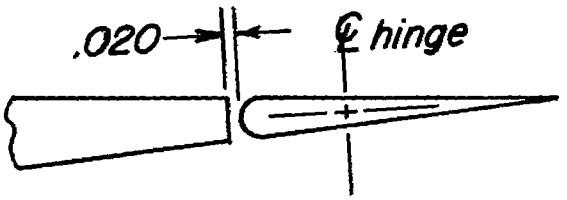

C_b/C_f = 0.50 ; $2M_1$ = .000319 ft^3

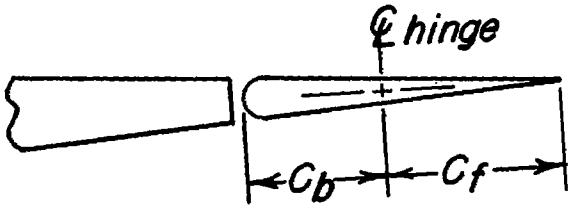

C_b/C_f = 0.79 ; $2M_1$ = .000225 ft^3

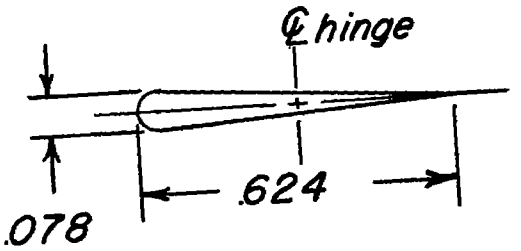

C_b/C_f = 1.03 ; $2M_1$ = .000174 ft^3

(b) Flap details.

Figure 1.- Concluded.

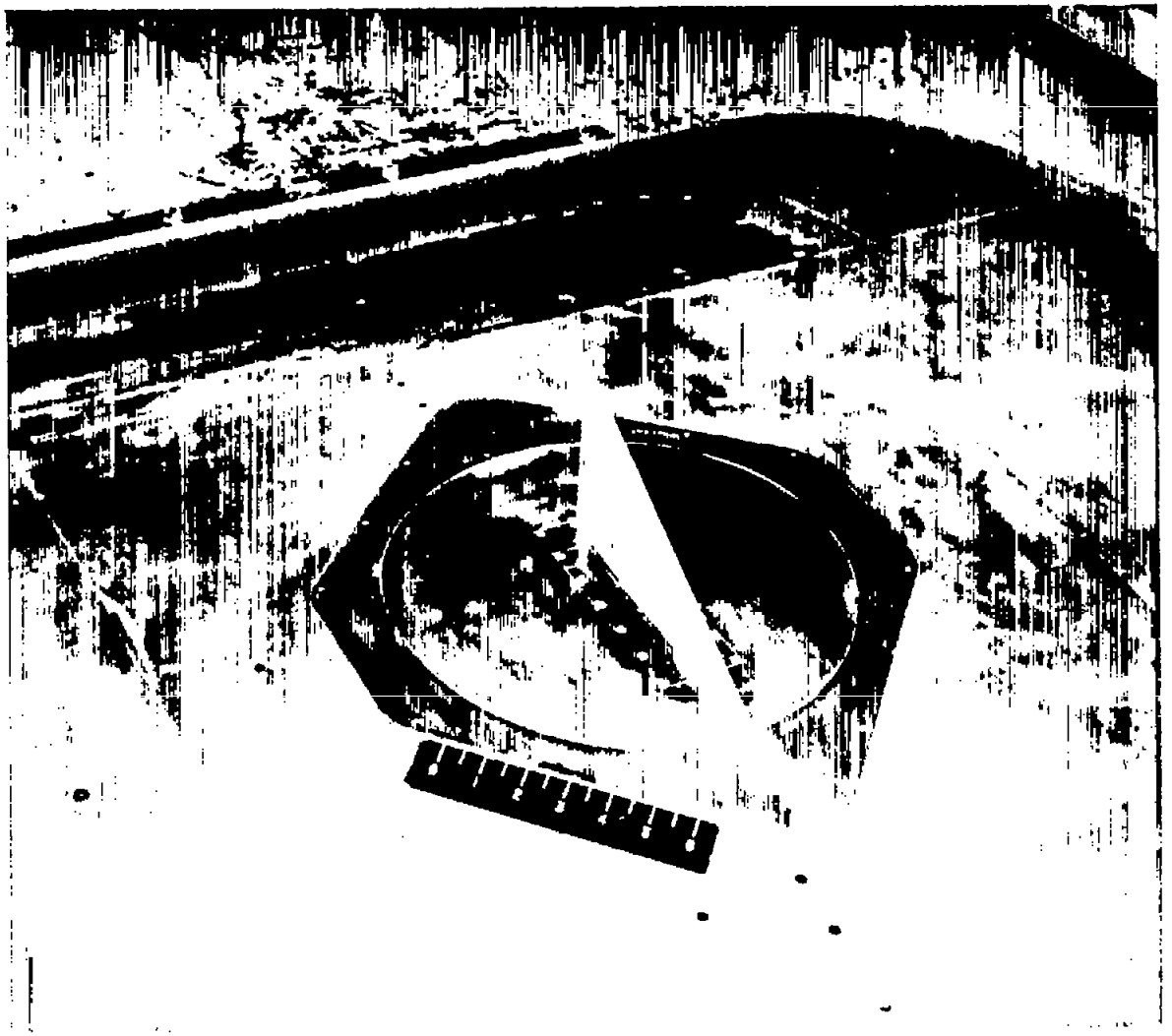

L-74129

Figure 2.- Photograph of the model as mounted on the bump in the Langley high-speed 7- by 10-foot tunnel.

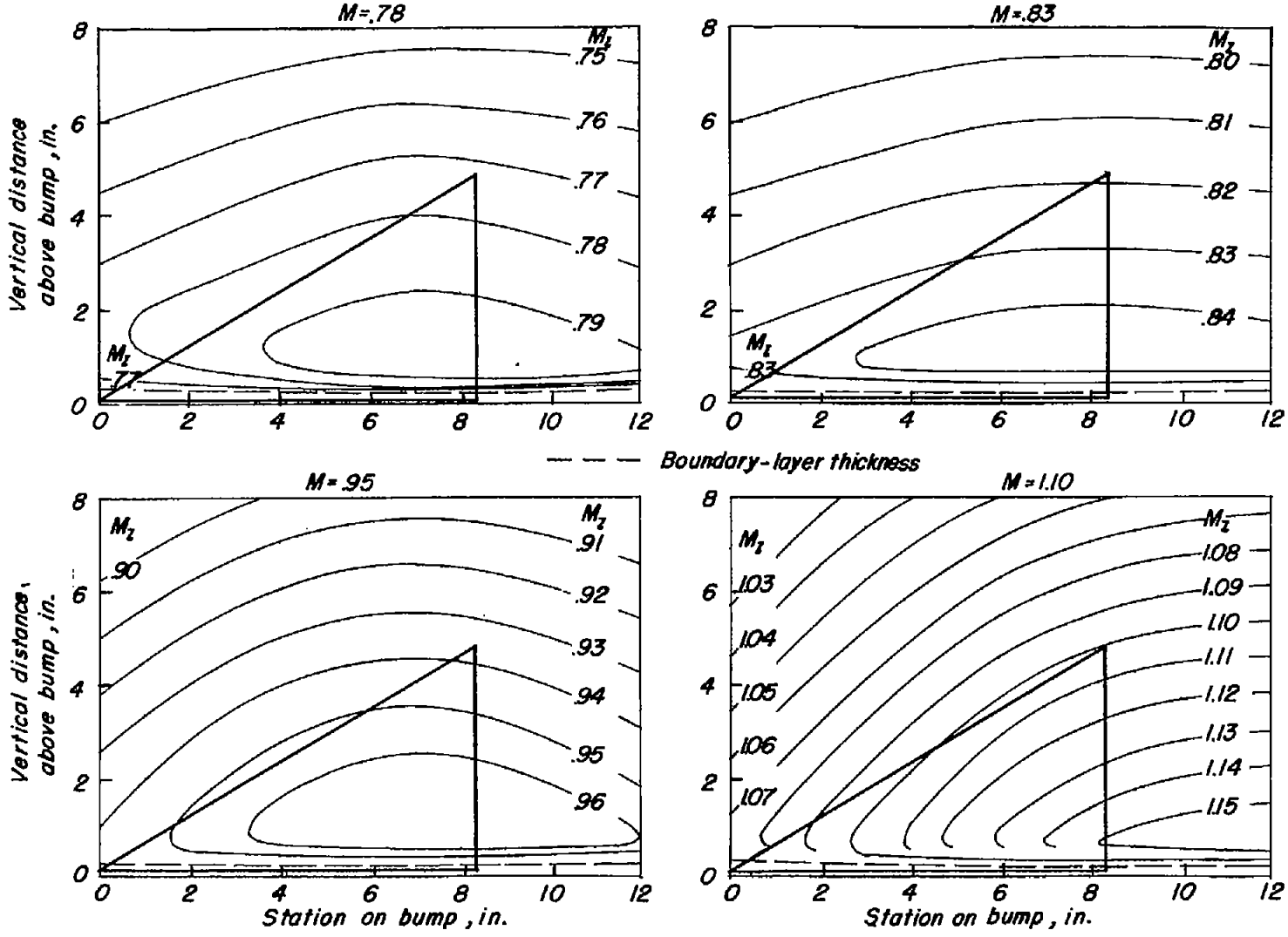

Figure 3.- Typical Mach number contours over transonic bump in region of model location.

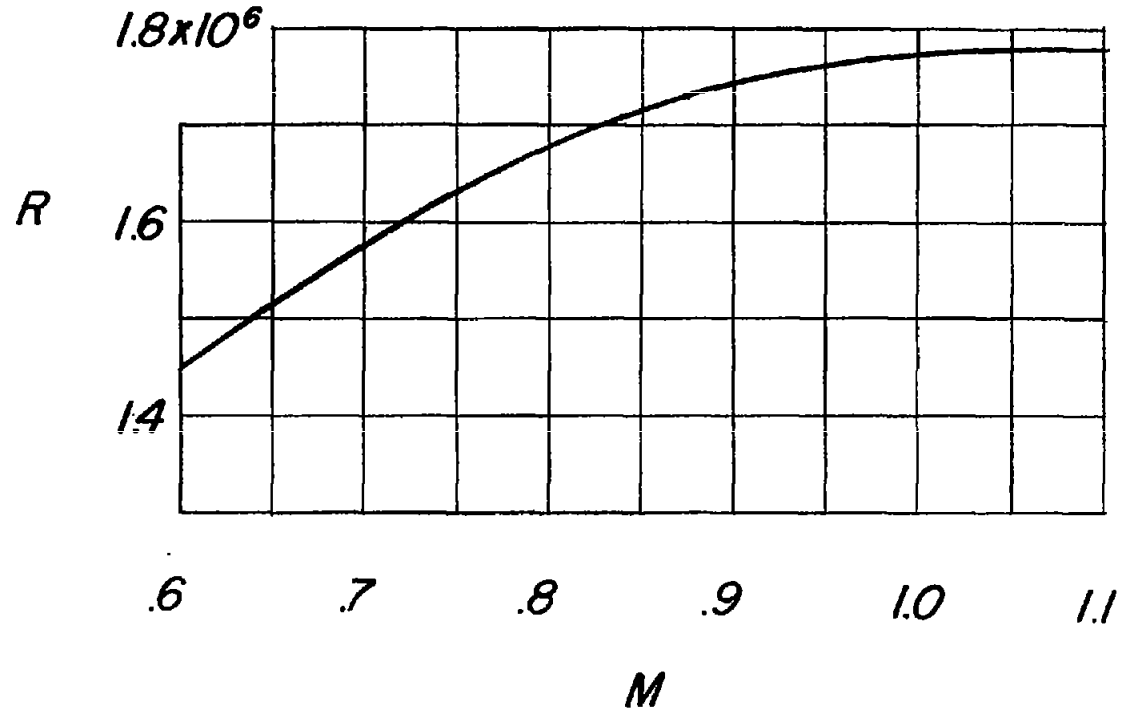

Figure 4.- Typical variation of test Reynolds number with Mach number.

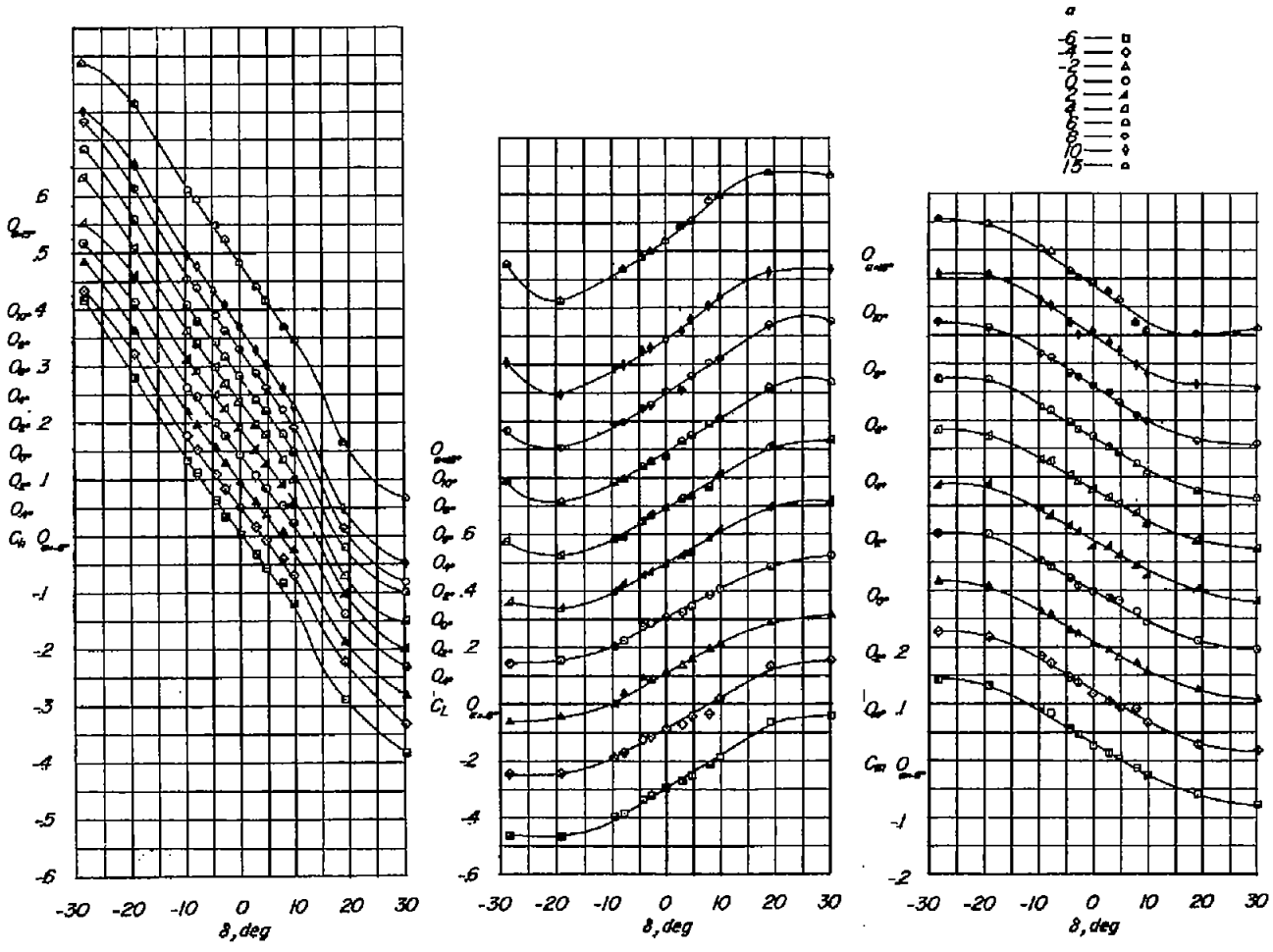

(a) M = 0.60.

Figure 5.- Variation of C_h, C_L, and C_m with δ for various angles of attack. $c_b/c_f = 0.07$.

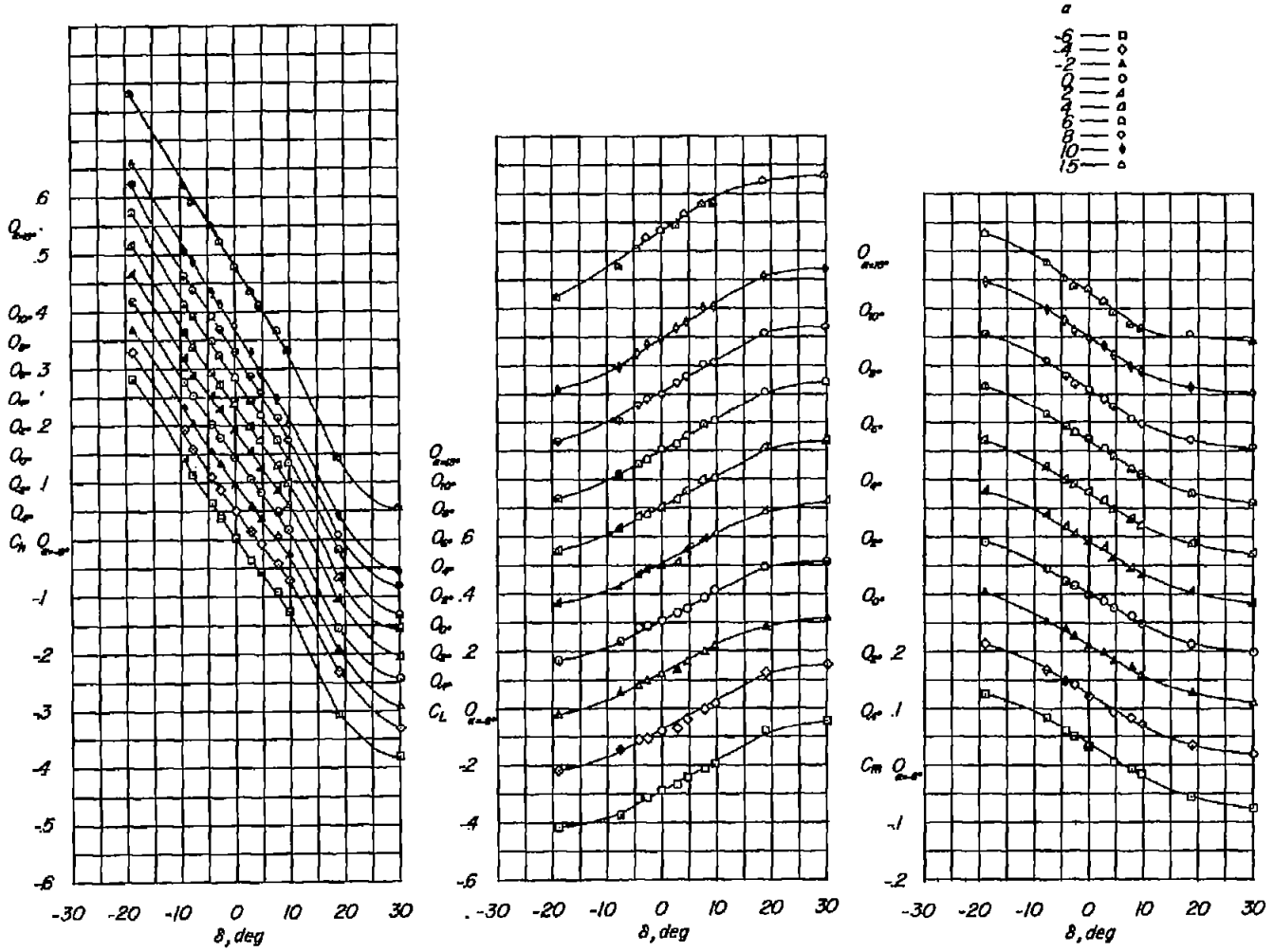

(b) M = 0.70; c_b/c_f = 0.07.

Figure 5.- Continued.

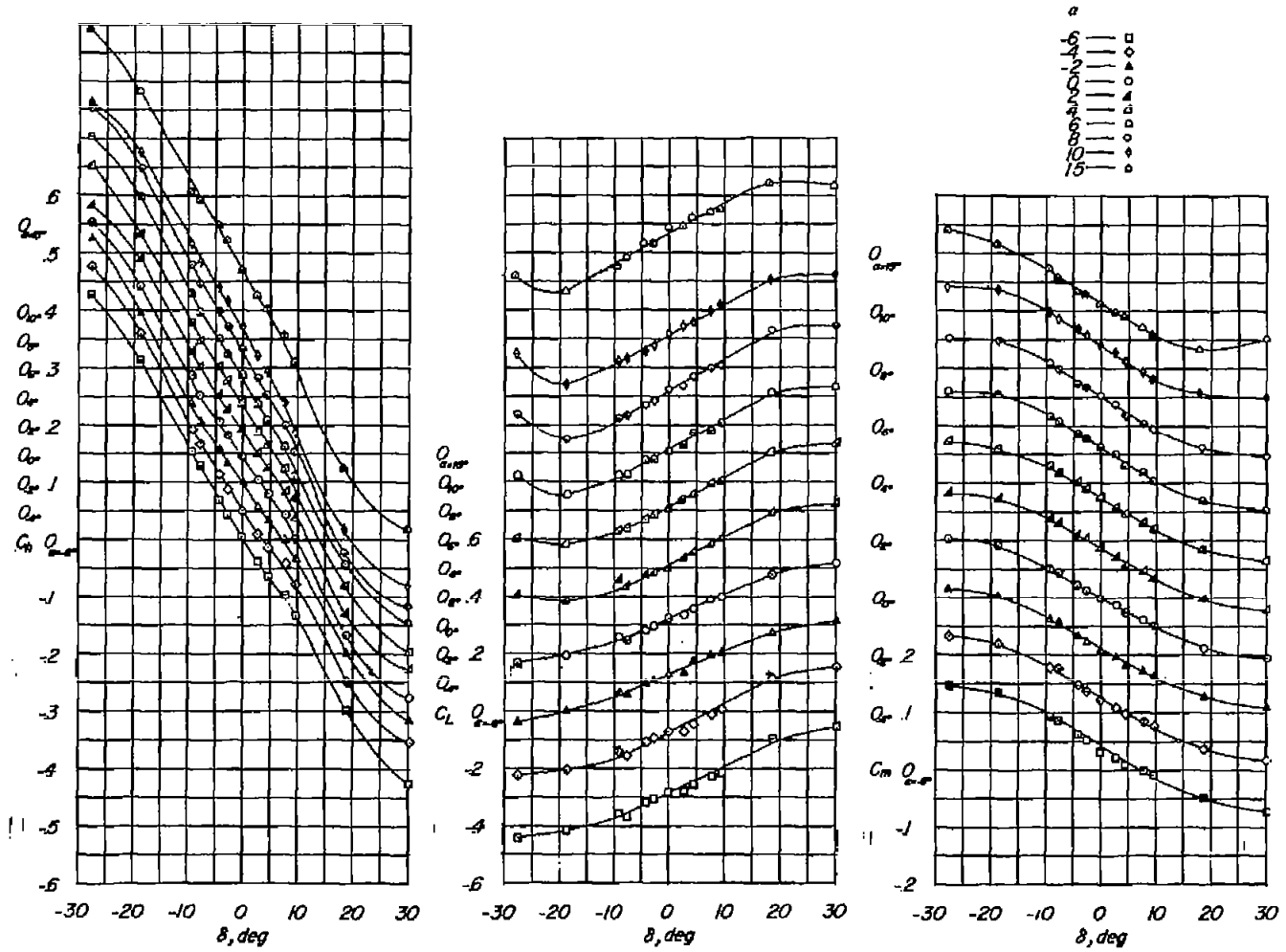

(c) M = 0.80; c_b/c_f = 0.07.

Figure 5.- Continued.

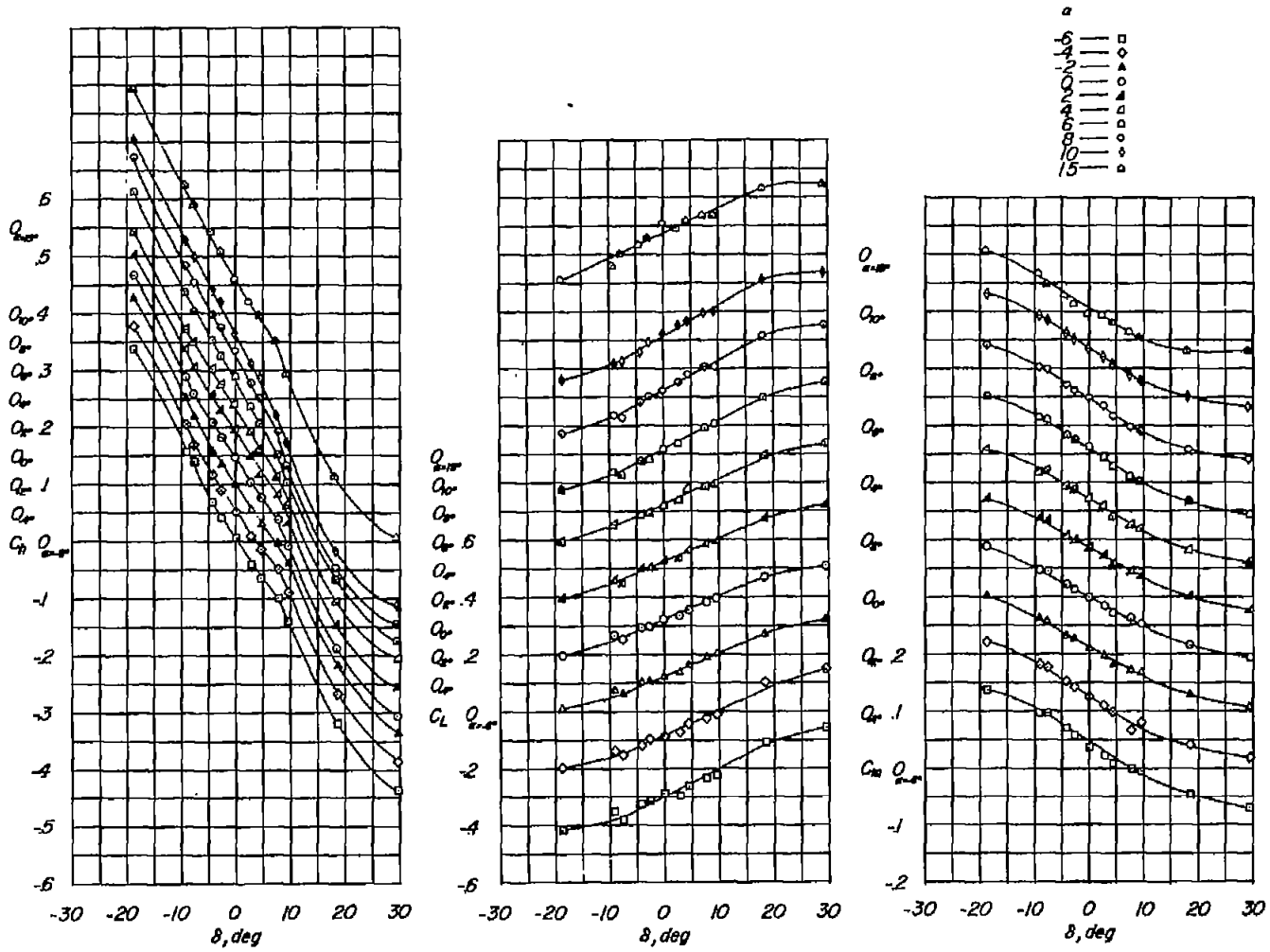

(d) M = 0.85; c_b/c_f = 0.07.

Figure 5.- Continued.

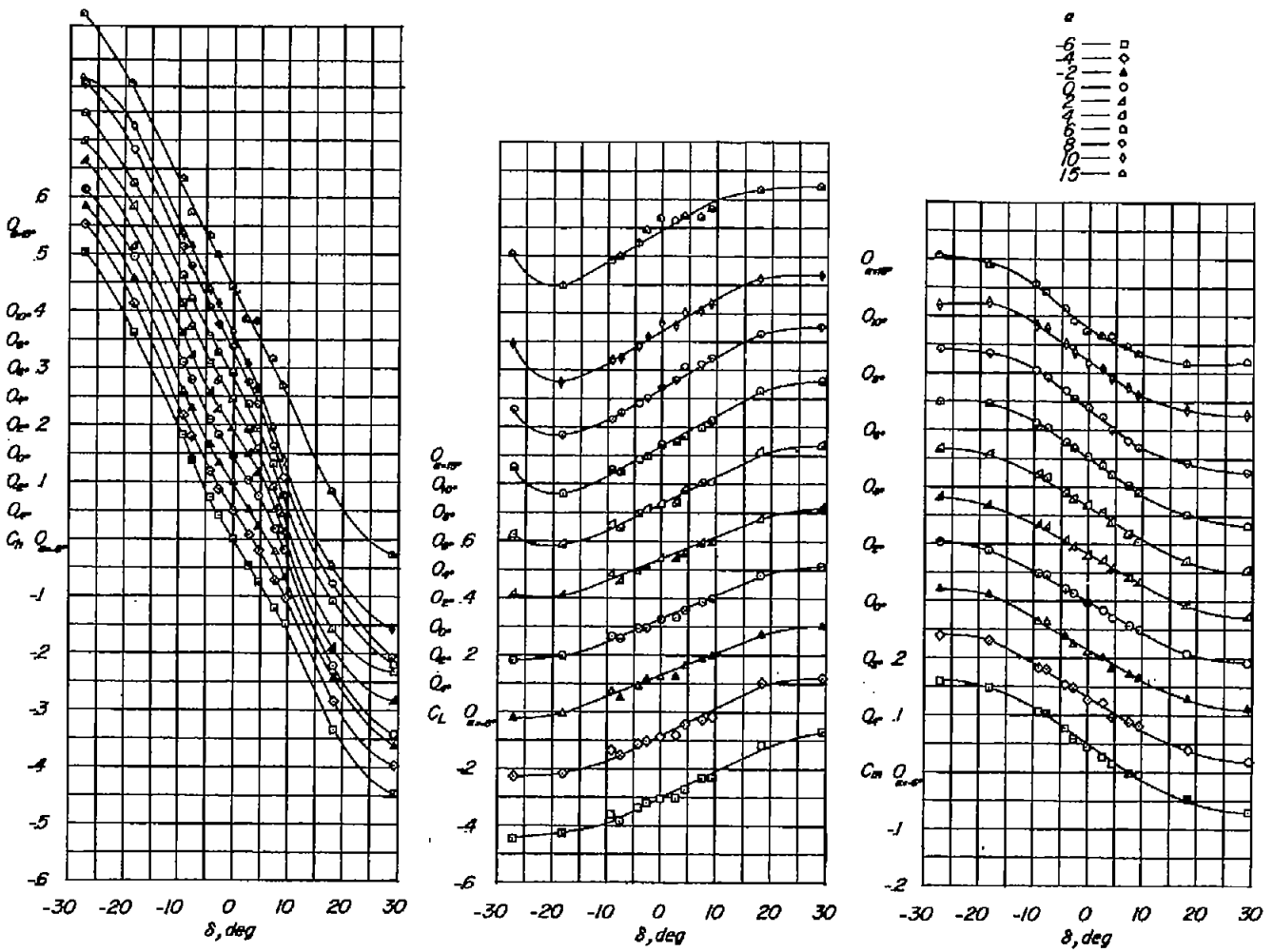

(e) $M = 0.90$; $c_b/c_f = 0.07$.

Figure 5.- Continued.

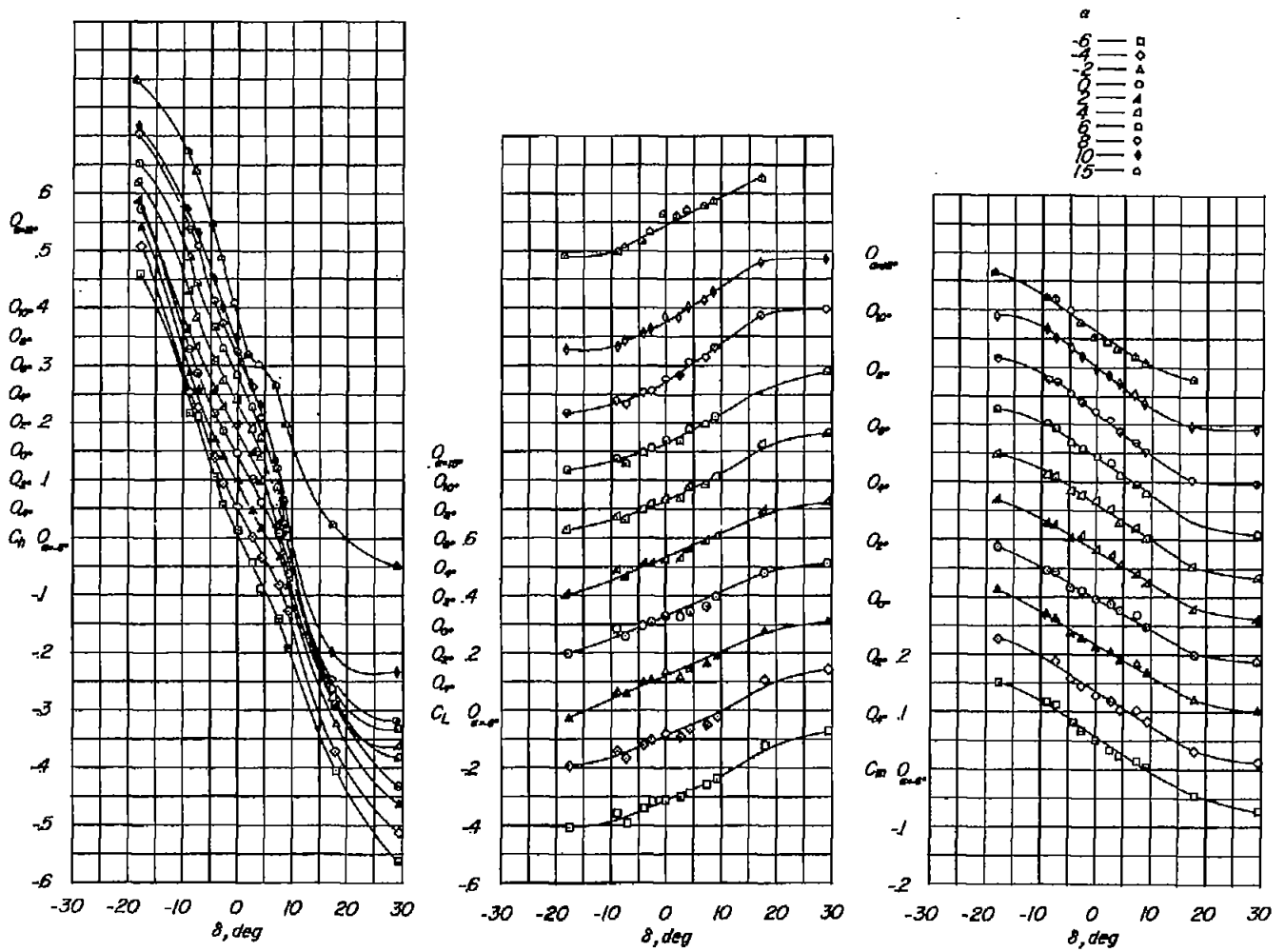

(f) M = 0.95; c_b/c_f = 0.07.

Figure 5.- Continued.

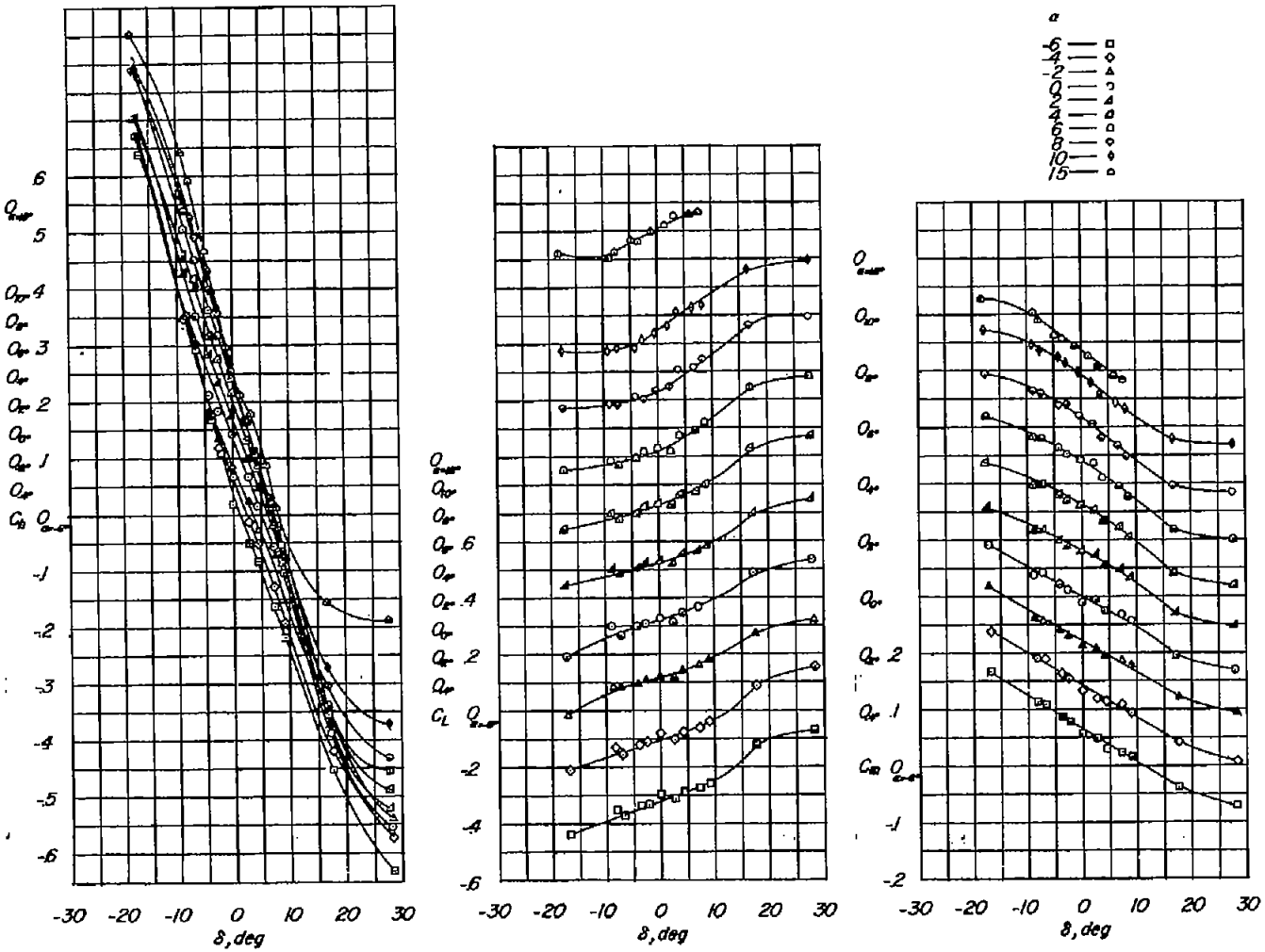

(g) M = 1.00; c_b/c_f = 0.07.

Figure 5.- Continued.

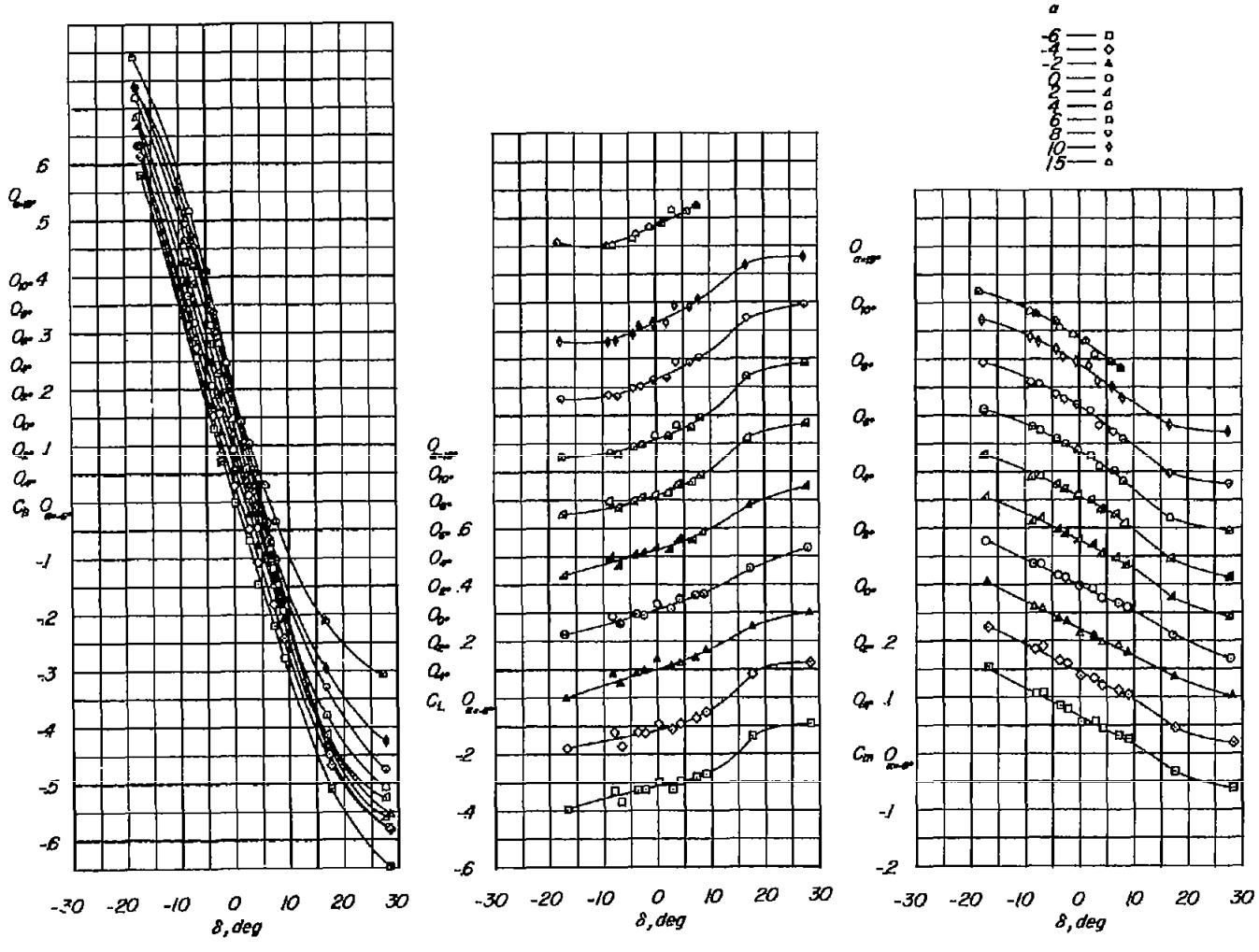

(h) M = 1.05; c_b/c_f = 0.07.

Figure 5.- Continued.

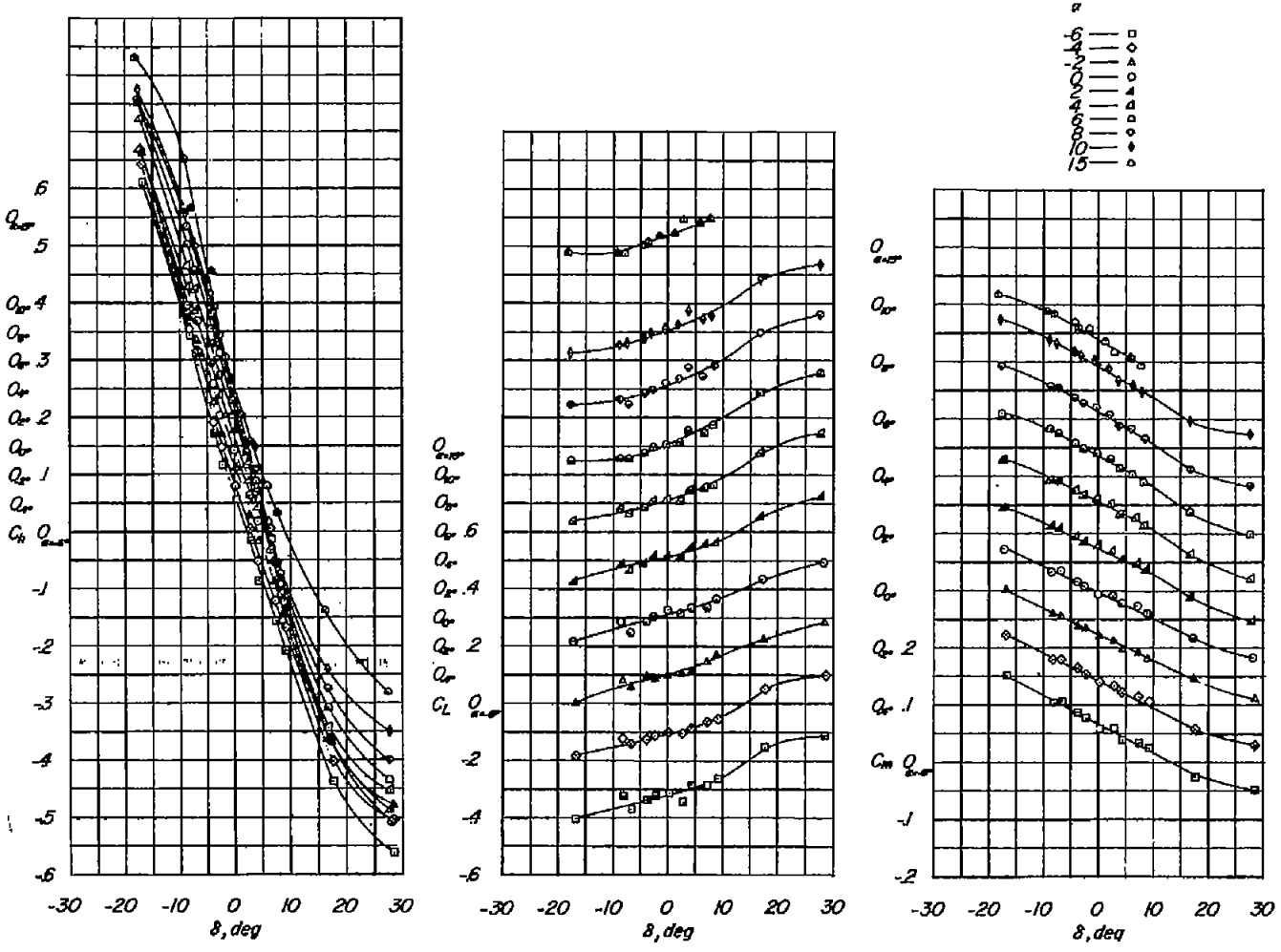

(i) M = 1.10; c_b/c_f = 0.07.

Figure 5.- Continued.

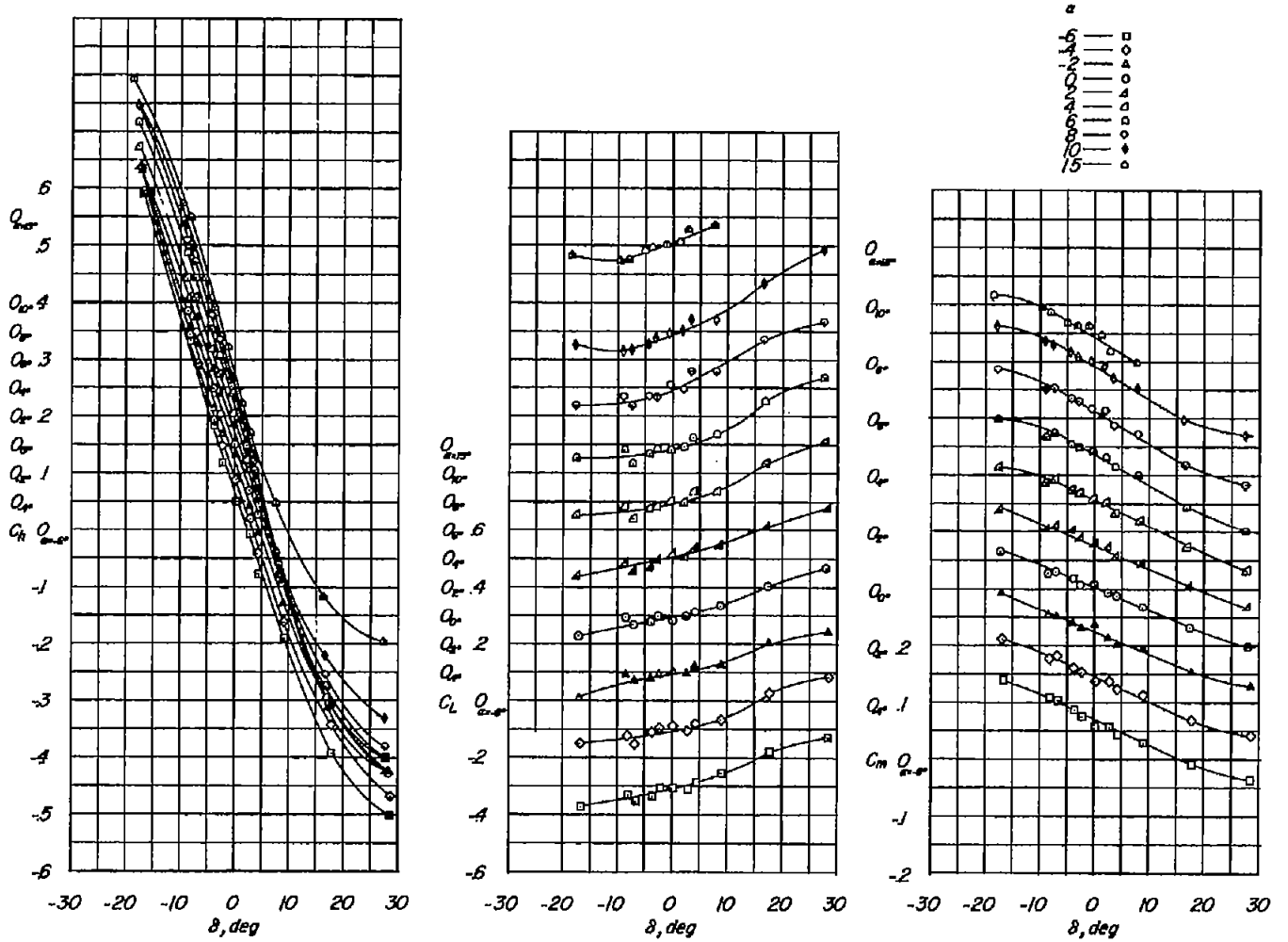

(j) M = 1.18; c_b/c_f = 0.07.

Figure 5.- Concluded.

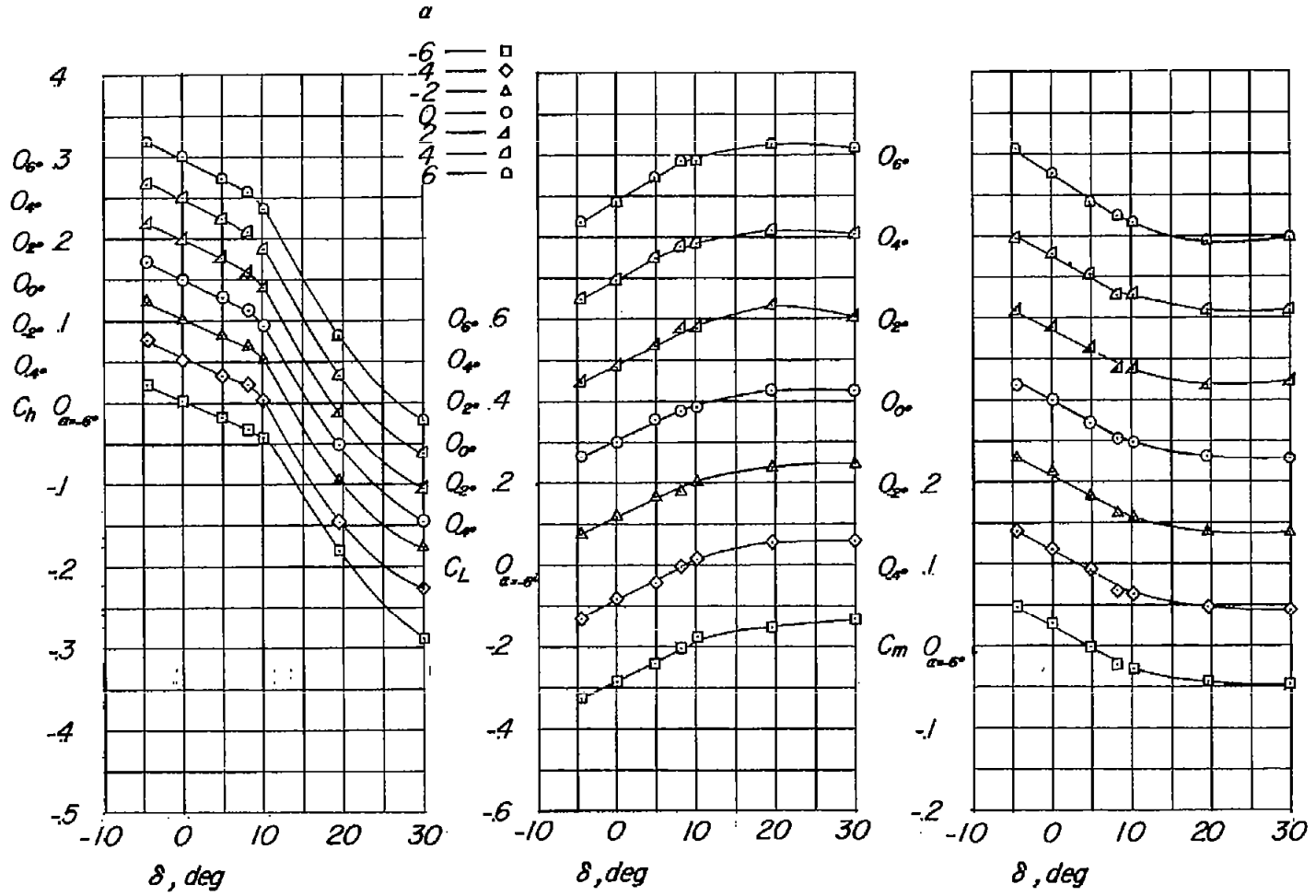

(a) M = 0.60.

Figure 6.- Variation of C_h, C_L, and C_m with δ for various angles of attack. $c_b/c_f = 0.32$.

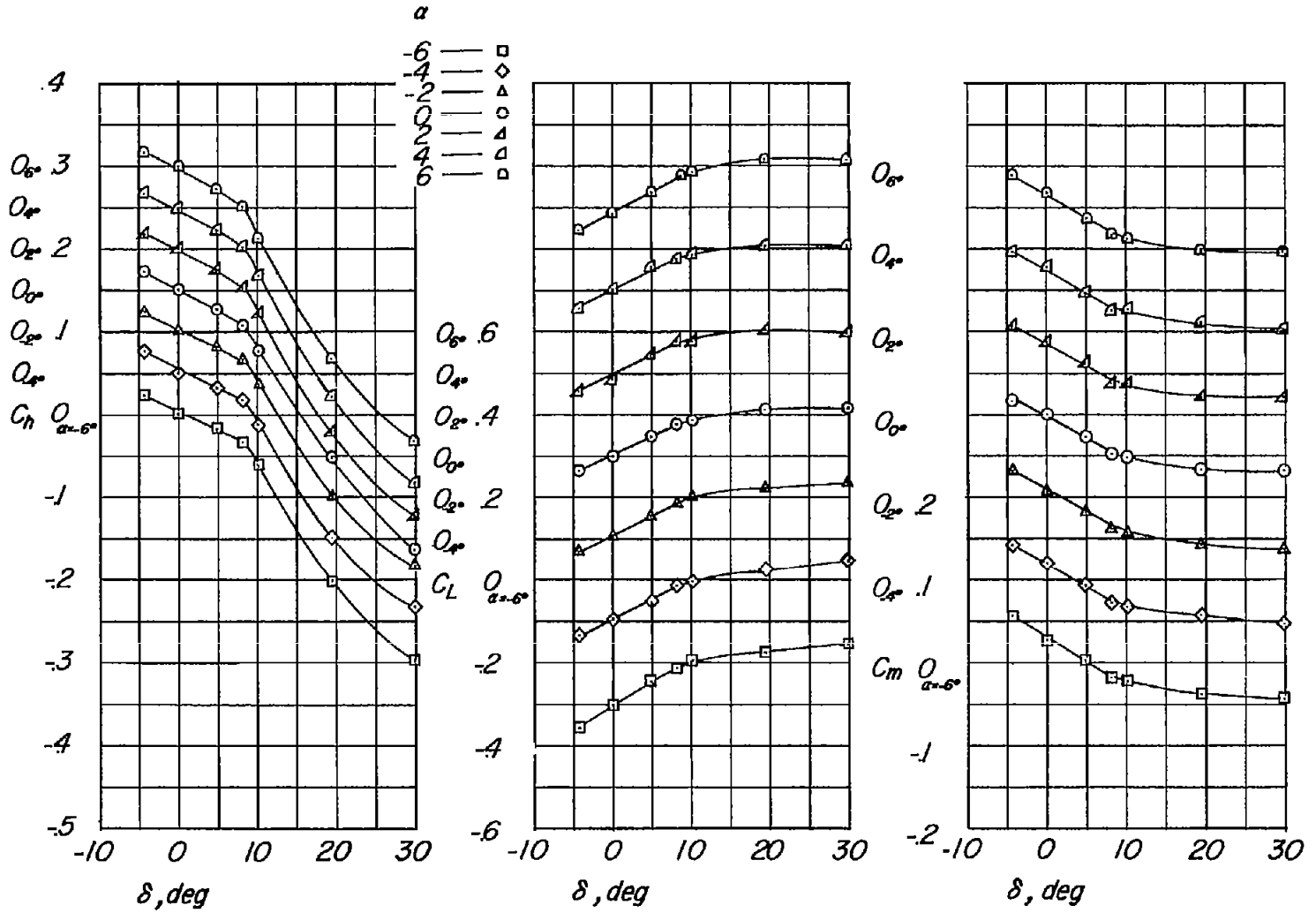

(b) M = 0.70; c_b/c_f = 0.32.

Figure 6.- Continued.

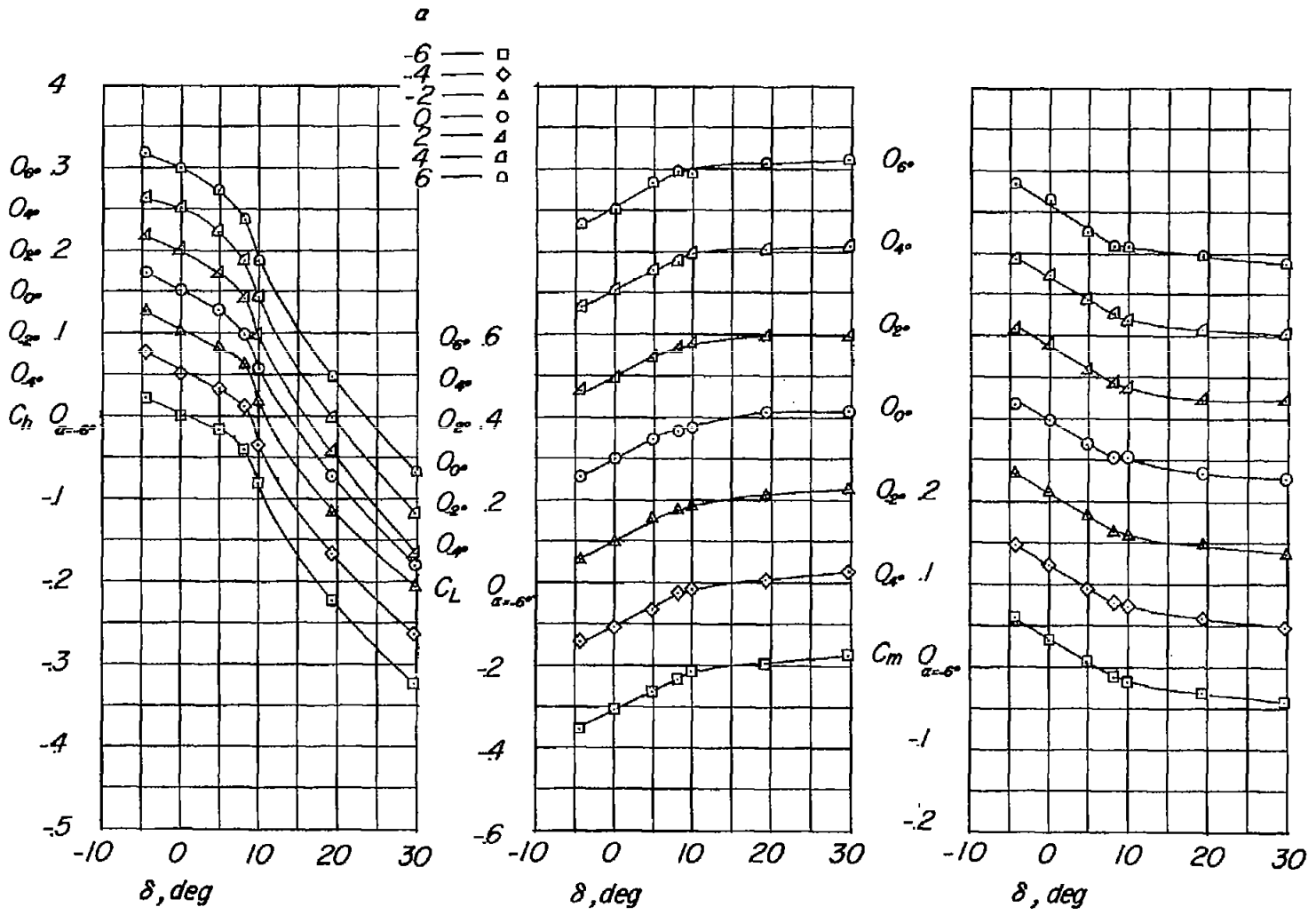

(c) M = 0.80; c_b/c_f = 0.32.

Figure 6.- Continued.

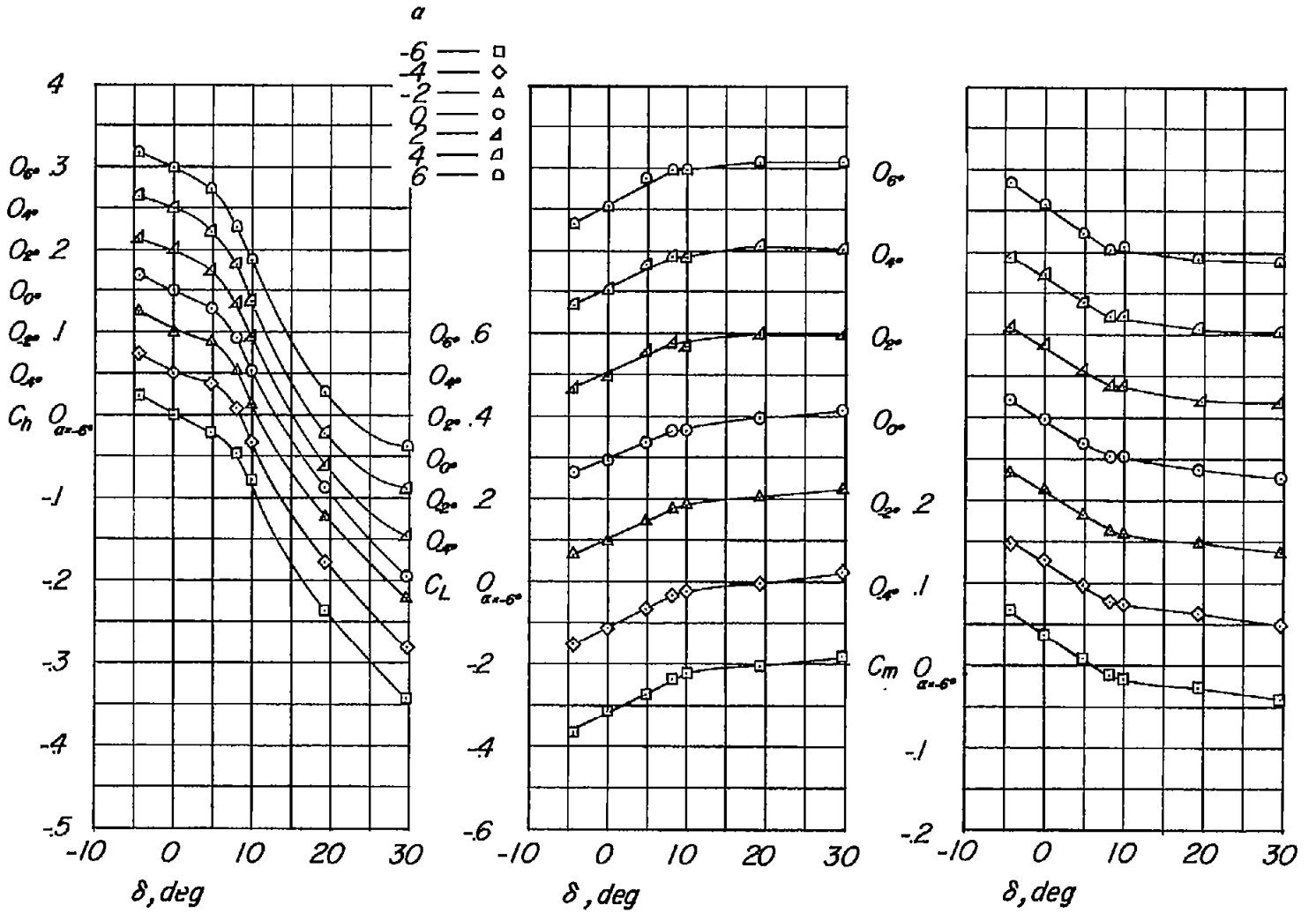

(d) M = 0.85; c_b/c_f = 0.32.

Figure 6.- Continued.

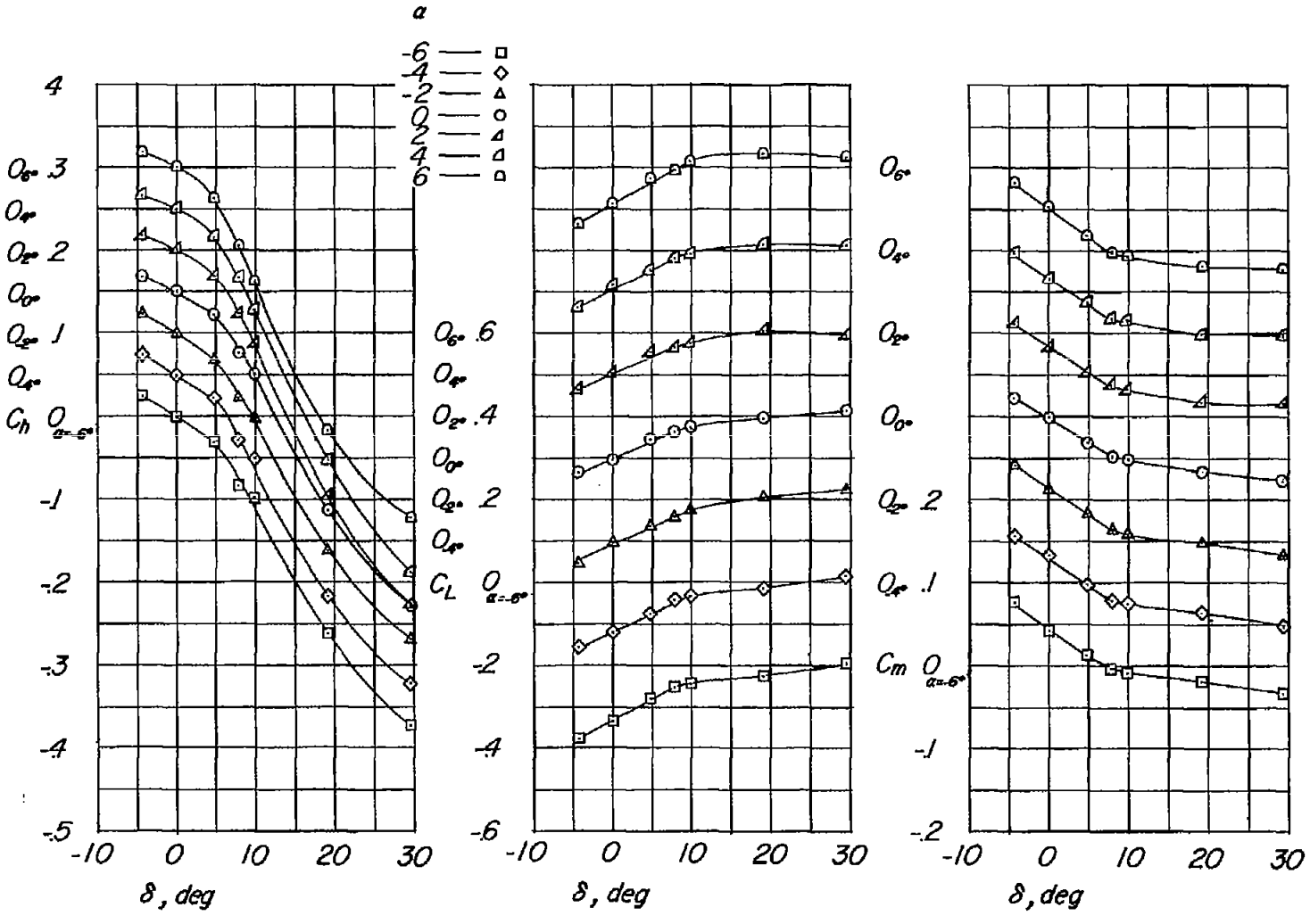

(e) M = 0.90; c_b/c_f = 0.32.

Figure 6.- Continued.

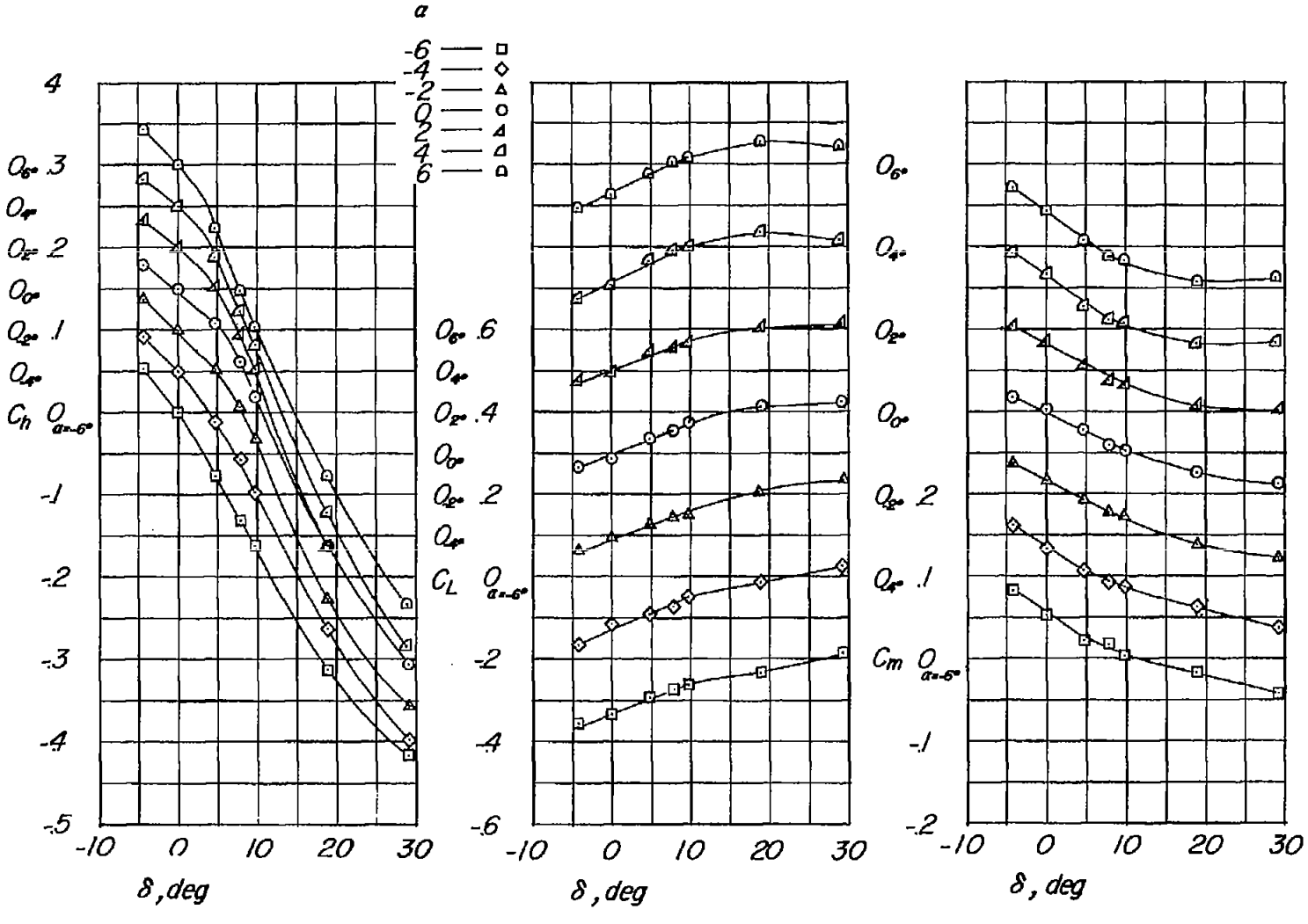

(f) M = 0.95; c_b/c_f = 0.32.

Figure 6.- Continued.

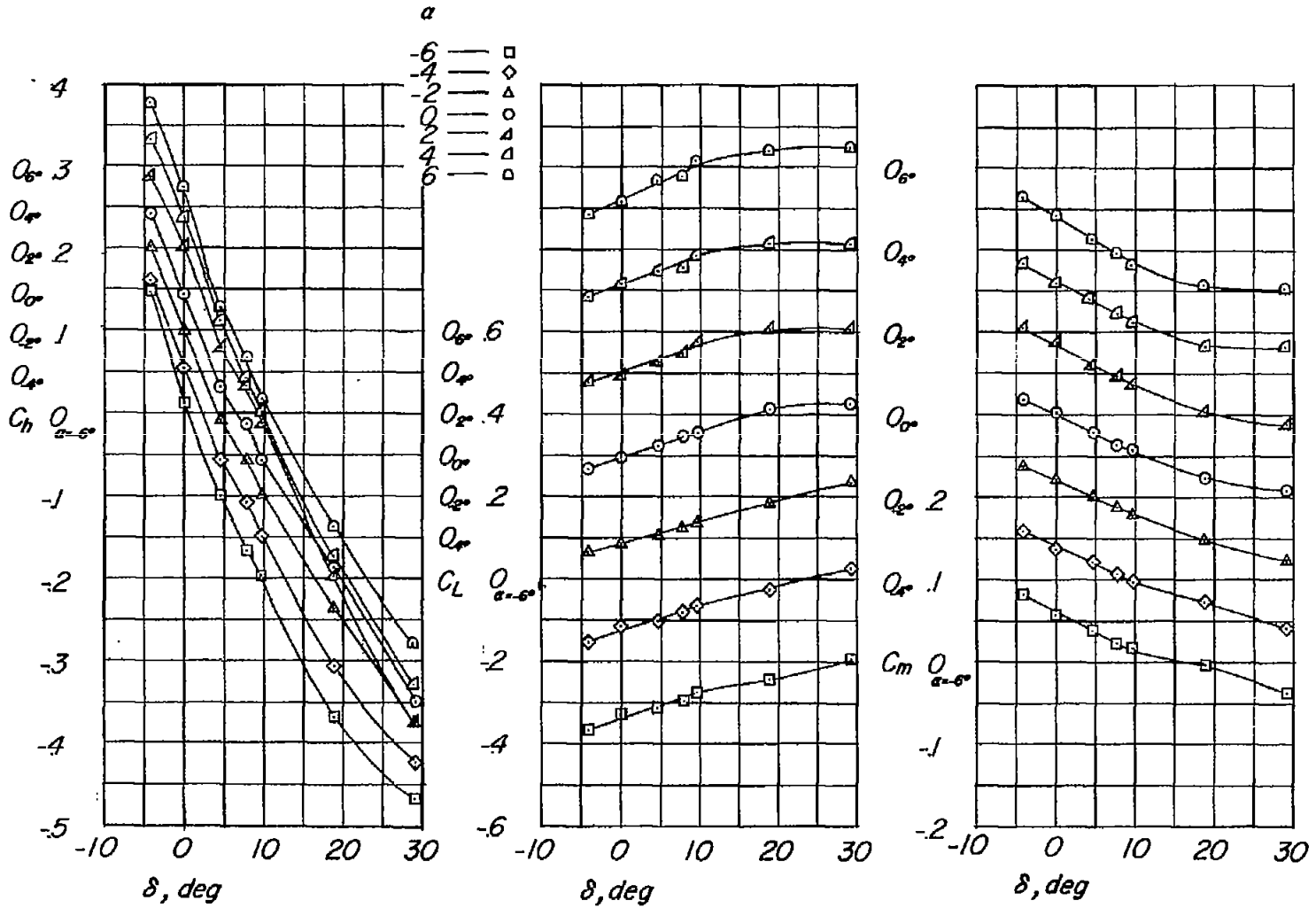

(g) M = 1.00; c_b/c_f = 0.32.

Figure 6.- Continued.

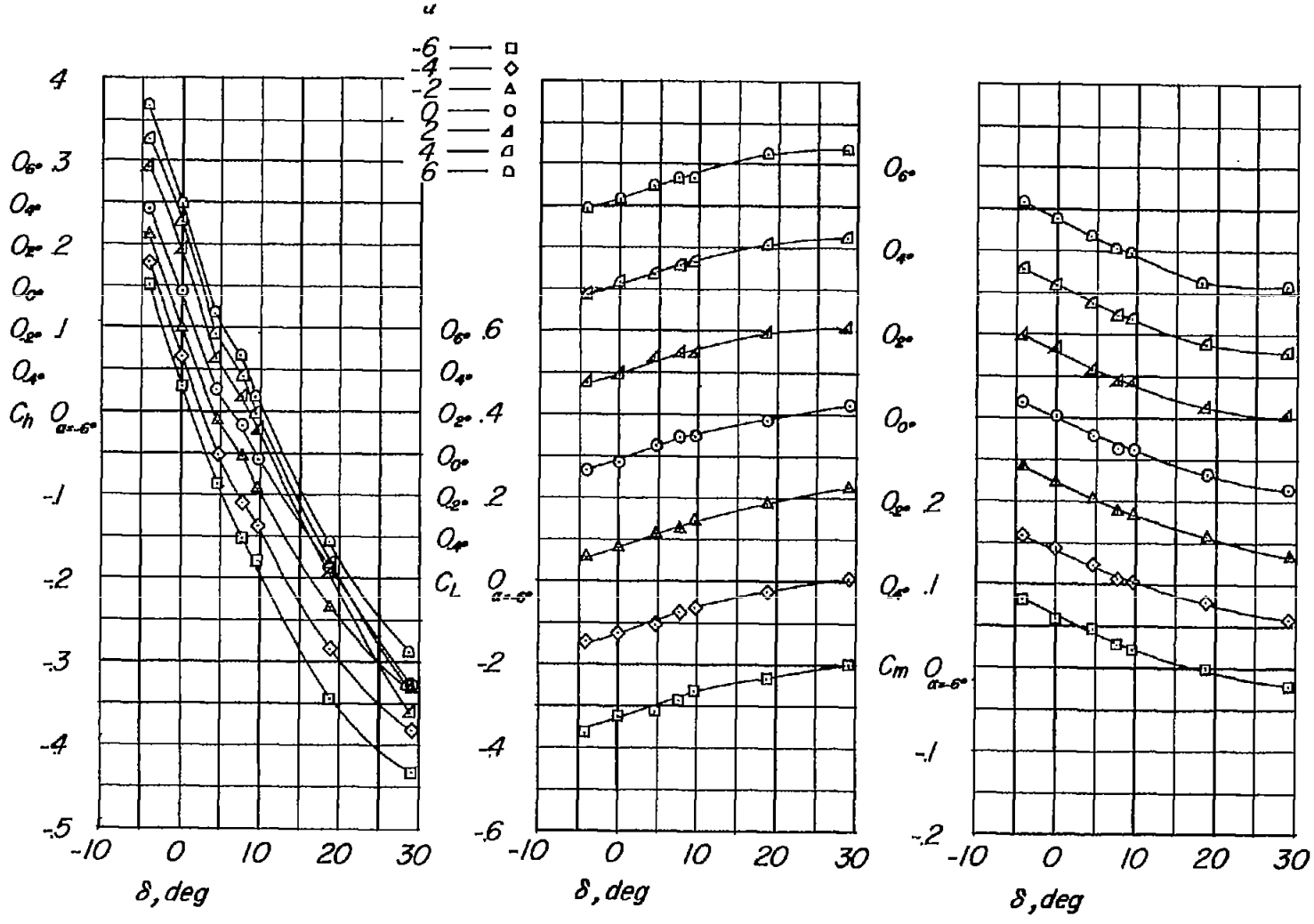

(h) M = 1.05; c_b/c_f = 0.32.

Figure 6.- Continued.

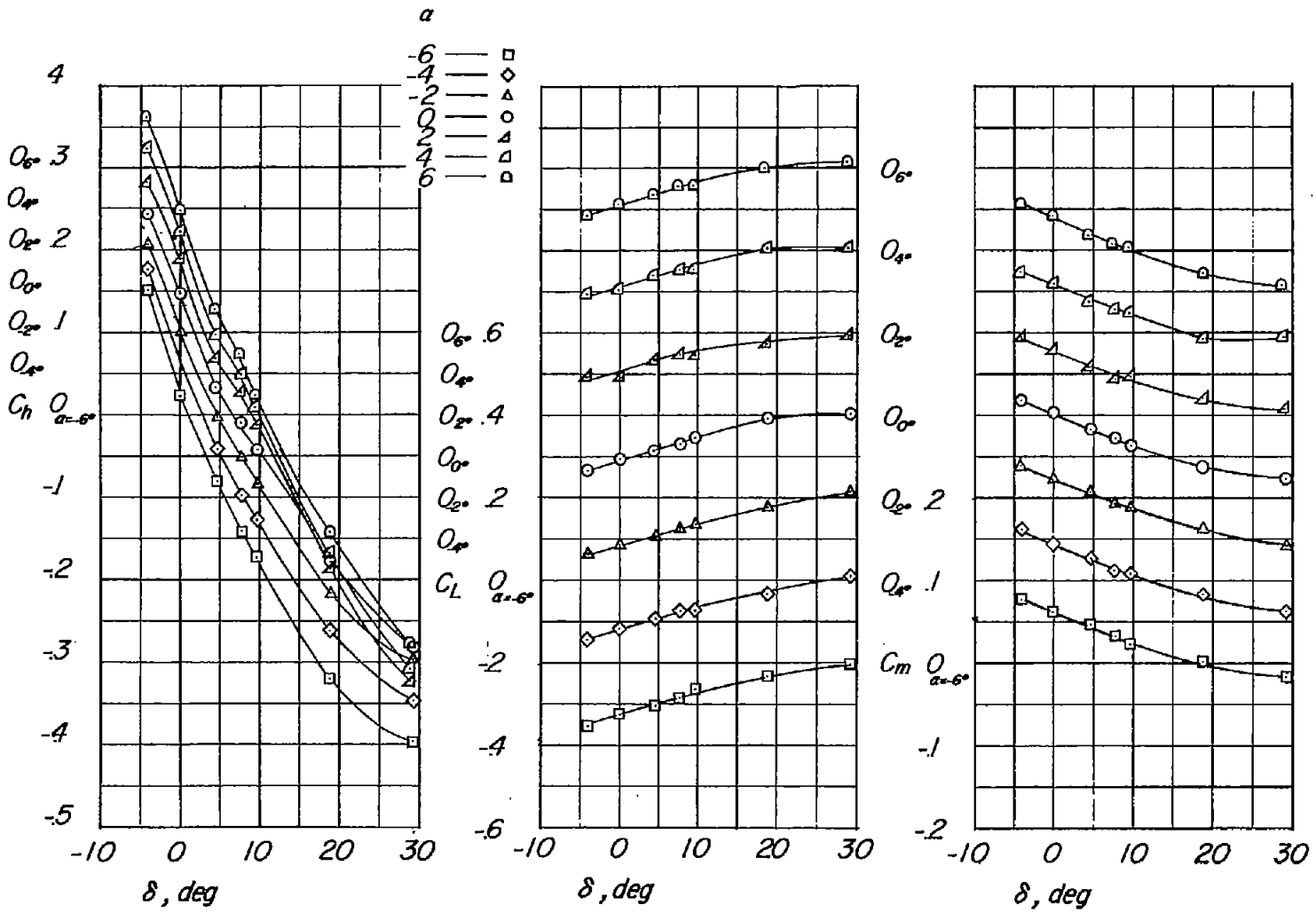

(i) M = 1.10; c_b/c_f = 0.32.

Figure 6.- Concluded.

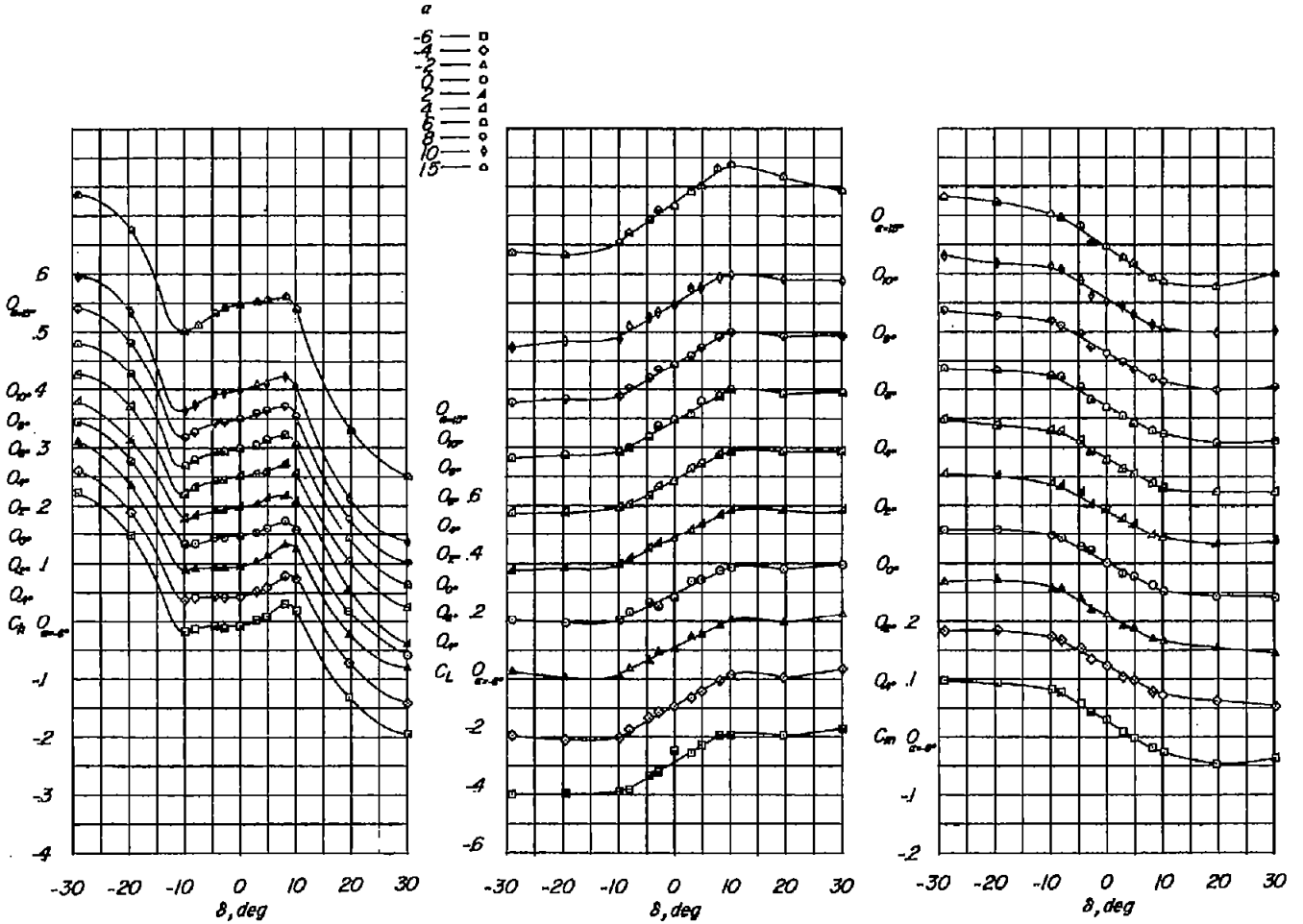

(a) M = 0.60.

Figure 7.- Variation of C_h, C_L, and C_m with δ for various angles of attack. $c_b/c_f = 0.50$.

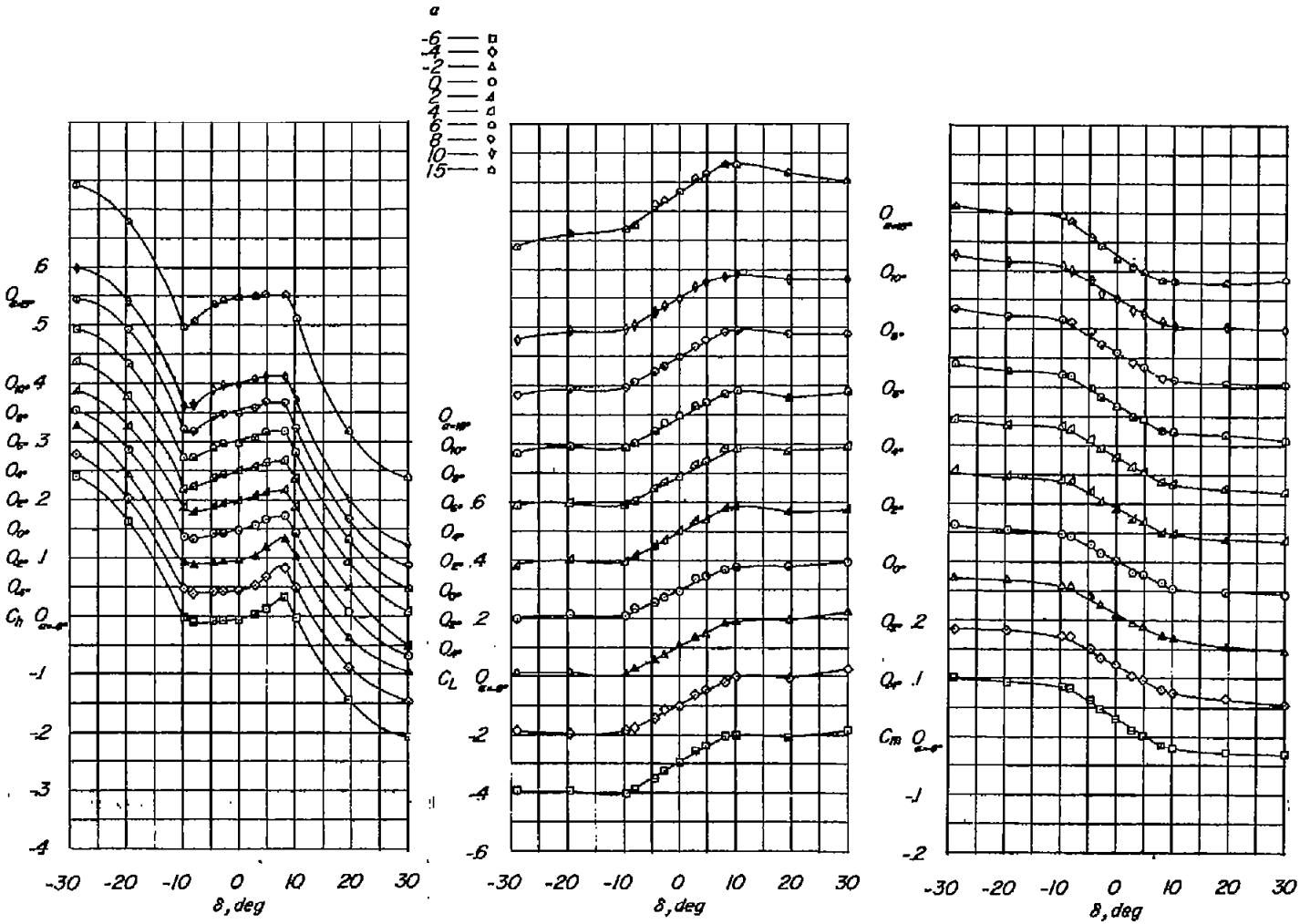

(b) M = 0.70; c_b/c_f = 0.50.

Figure 7.- Continued.

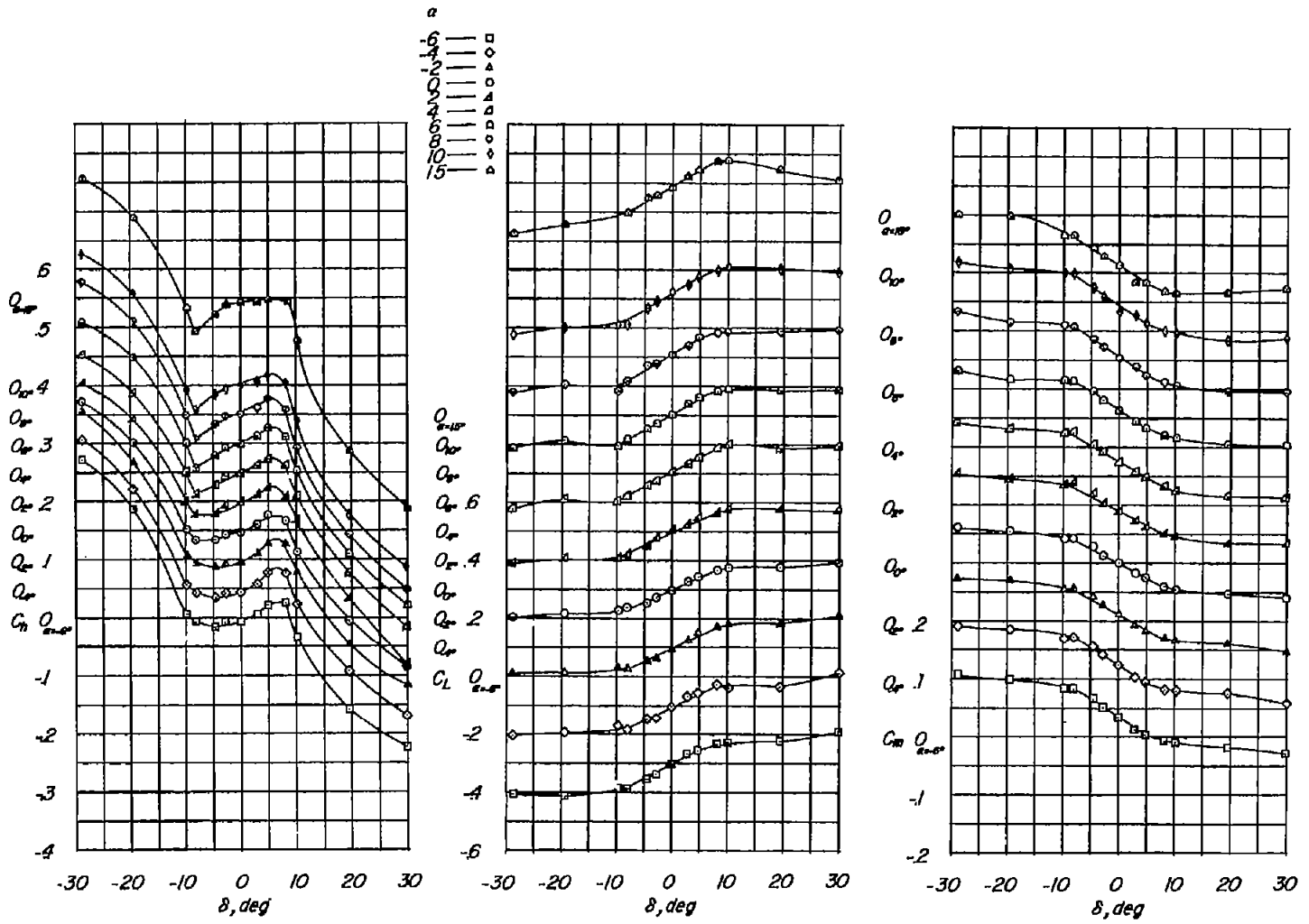

(c) M = 0.80; c_b/c_f = 0.50.

Figure 7.- Continued.

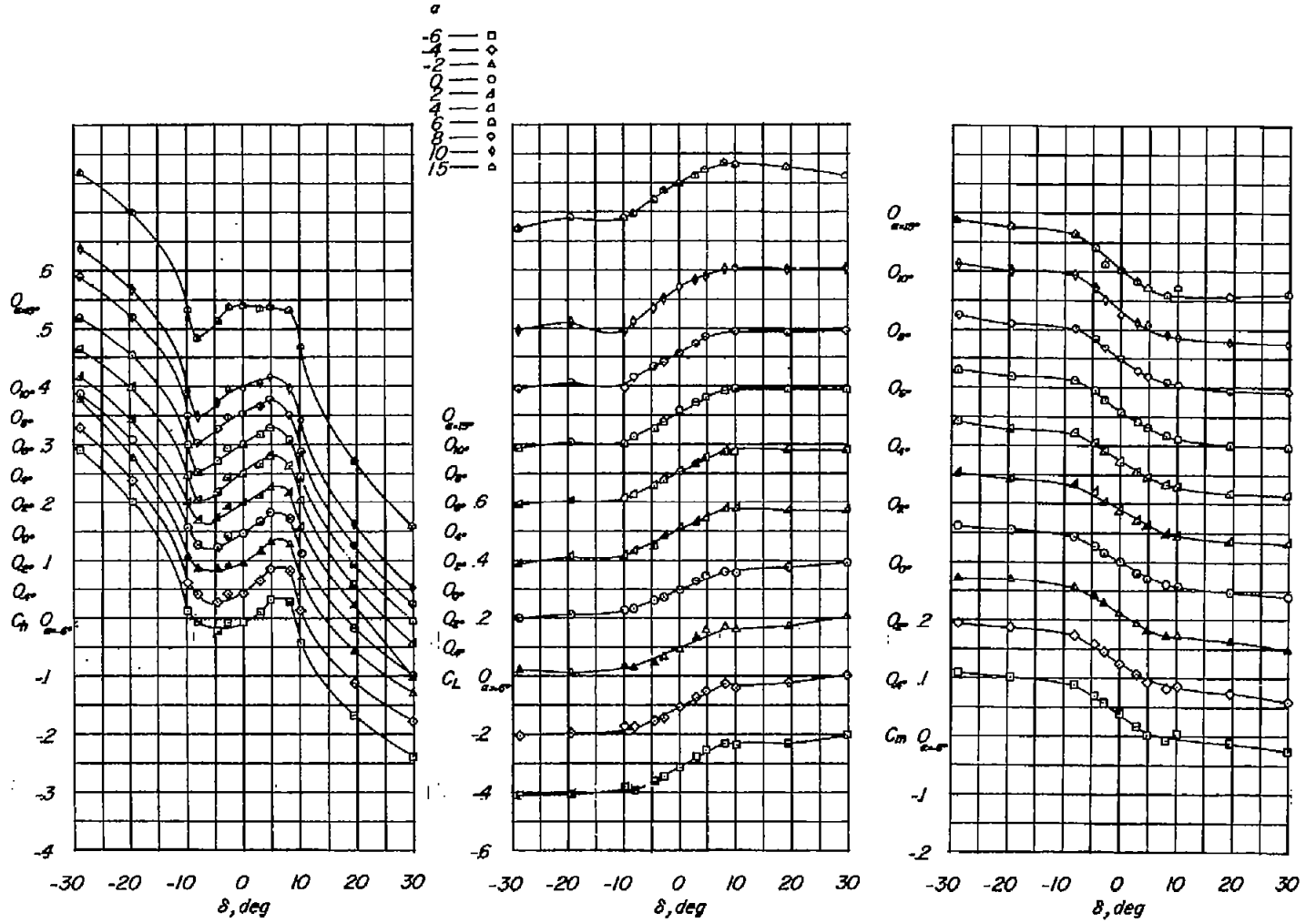

(d) M = 0.85; c_b/c_f = 0.50.

Figure 7.- Continued.

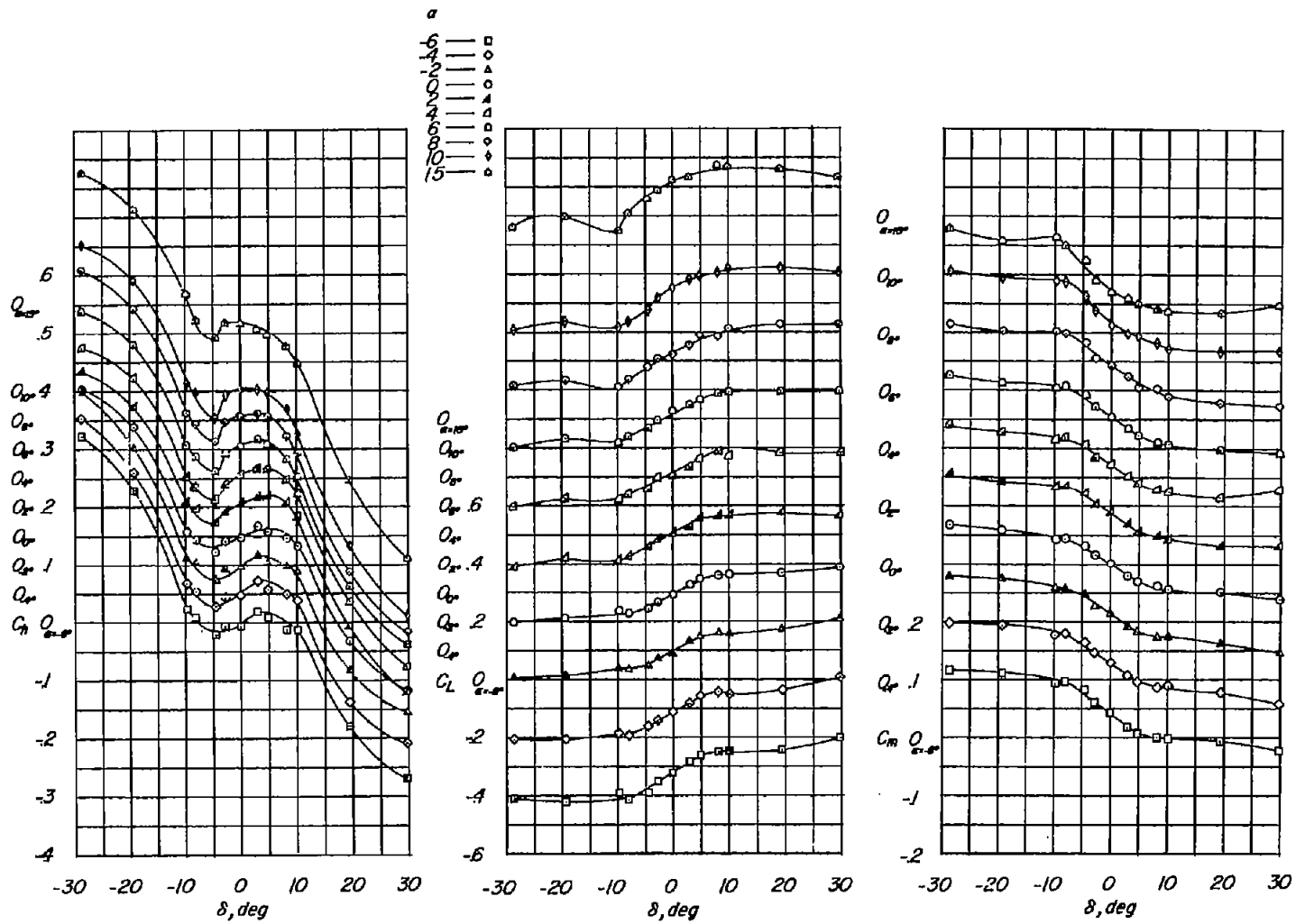

(e) M = 0.90; c_b/c_f = 0.50.

Figure 7.- Continued.

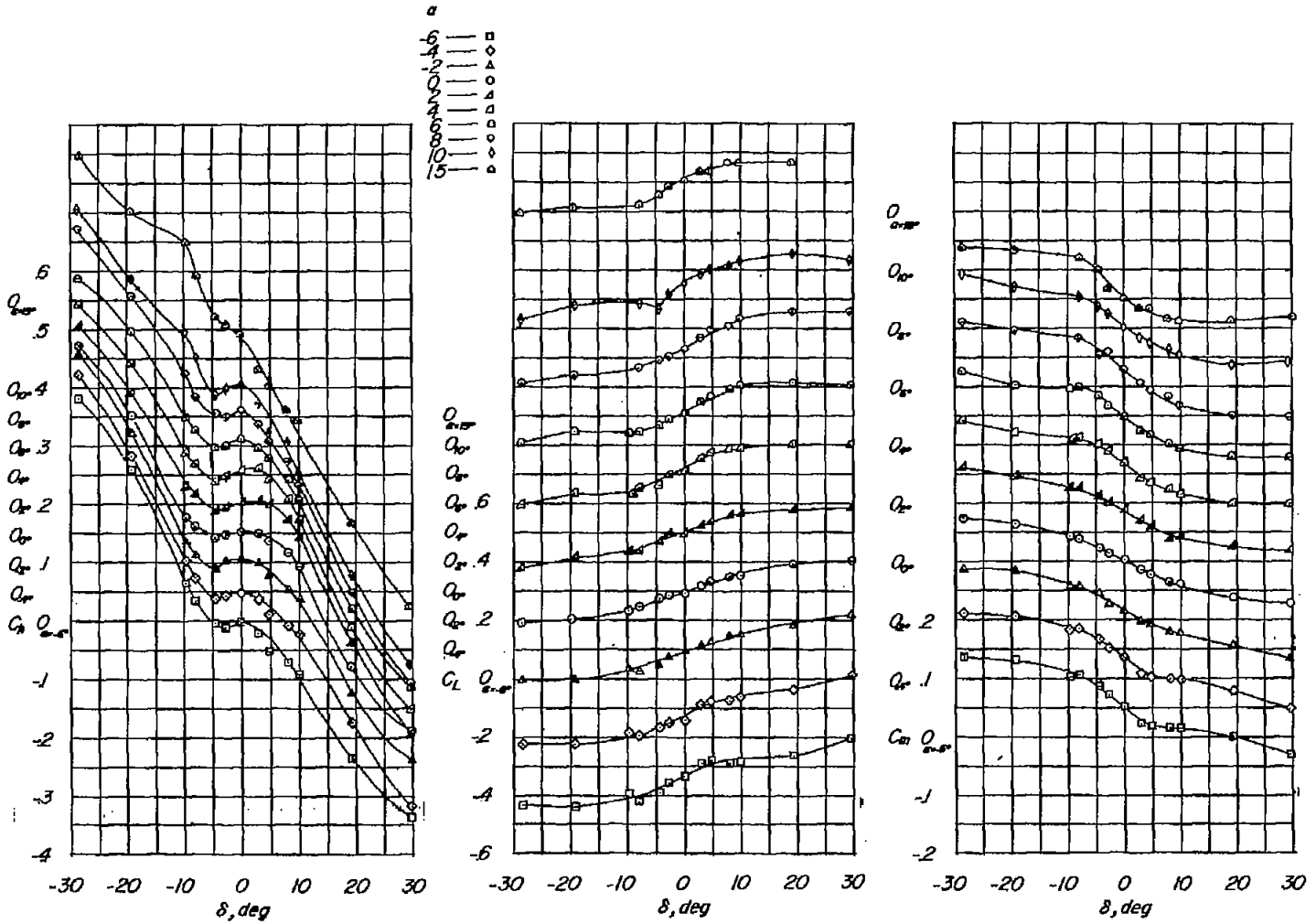

(f) M = 0.95; c_b/c_f = 0.50.

Figure 7.- Continued.

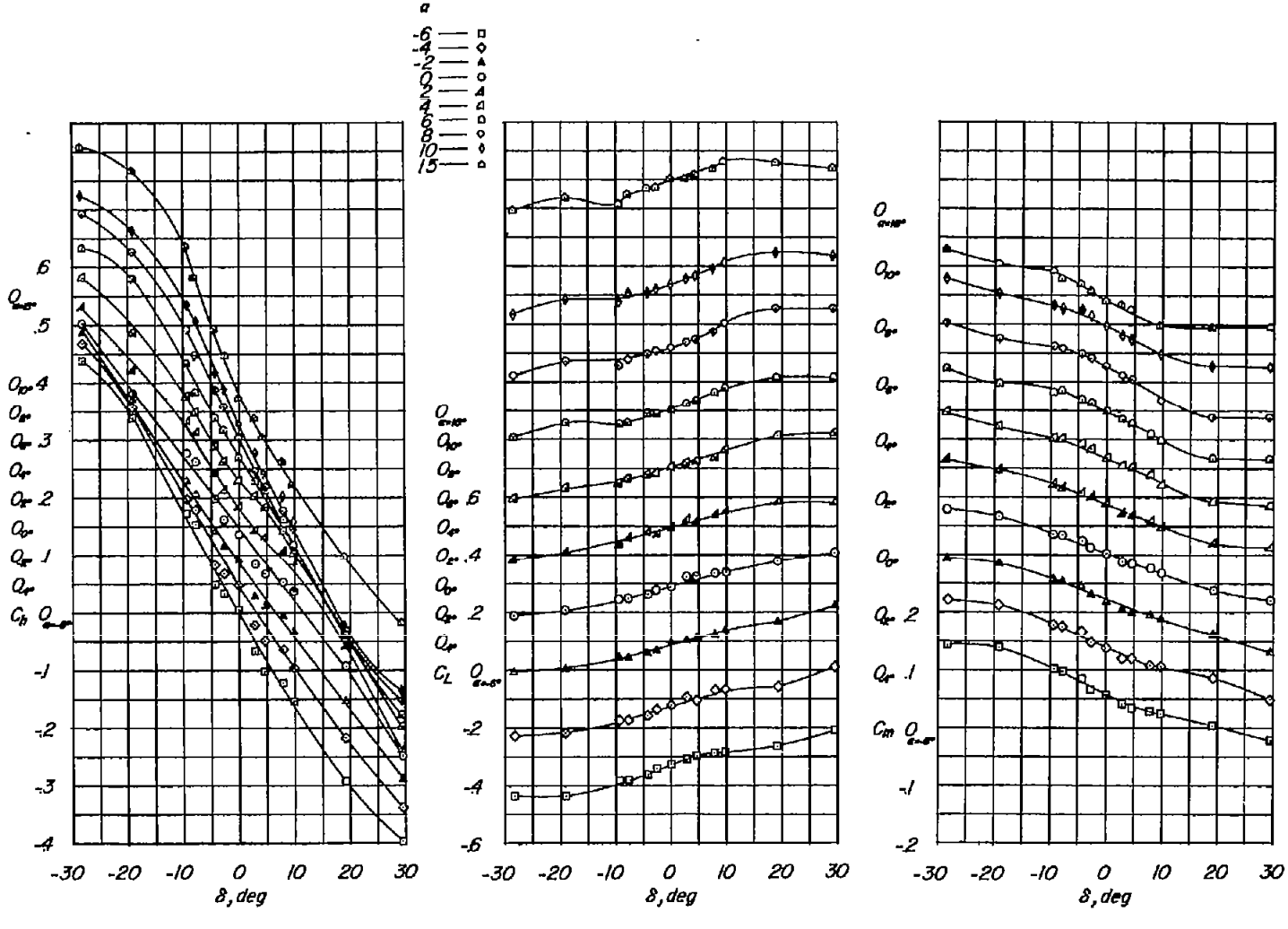

(g) M = 1.00; c_b/c_f = 0.50.

Figure 7.- Continued.

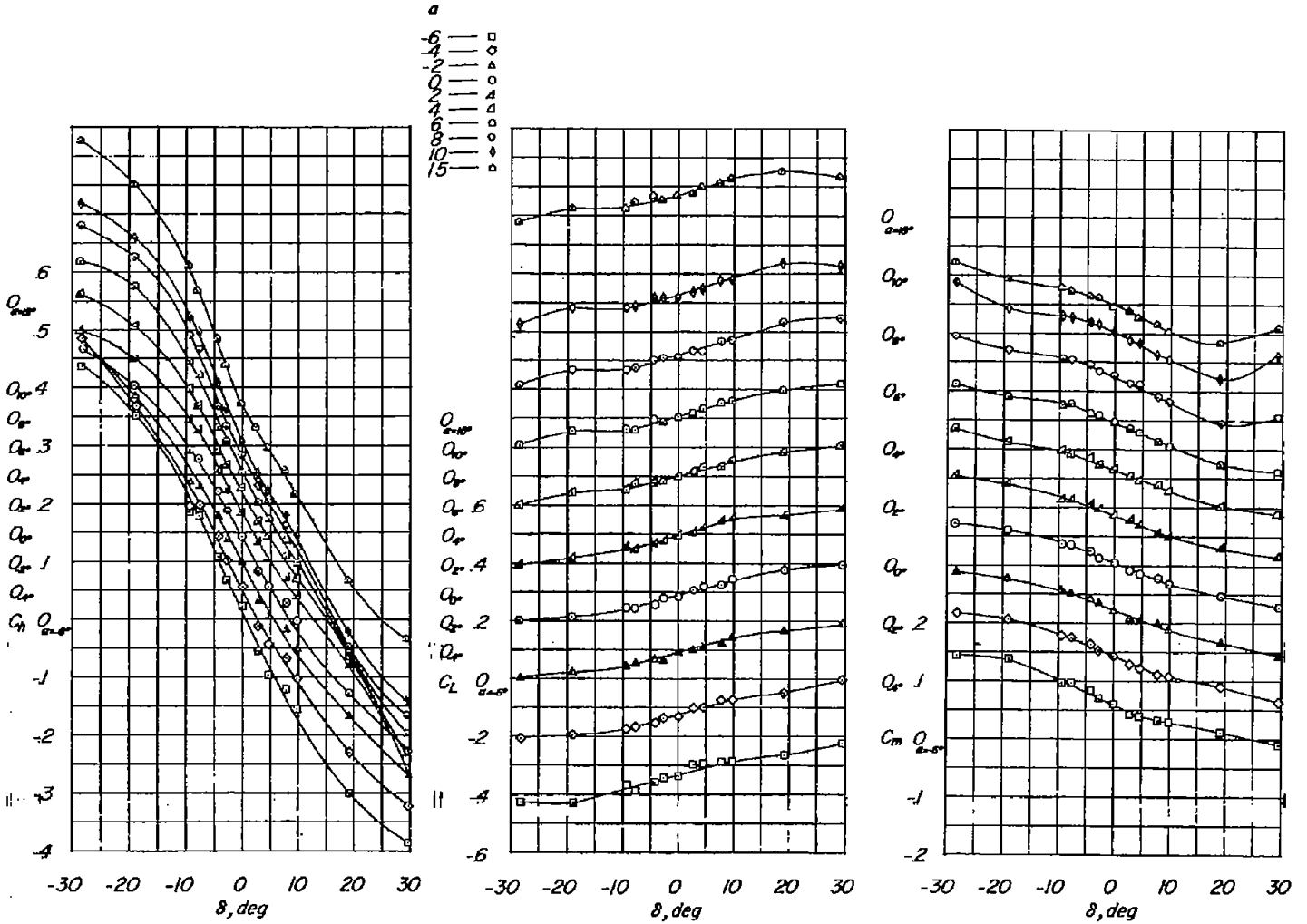

(h) M = 1.05; c_b/c_f = 0.50.

Figure 7.- Continued.

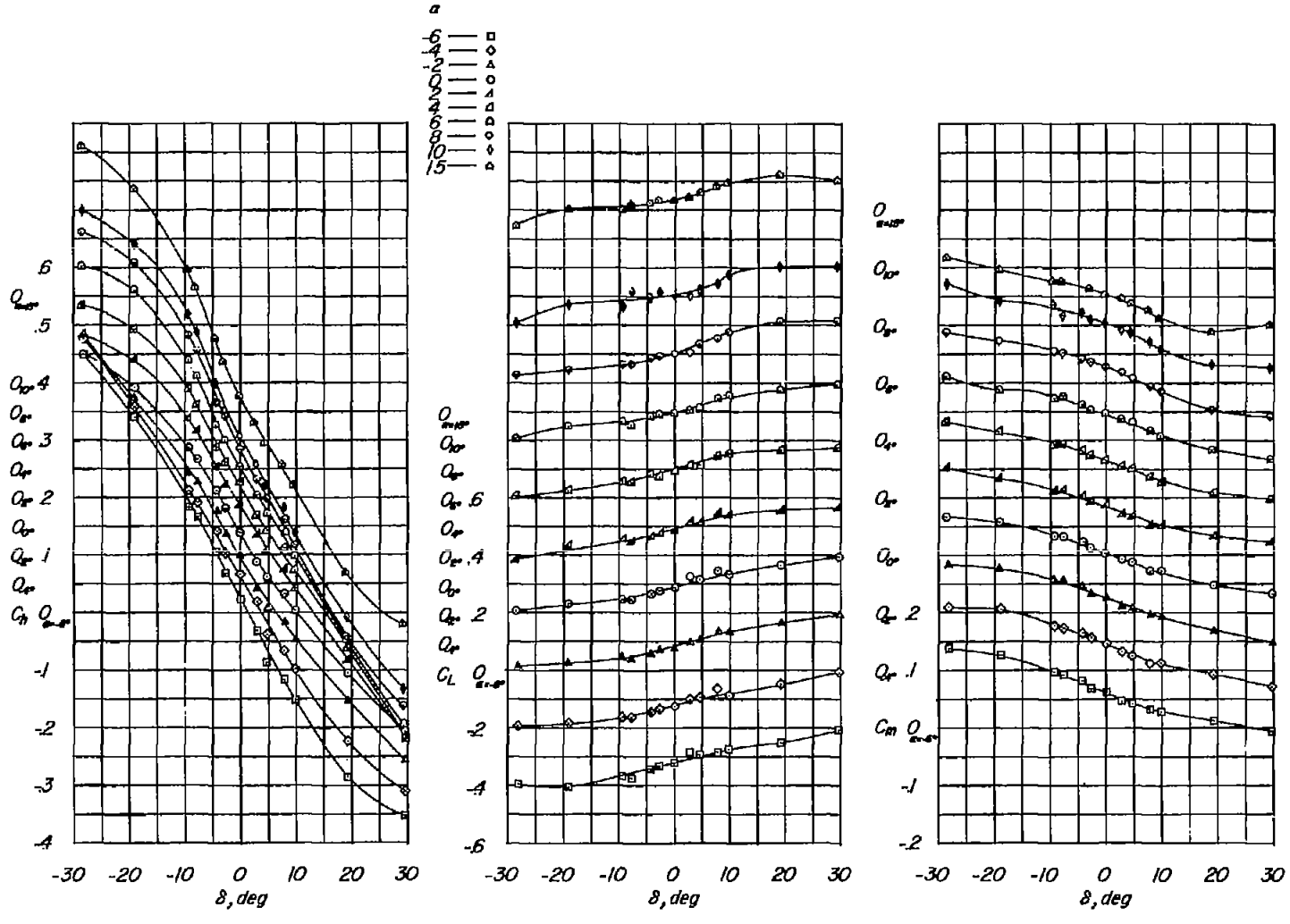

(i) M = 1.10; c_b/c_f = 0.50.

Figure 7.- Continued.

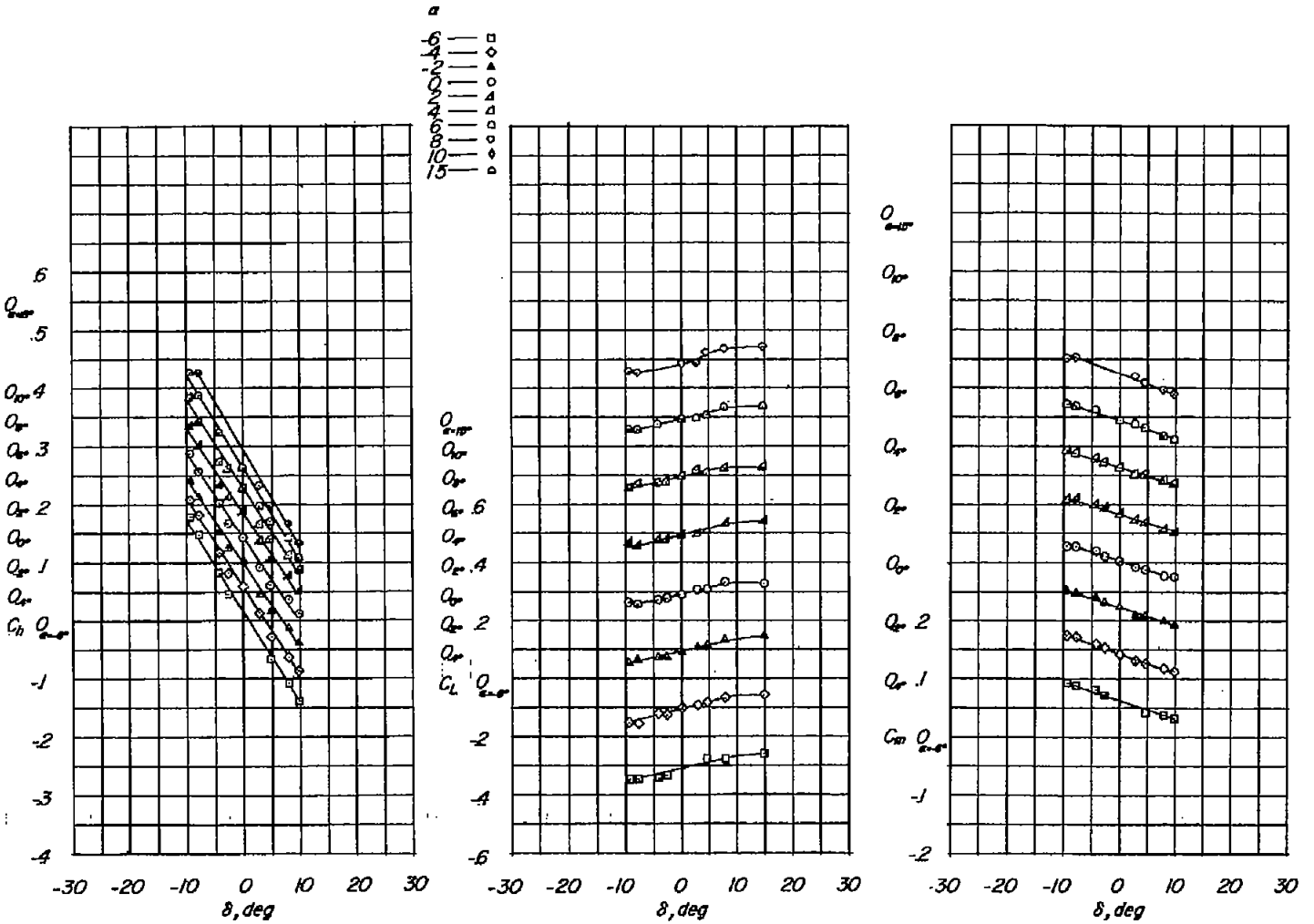

(j) M = 1.18; c_b/c_f = 0.50.

Figure 7.- Concluded.

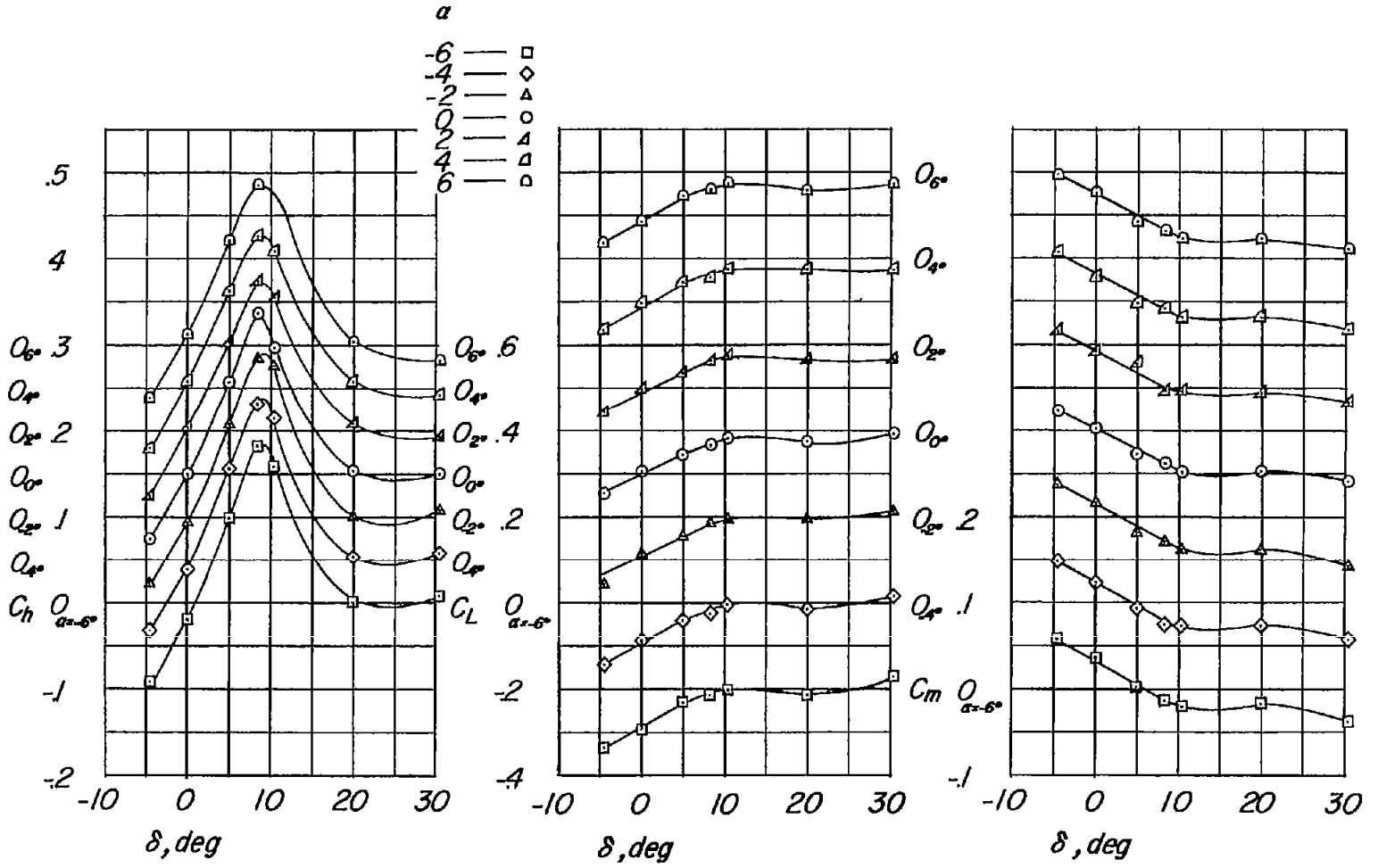

(a) M = 0.60.

Figure 8.- Variation of C_h, C_L, and C_m with δ for various angles of attack. c_b/c_f = 0.79.

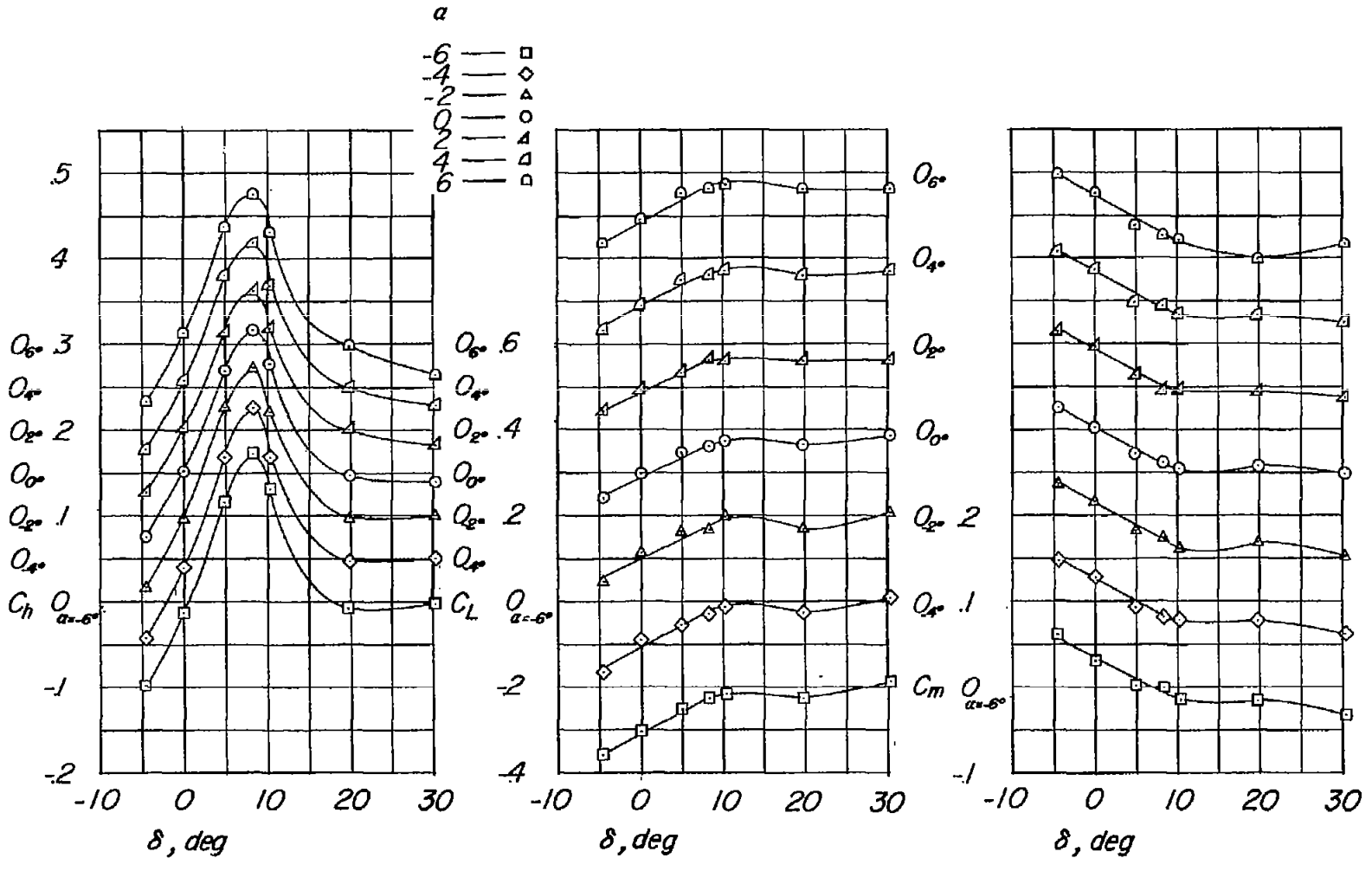

(b) M = 0.70; c_b/c_f = 0.79.

Figure 8.- Continued.

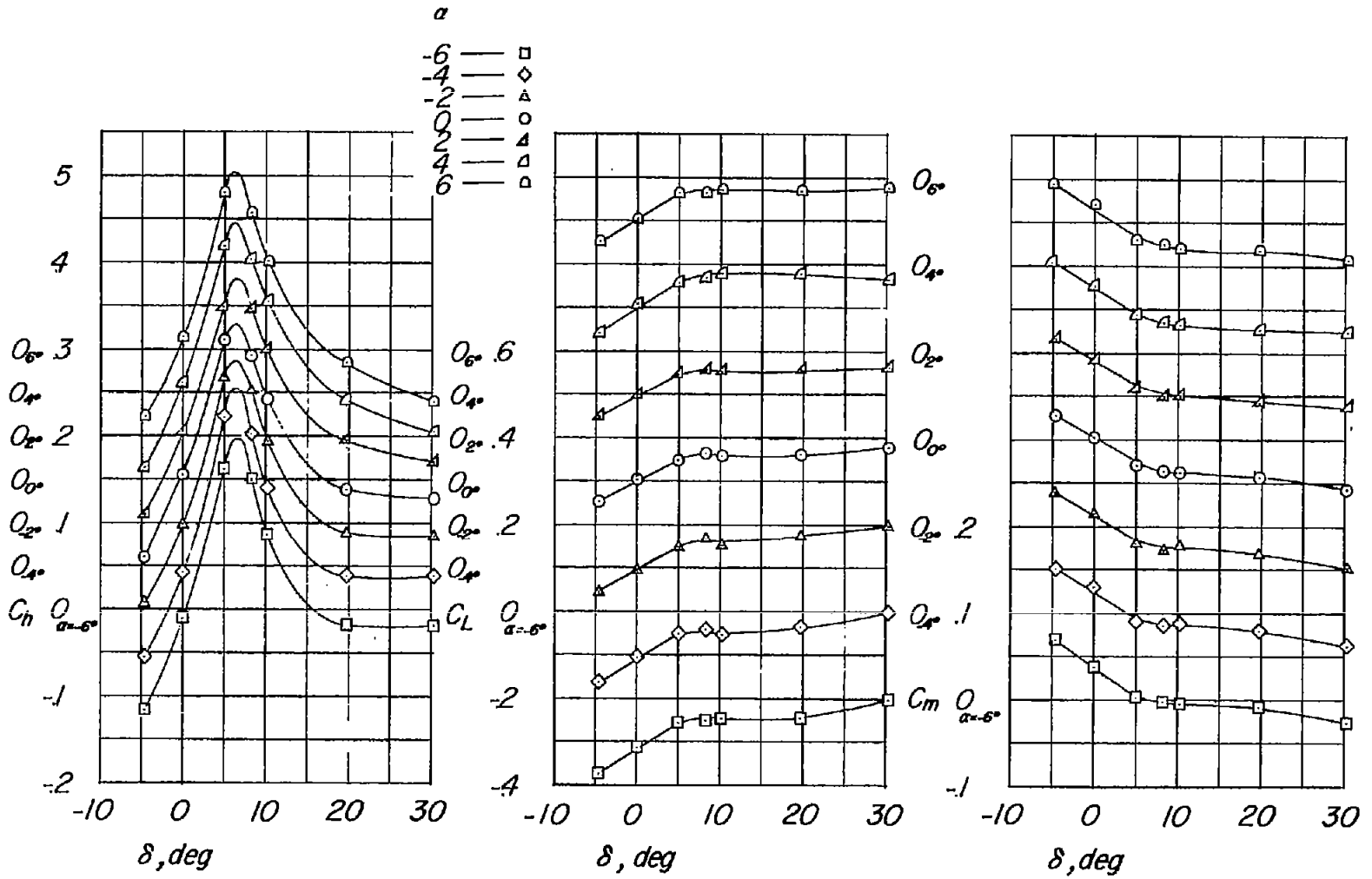

(c) M = 0.80; c_b/c_f = 0.79.

Figure 8.- Continued.

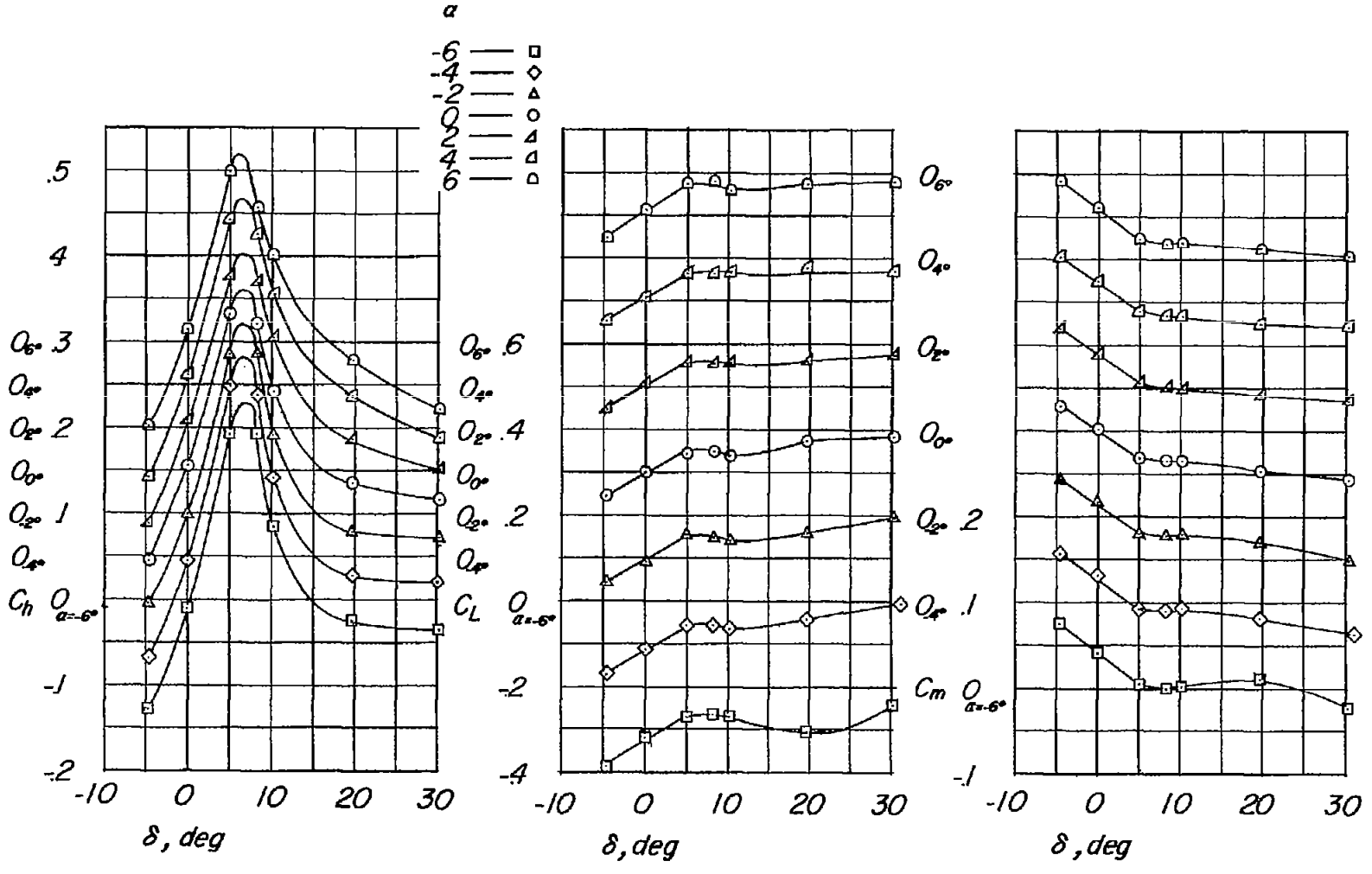

(d) M = 0.85; c_b/c_f = 0.79.

Figure 8.- Continued.

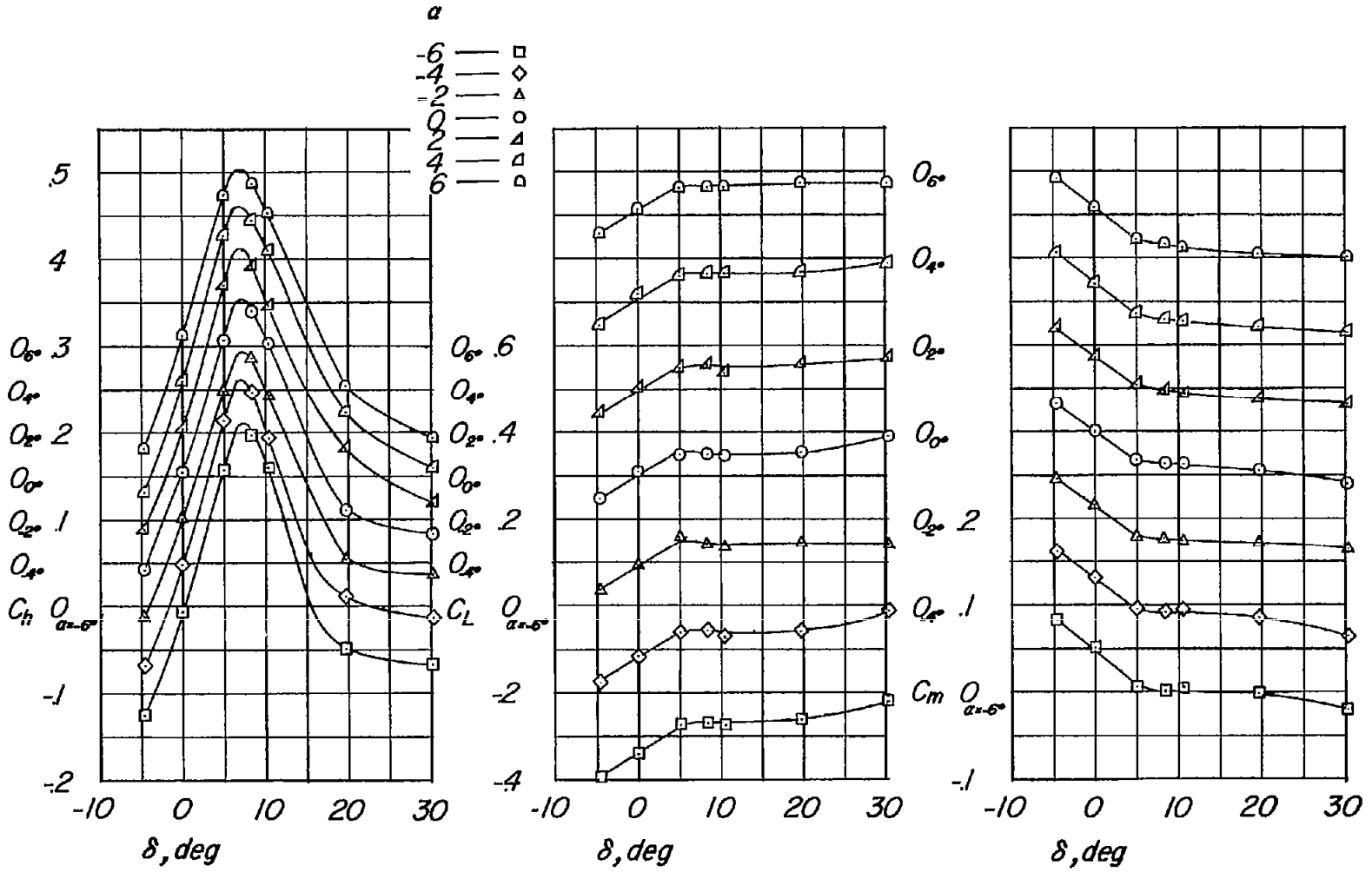

(e) M = 0.90; c_b/c_f = 0.79.

Figure 8.- Continued.

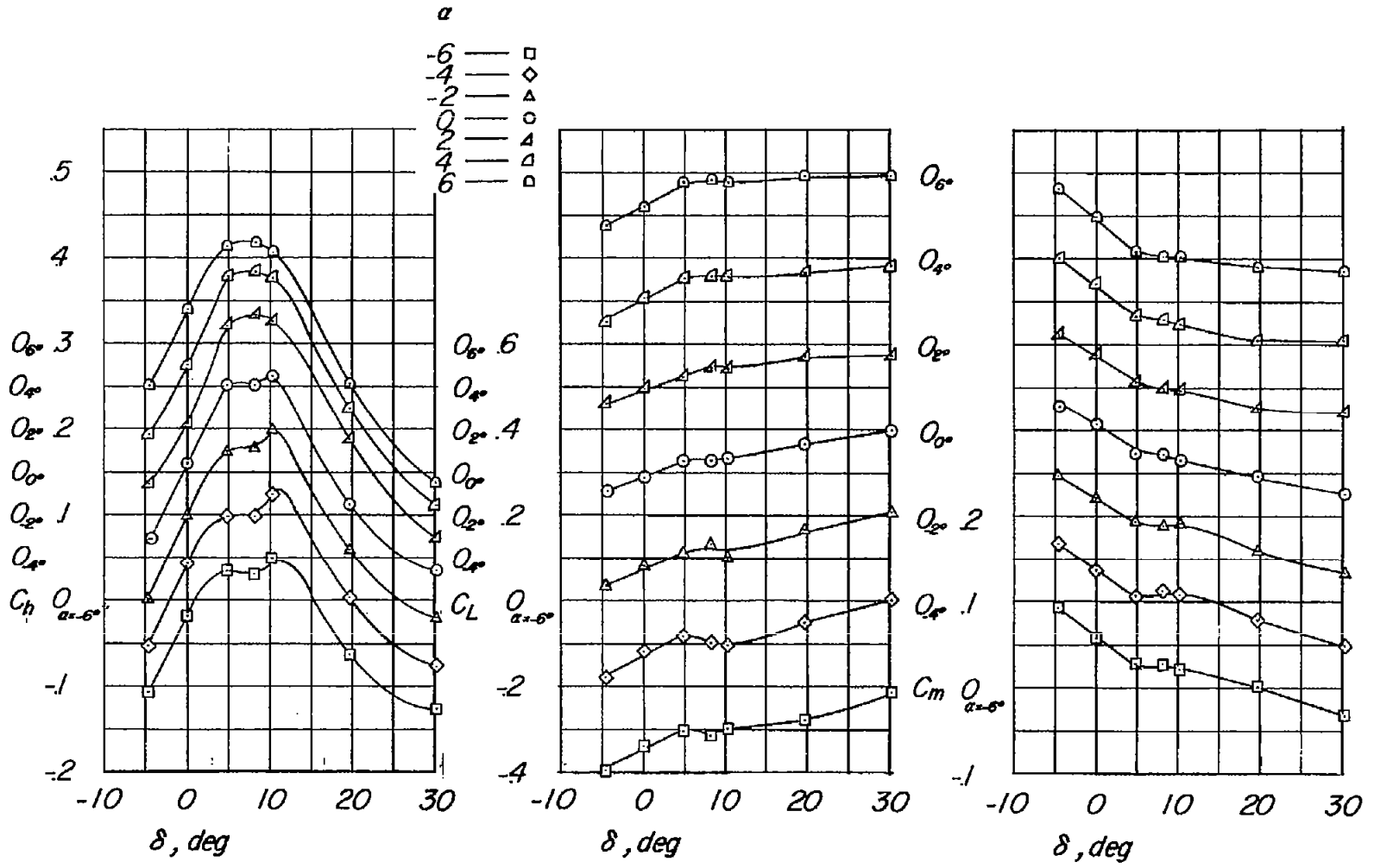

(f) M = 0.95; c_b/c_f = 0.79.

Figure 8.- Continued.

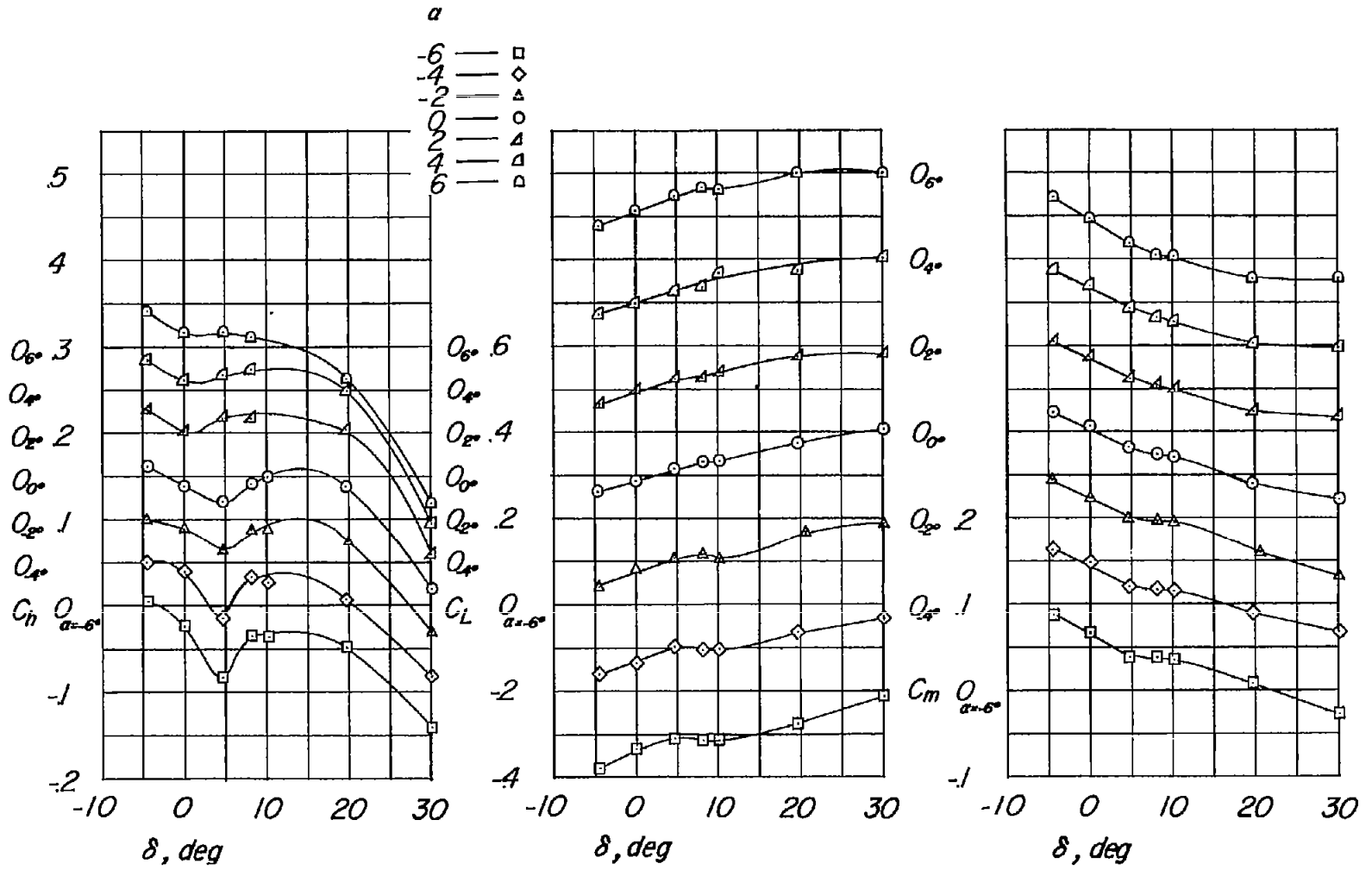

(g) M = 1.00; c_b/c_f = 0.79.

Figure 8.- Continued.

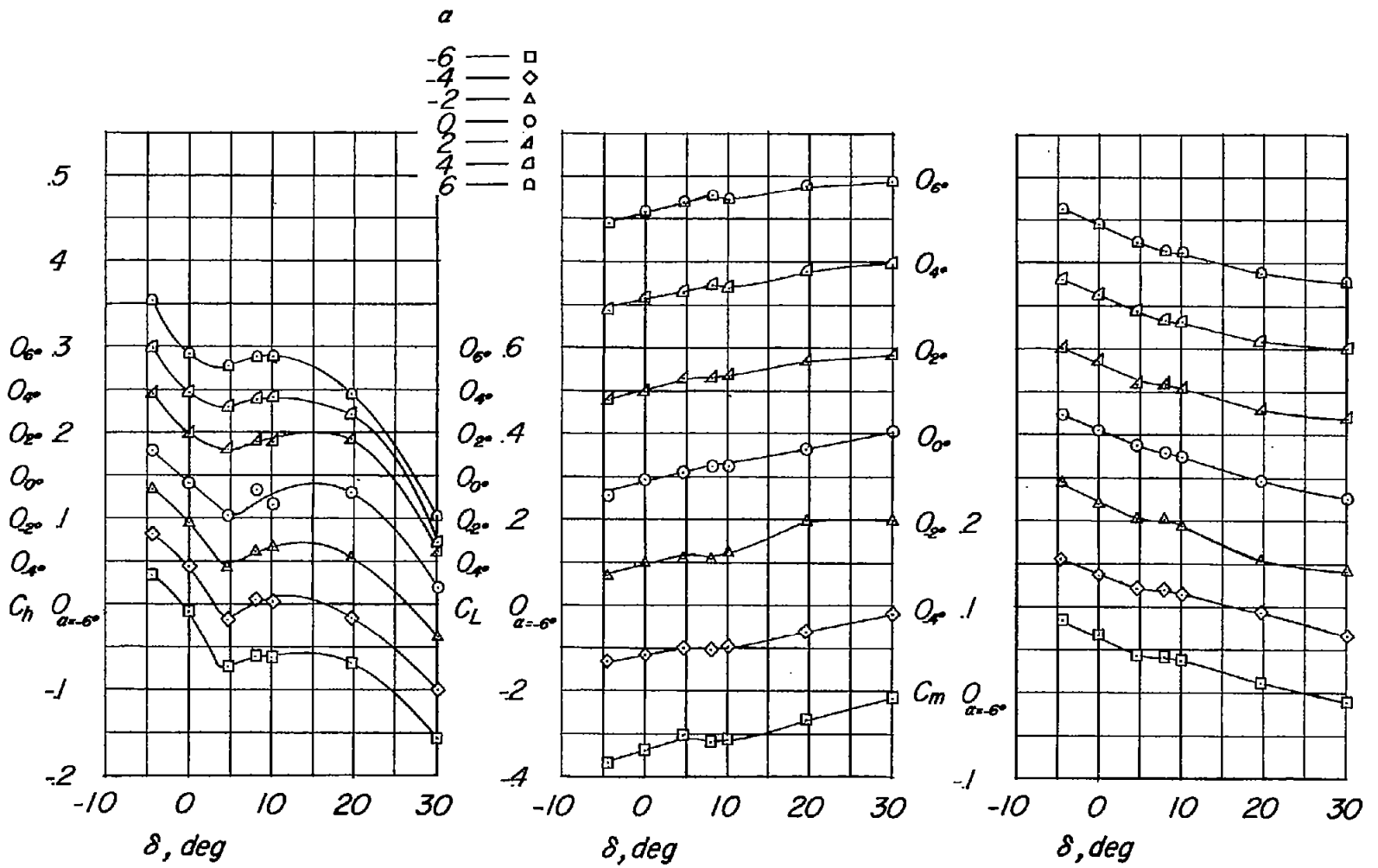

(h) M = 1.05; c_b/c_f = 0.79.

Figure 8.- Continued.

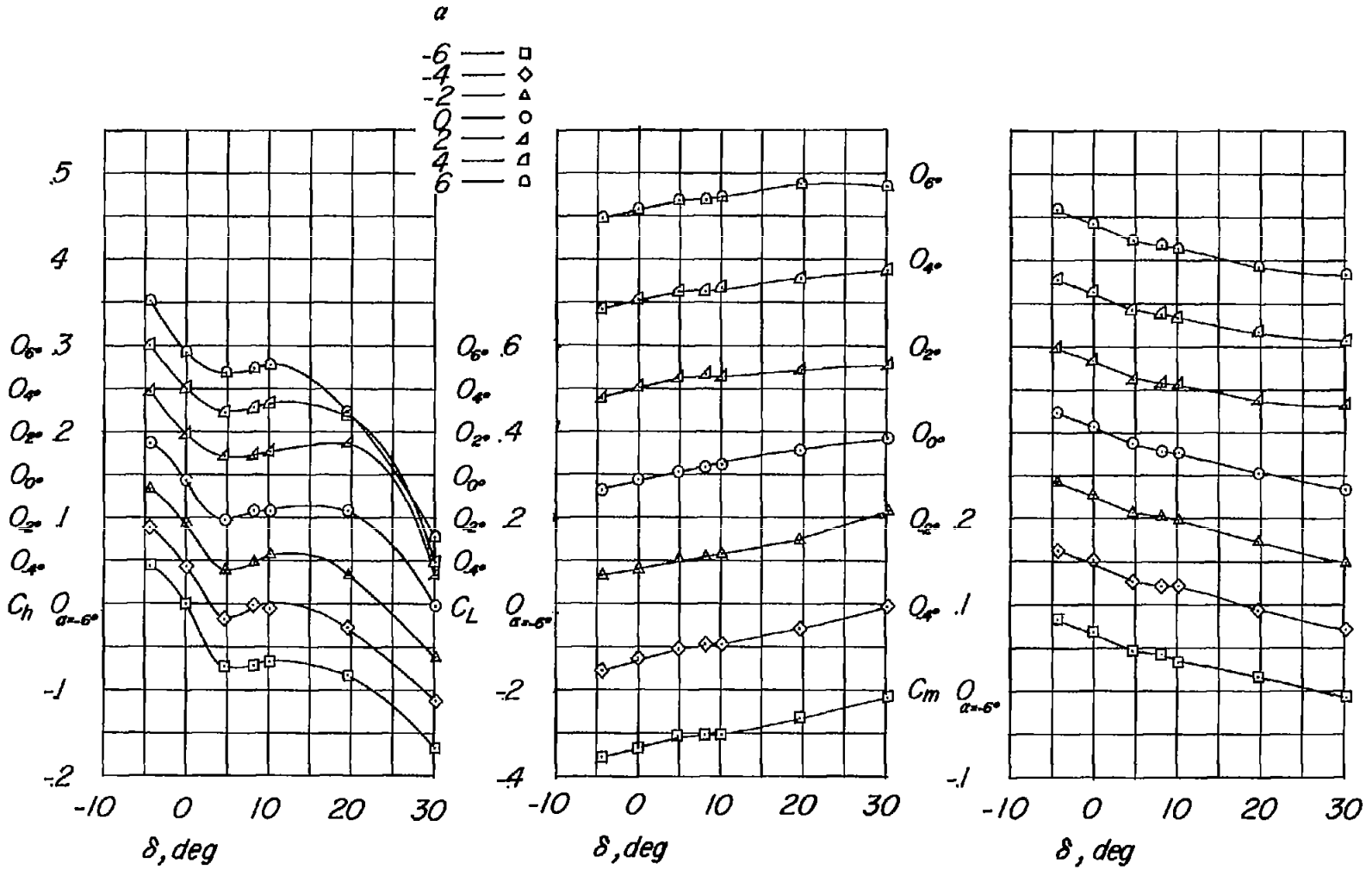

(i) M = 1.10; c_b/c_f = 0.79.

Figure 8.- Concluded.

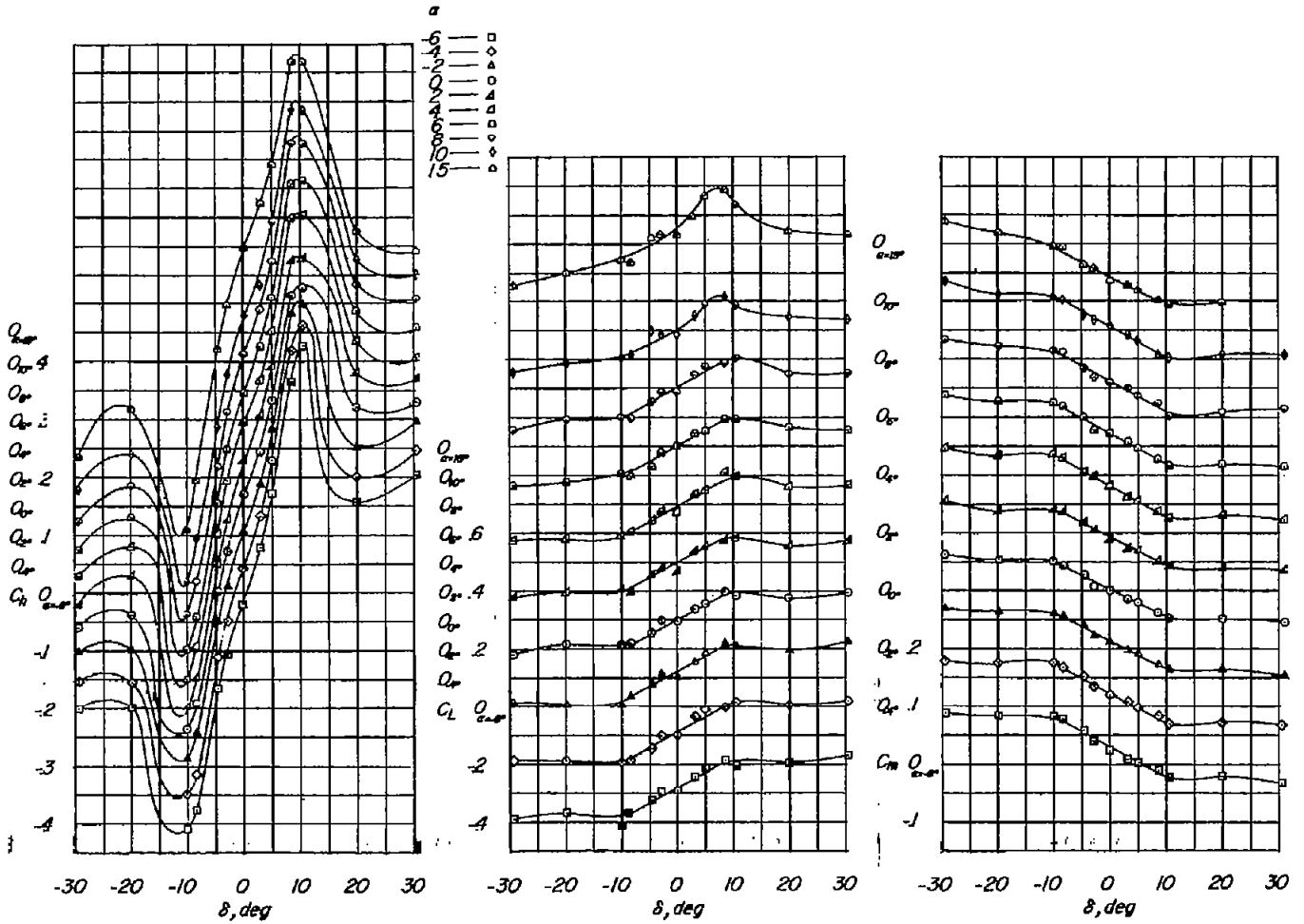

(a) M = 0.60.

Figure 9.- Variation of C_h, C_L, and C_m with δ for various angles of attack. $c_b/c_f = 1.03$.

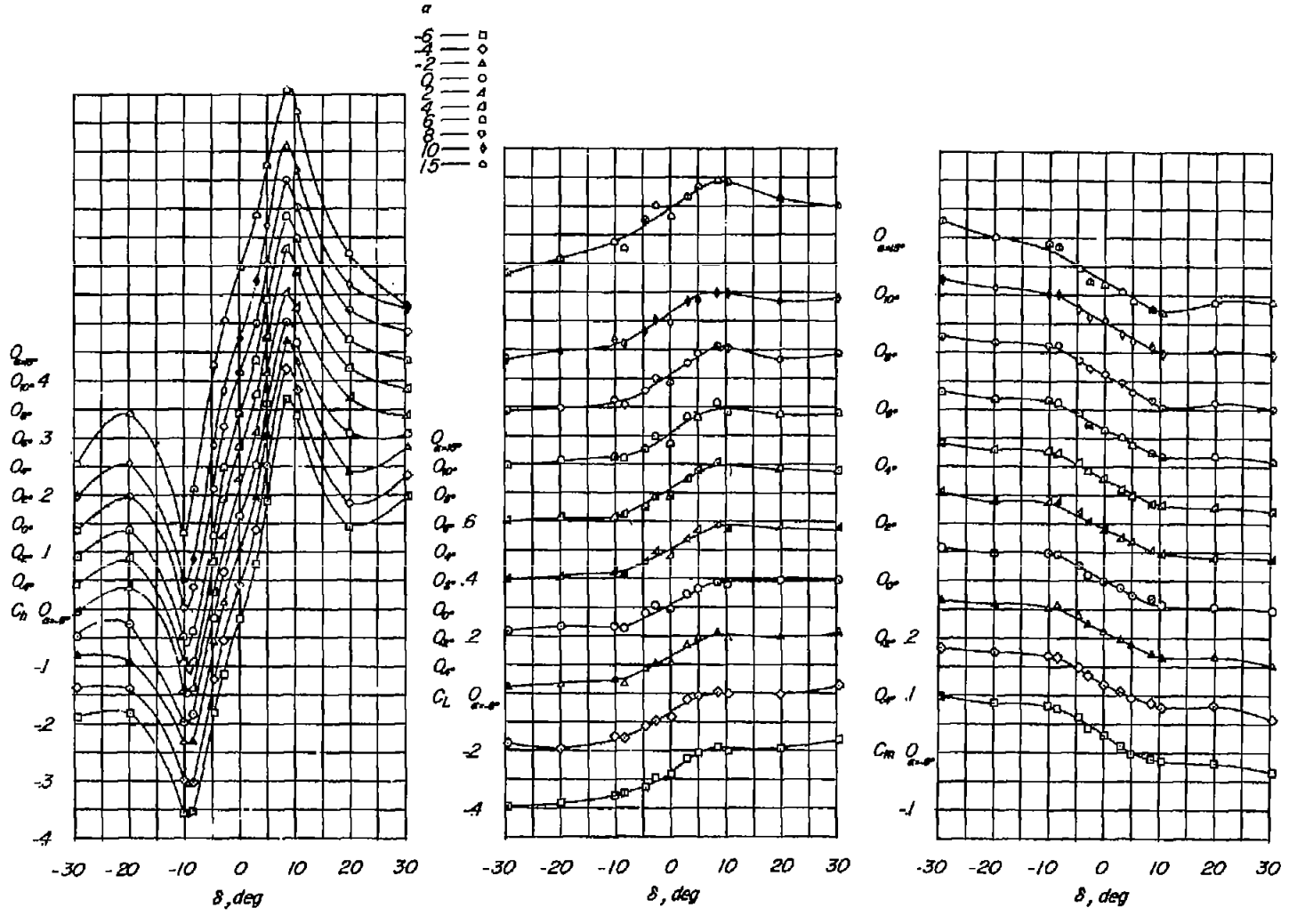

(b) M = 0.70; c_b/c_f = 1.03.

Figure 9.- Continued.

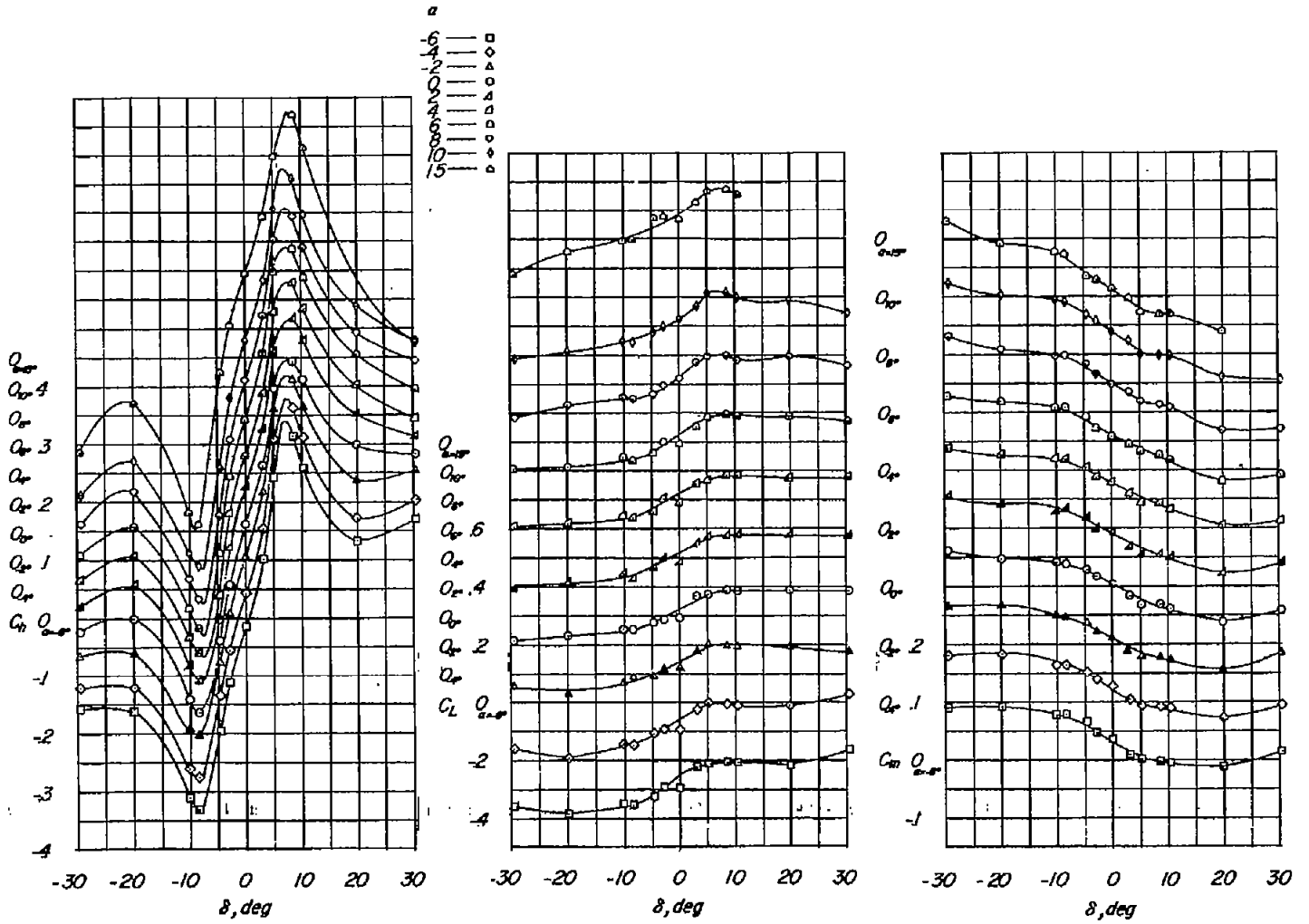

(c) M = 0.80; c_b/c_f = 1.03.

Figure 9.- Continued.

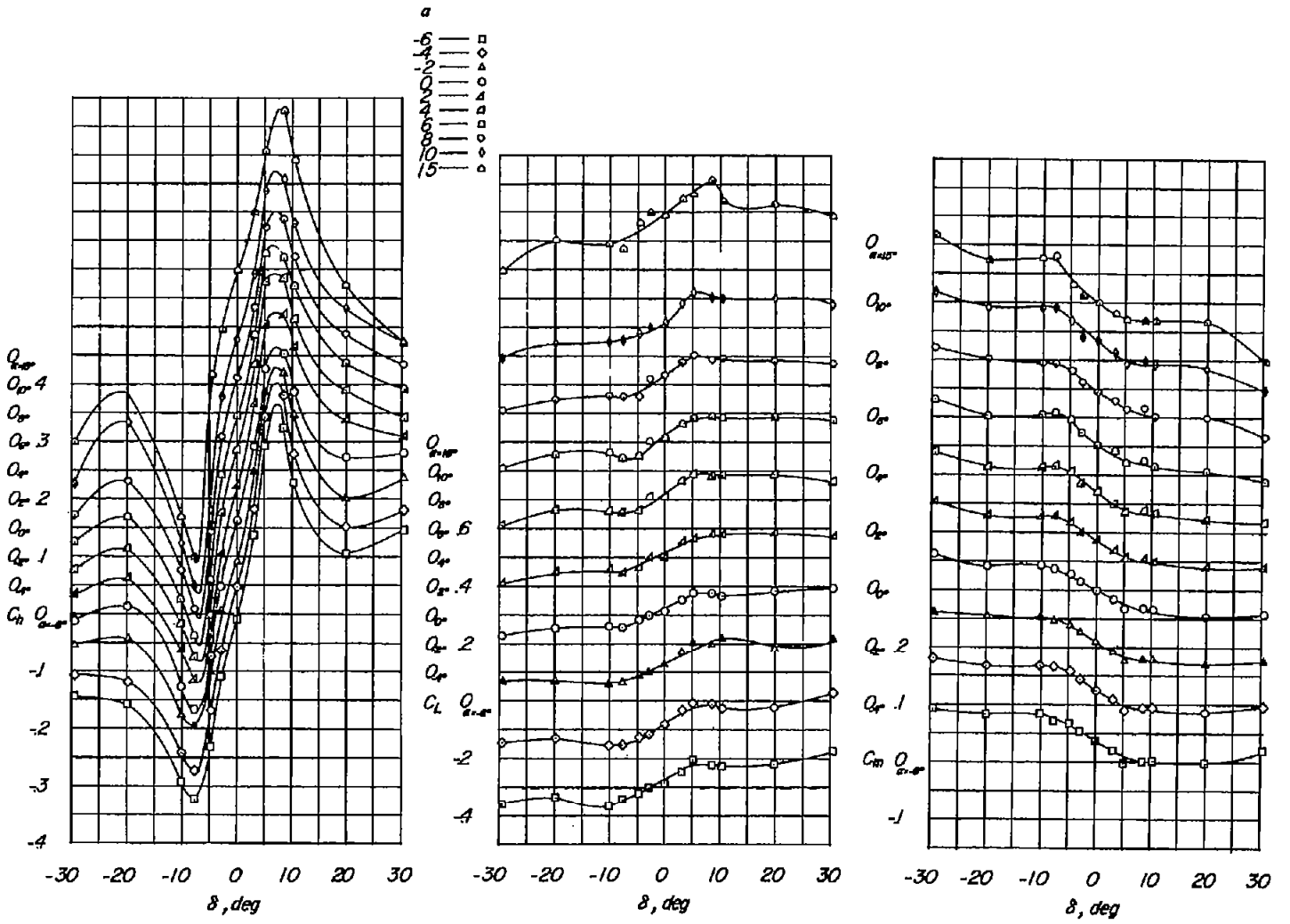

(d) M = 0.85; c_b/c_f = 1.03.

Figure 9.- Continued.

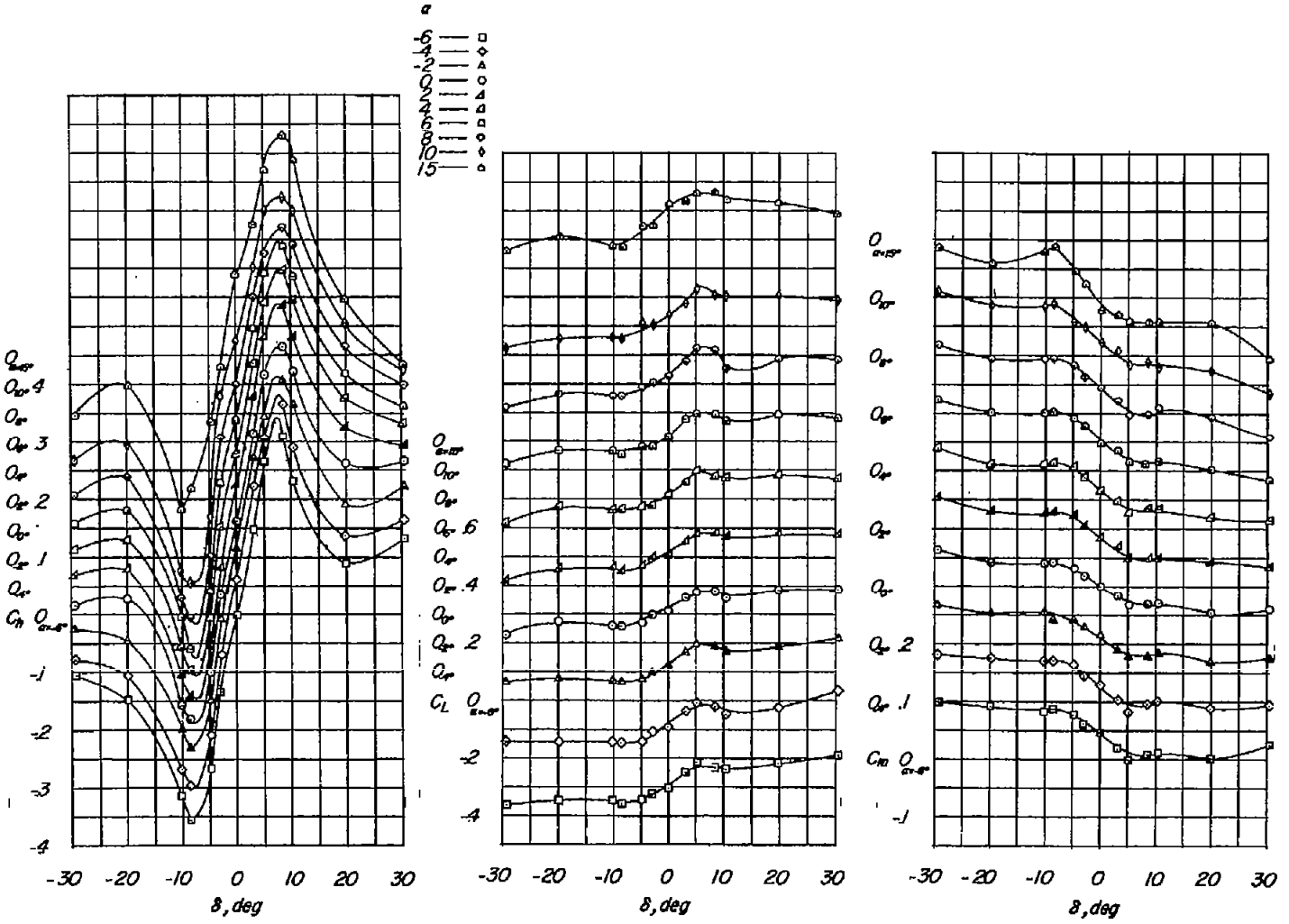

(e) M = 0.90; c_b/c_f = 1.03.

Figure 9.- Continued.

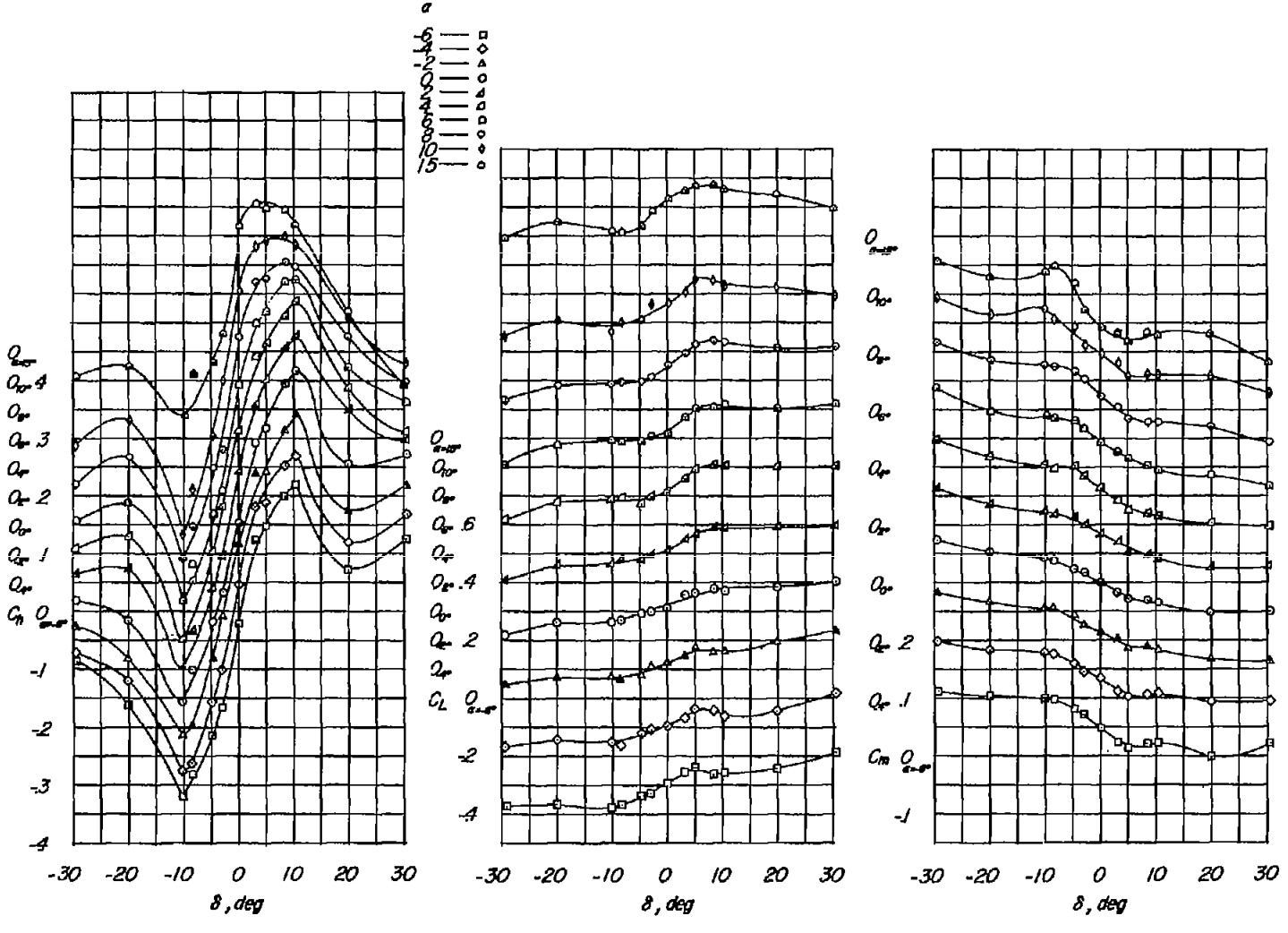

(f) M = 0.95; c_b/c_f = 1.03.

Figure 9.- Continued.

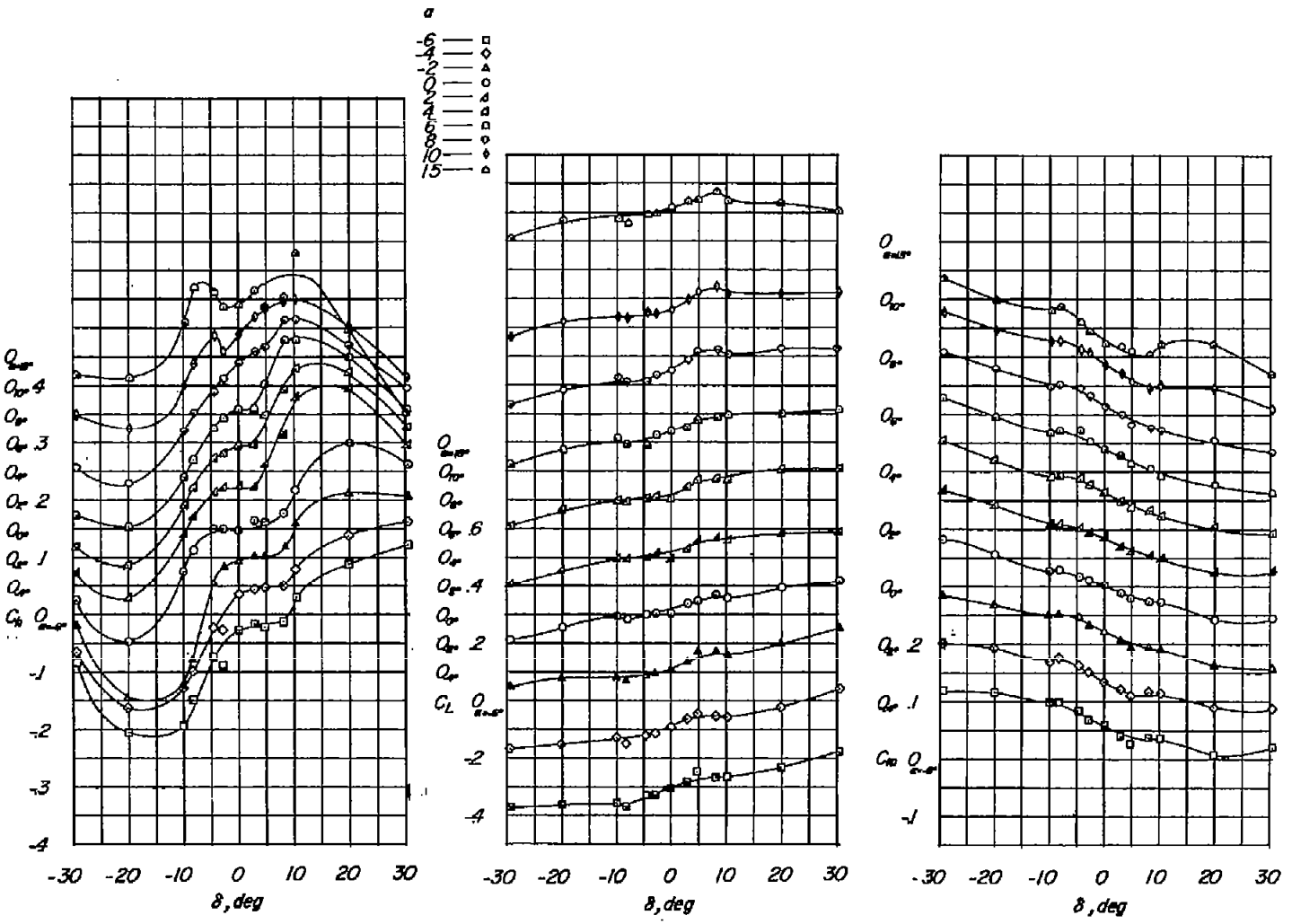

(g) M = 1.00; c_b/c_f = 1.03.

Figure 9.- Continued.

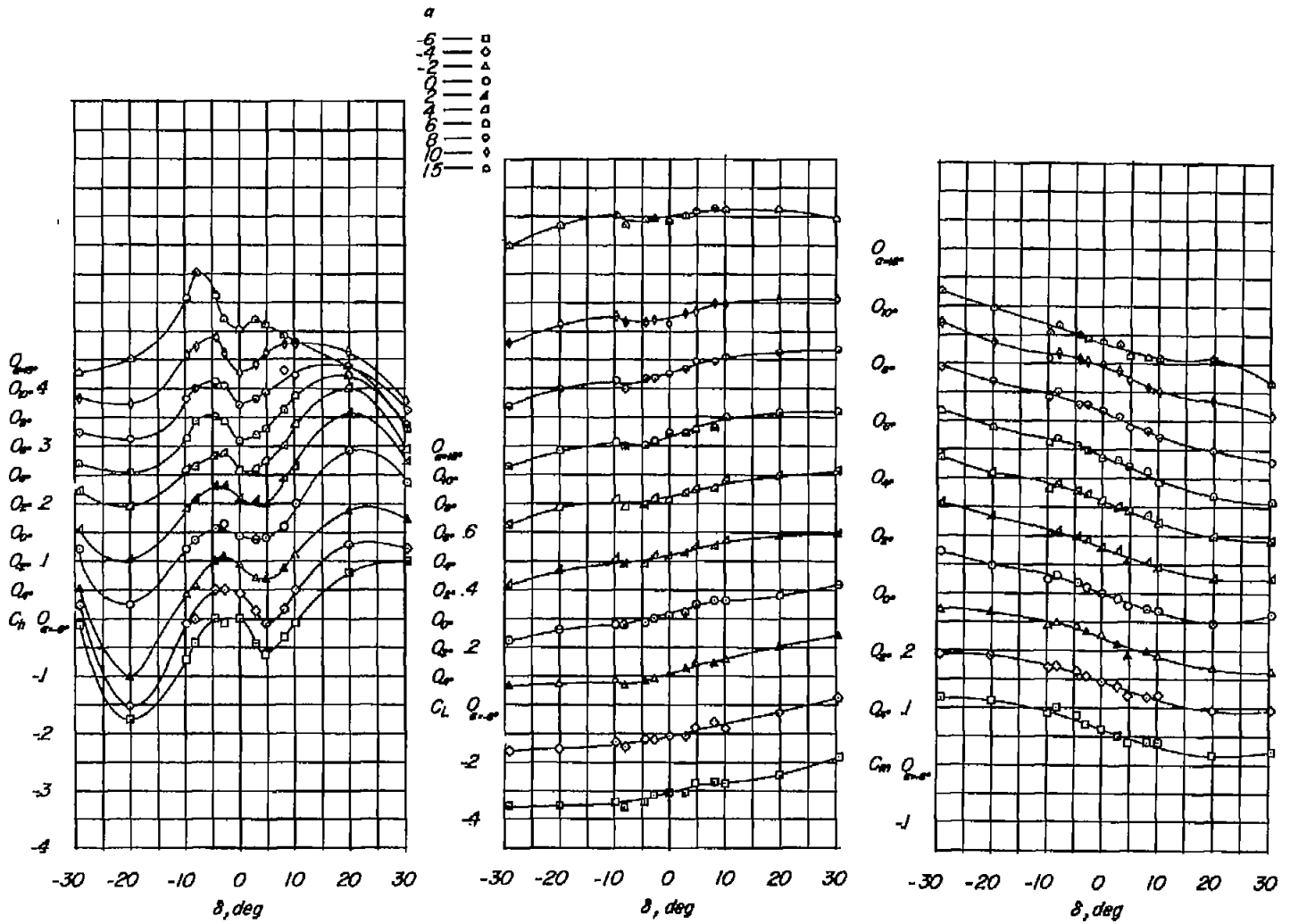

(h) M = 1.05; c_b/c_f = 1.03.

Figure 9.- Continued.

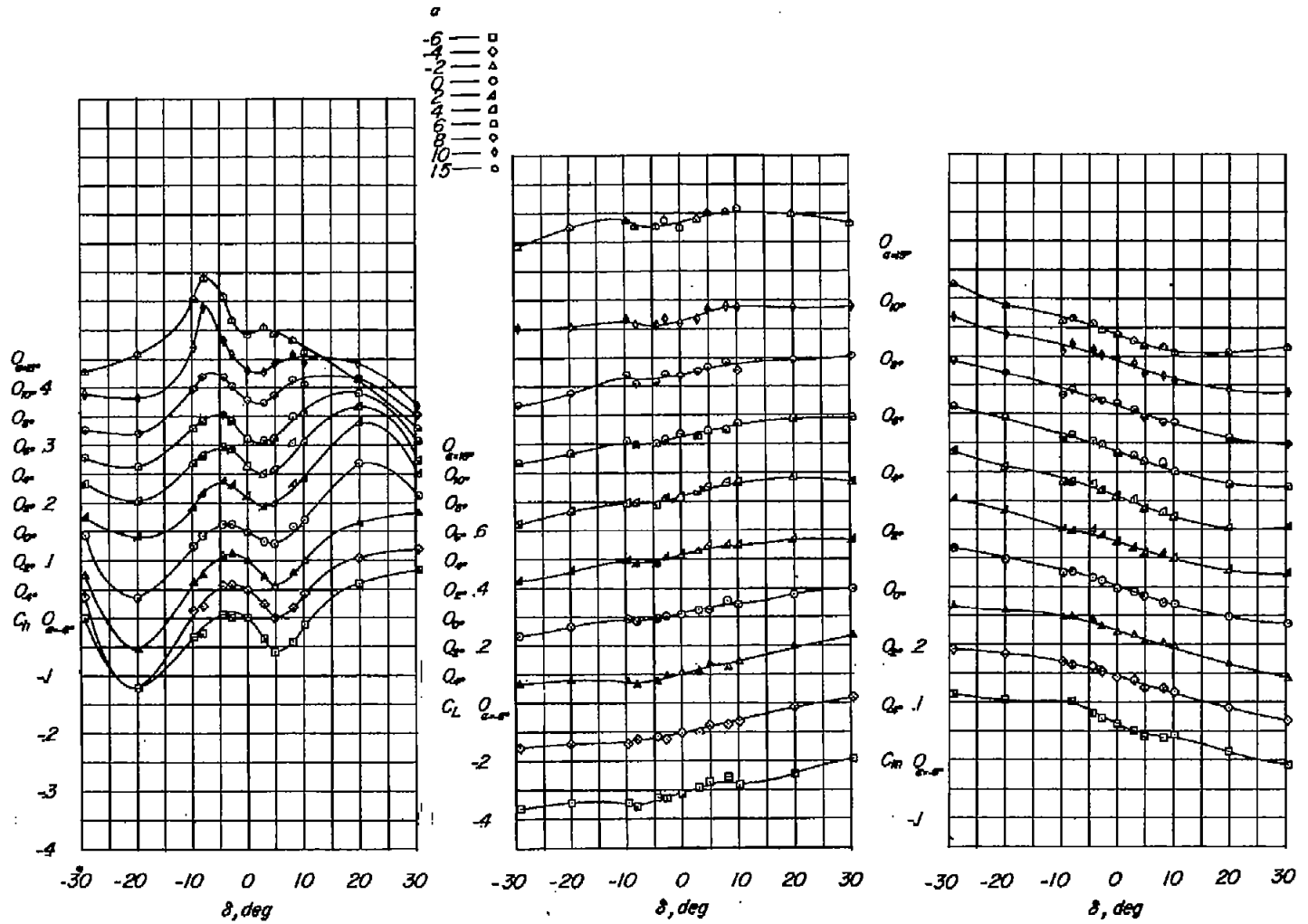

(i) M = 1.10; c_b/c_f = 1.03.

Figure 9.- Continued.

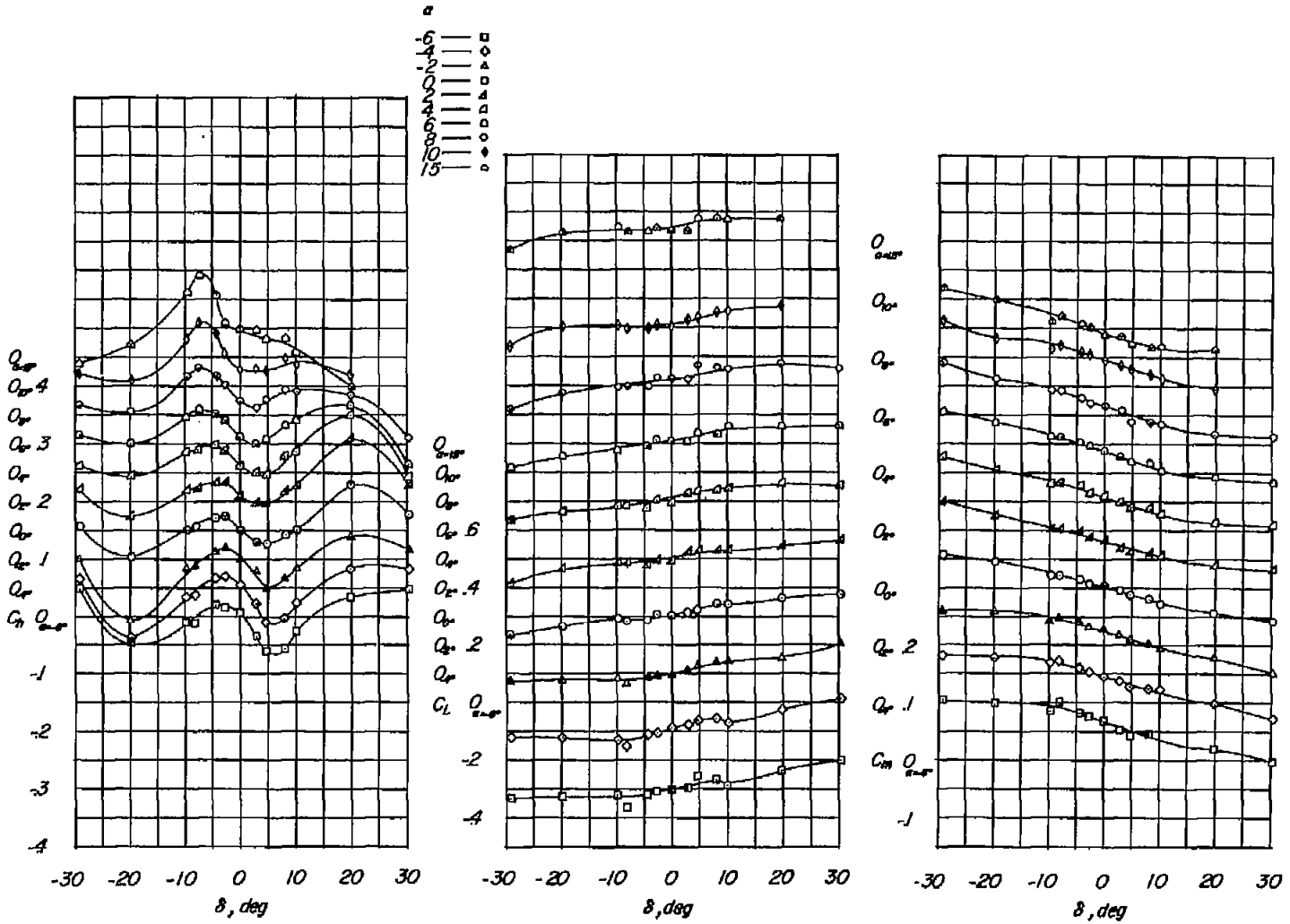

(j) M = 1.18; c_b/c_f = 1.03.

Figure 9.- Concluded.

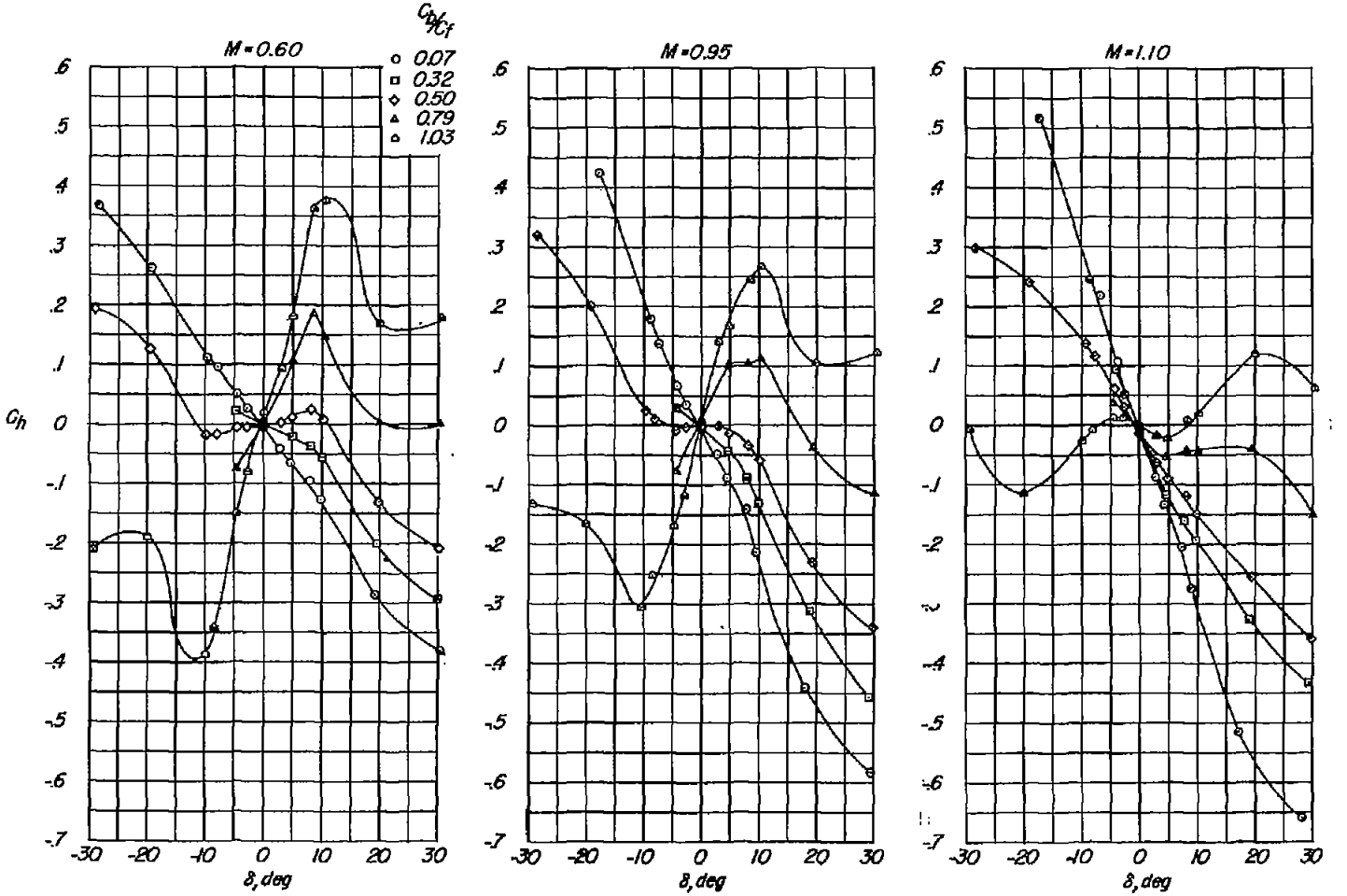

(a) C_h plotted against δ.

Figure 10.- The effect of hinge location for three test Mach numbers. $\alpha = 0^\circ$.

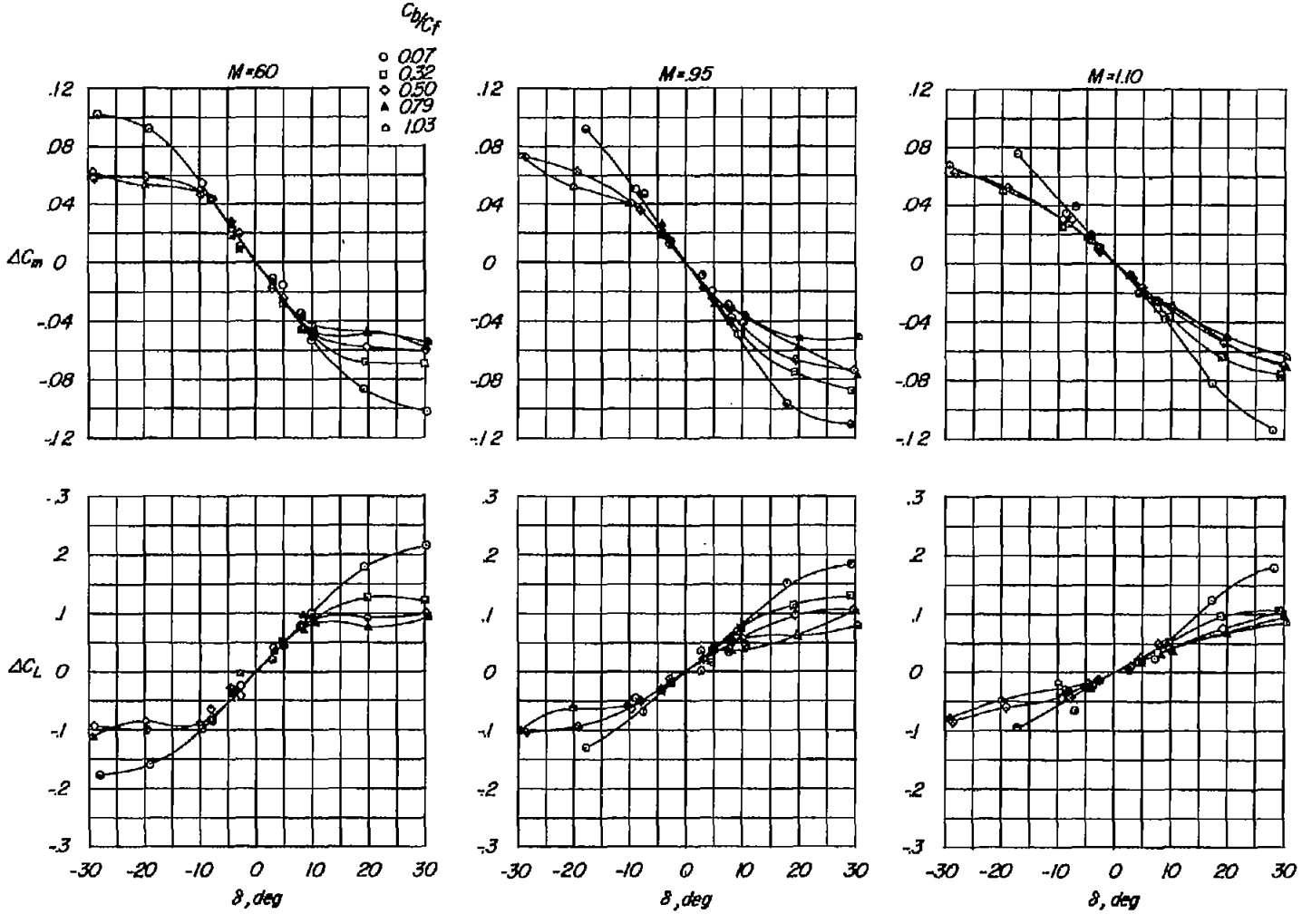

(b) ΔC_L and ΔC_m plotted against δ.

Figure 10.- Concluded.

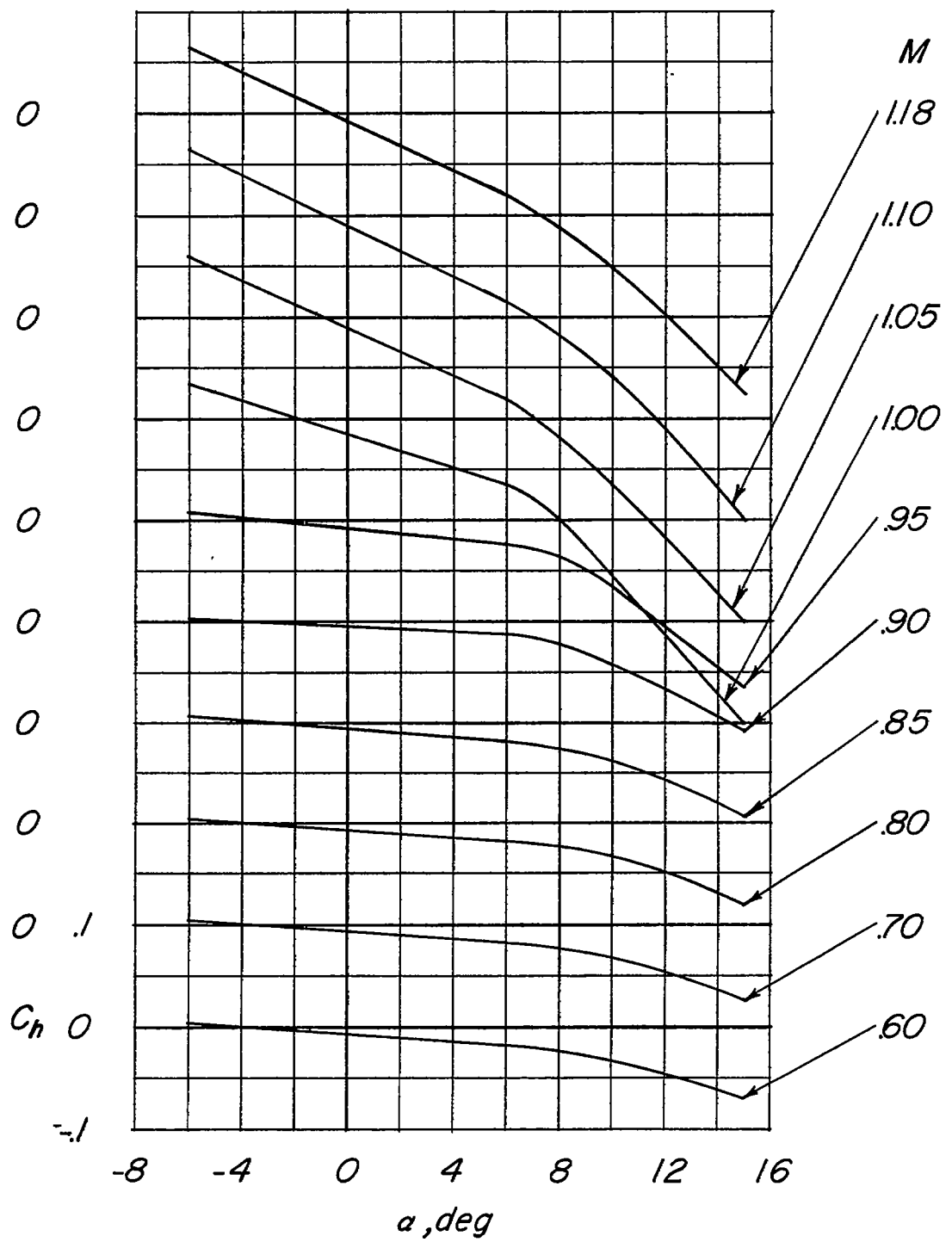

(a) $c_b/c_f = 0.07$.

Figure 11.- Variation of C_h with α for various Mach numbers. $\delta = 0^\circ$.

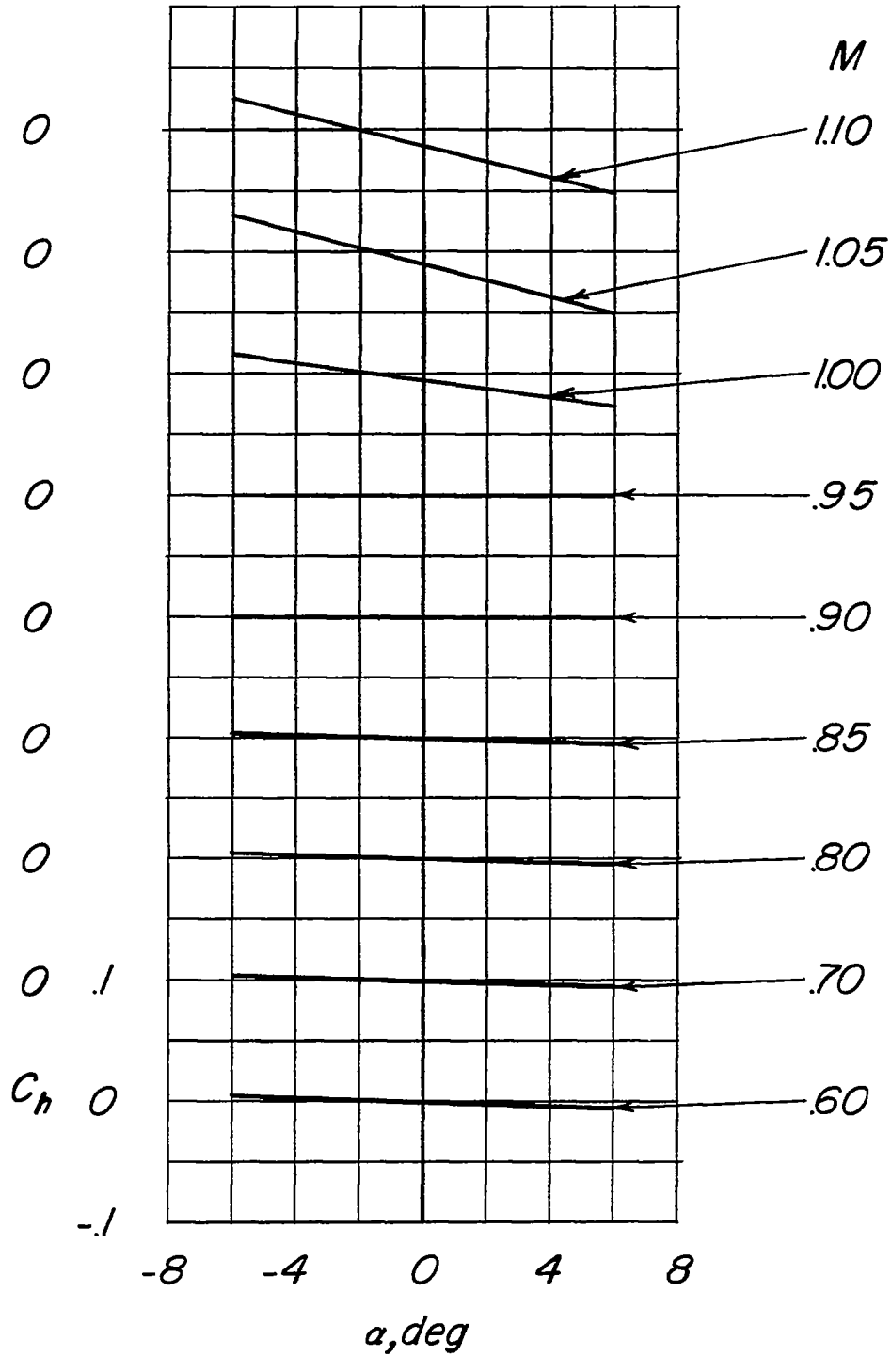

(b) $c_b/c_f = 0.32$.

Figure 11.- Continued.

[redacted]

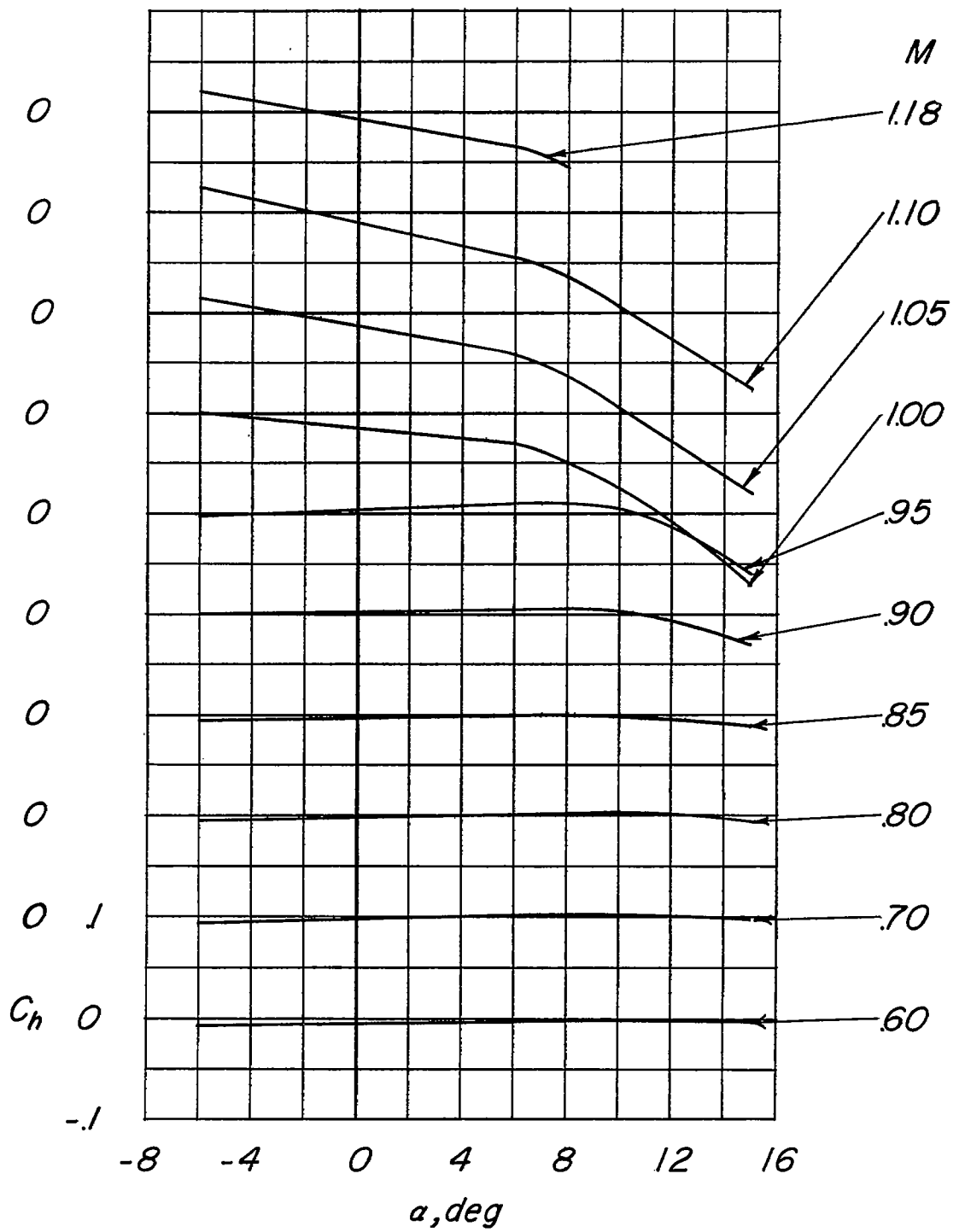

(c) $c_b/c_f = 0.50$.

Figure 11.- Continued.

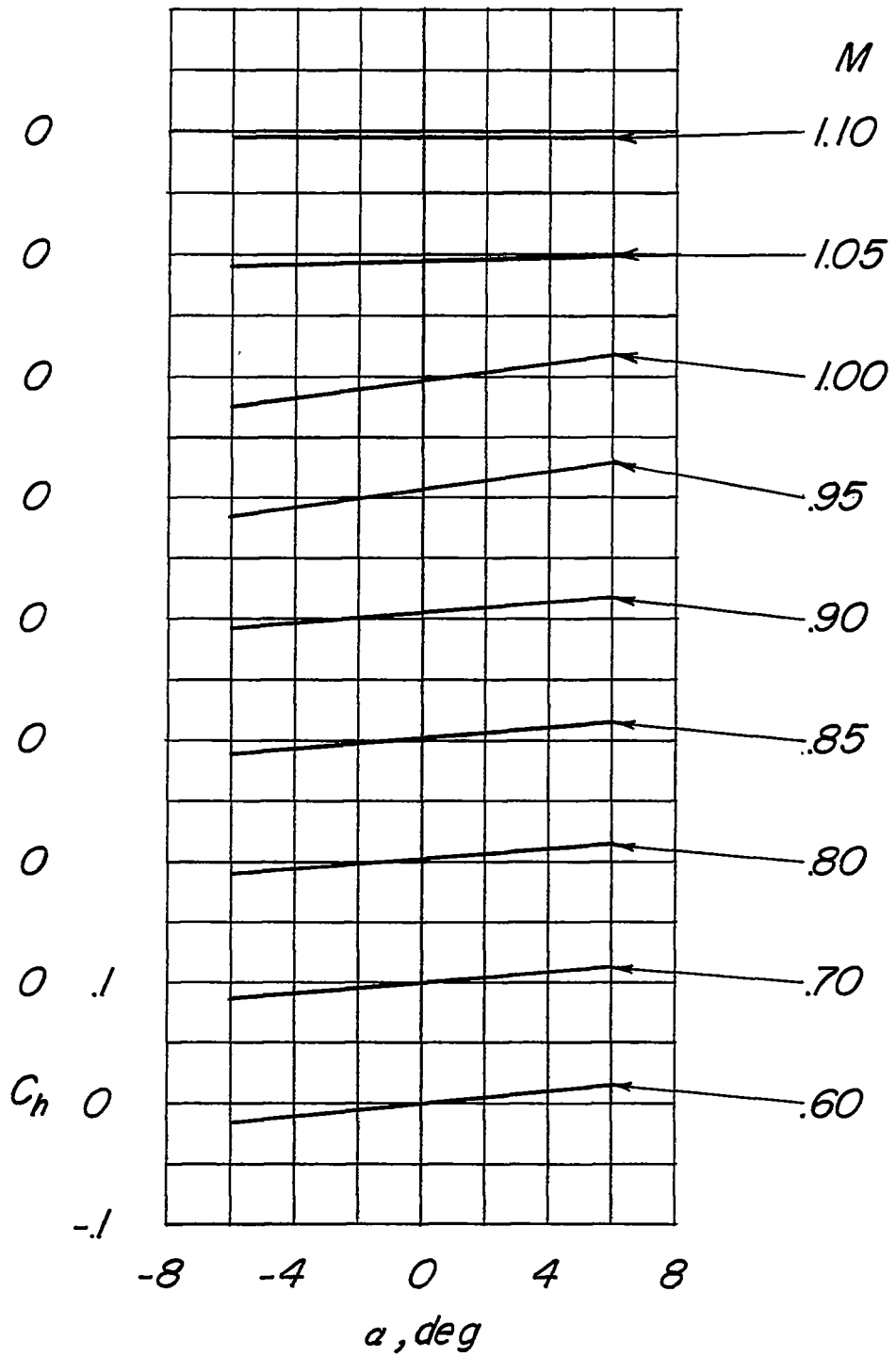

(d) $c_b/c_f = 0.79$.

Figure 11.- Continued.

[redacted]

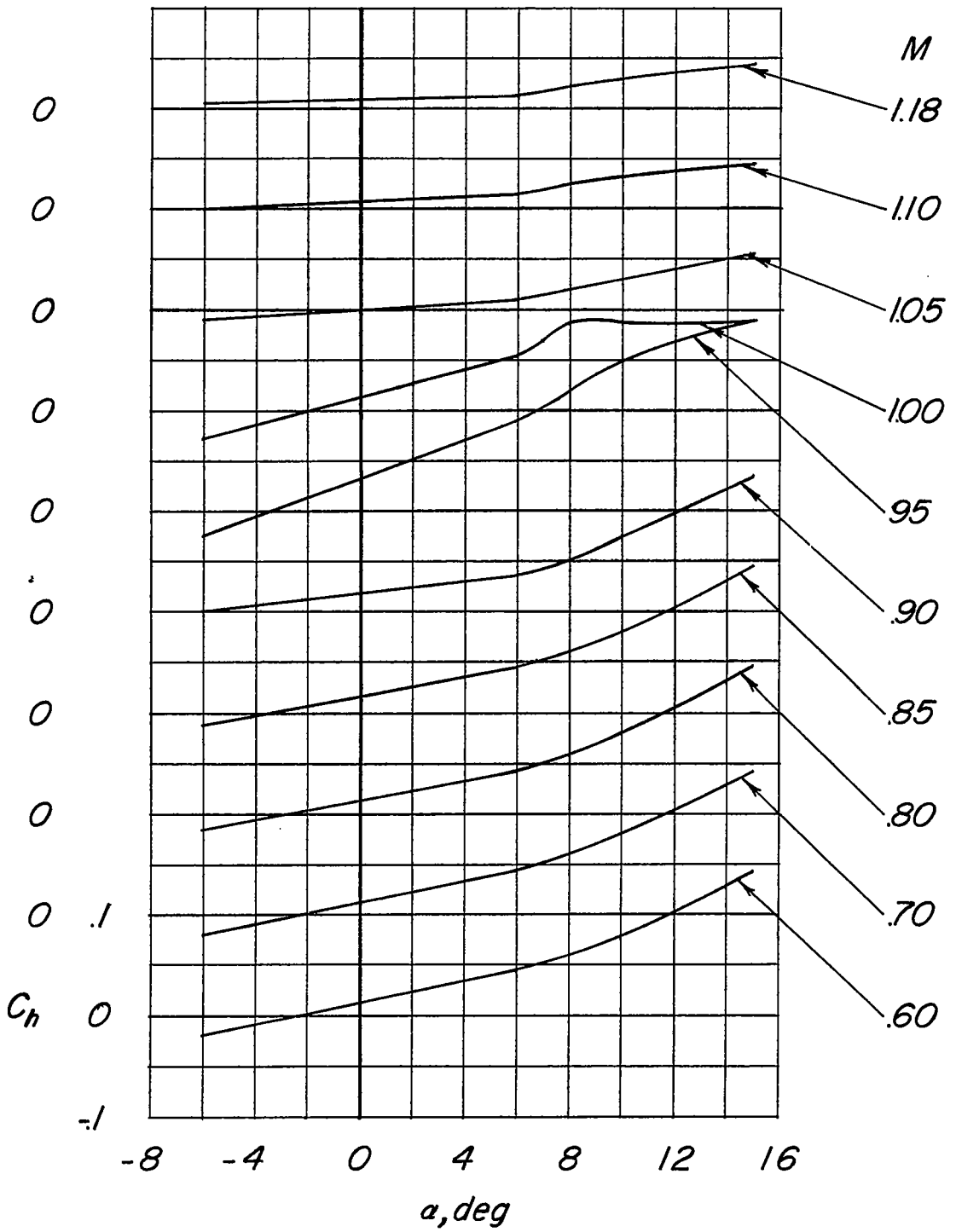

(e) $c_b/c_f = 1.03$.

Figure 11.- Concluded.

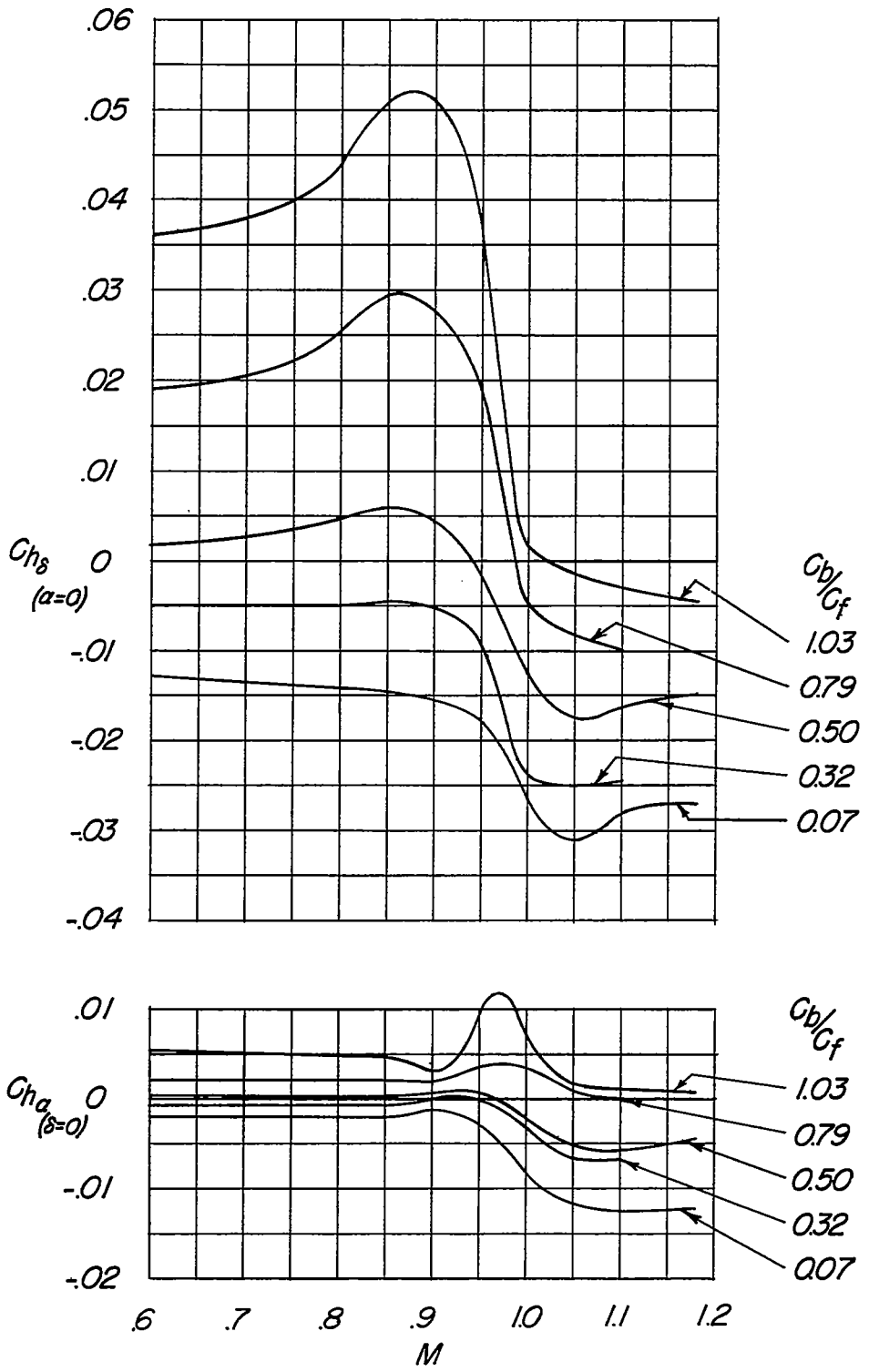

Figure 12.- Effect of hinge location on the variation with Mach number of the hinge-moment parameters C_{h_δ} and C_{h_α}.

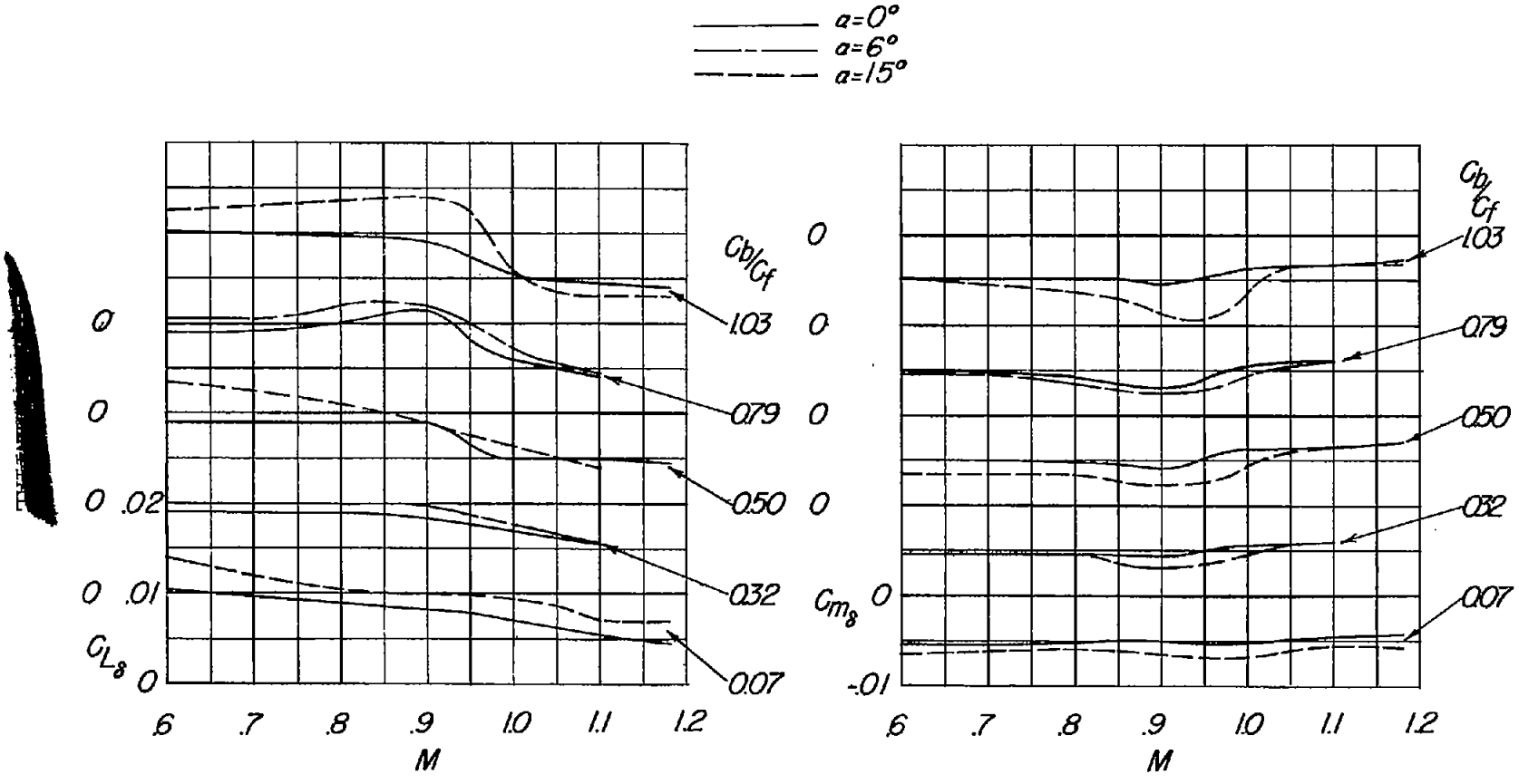

Figure 13.- Effect of hinge location and α on the variation with Mach number of C_{L_δ} and C_{m_δ}.

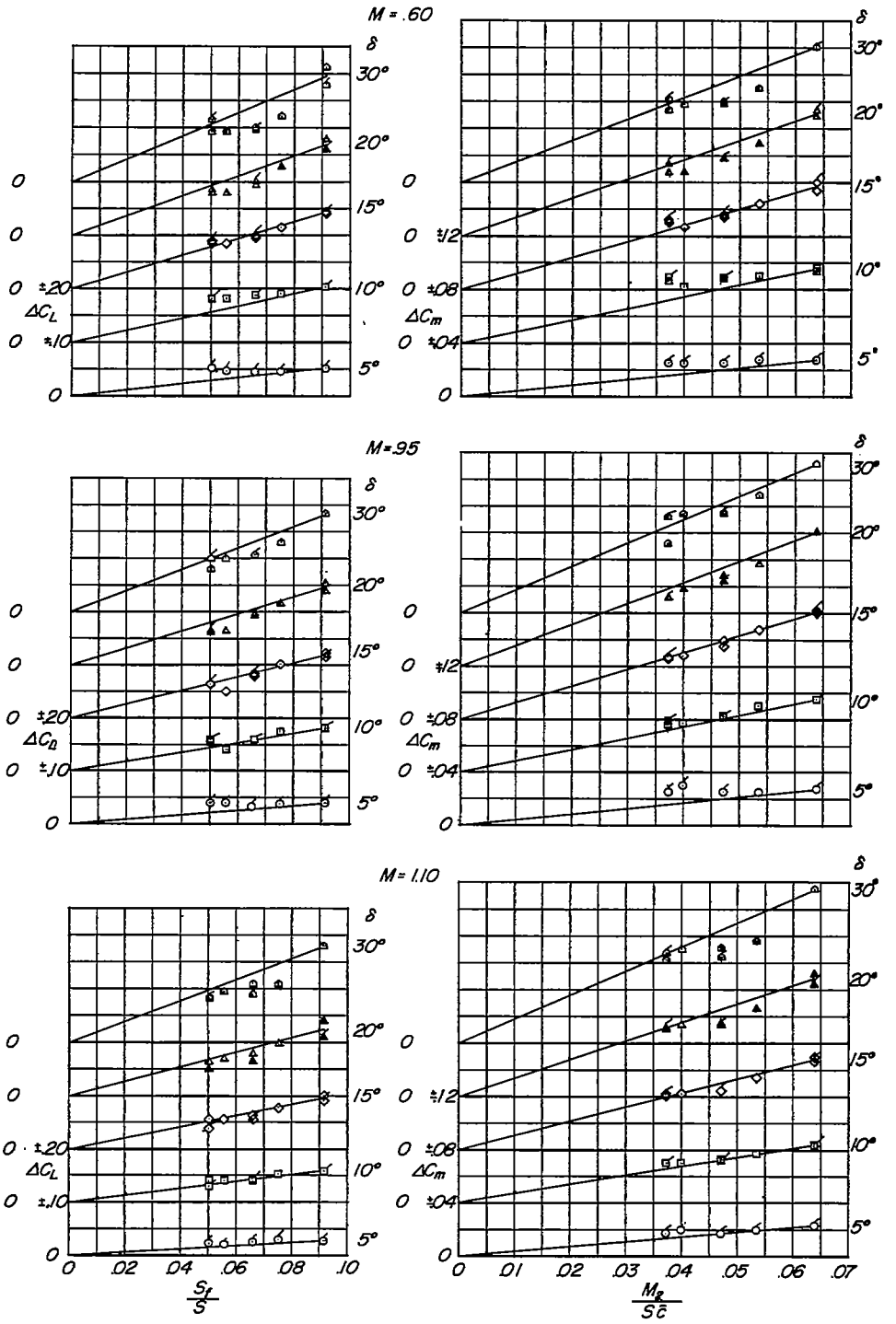

Figure 14.- Variation of ΔC_L and ΔC_m with a nondimensional ratio based on the area and area moment of the control area rearward of the hinge line. Flagged symbols denote negative flap deflections.